

**SELF-INDUCED BACK ACTION ACTUATED  
NANOPORE ELECTROPHORESIS (SANE) SENSOR  
FOR MOLECULAR DETECTION AND ANALYSIS**

by

SAI SANTOSH SASANK PERI

DISSERTATION

Submitted in partial fulfillment of the requirements  
for the degree of Doctor of Philosophy at  
The University of Texas at Arlington  
May 2019

Arlington, Texas

Supervising Committee:

George Alexandrakis, Supervising Professor

Jon Weidanz

Weidong Zhou

Yuze Sun

Michael Vasilyev

Copyright by  
Sai Santosh Sasank Peri  
2019

## ACKNOWLEDGEMENTS

Firstly, I would like to thank my supervisor, Dr. George Alexandrakis, for his trust in me to pursue scientific research. He constantly supported and encouraged me through every obstacle I faced through the process of turning this work from an idea into reality. This doctoral dissertation would not have been possible without his invaluable inputs derived from his expertise and experience.

I would like to thank the Office of Vice-President of Research at the University of Texas at Arlington for supporting this work through a Pilot Research Program for Interdisciplinary Collaboration.

I am thankful to my dear friend and co-worker Dr. Muhammad Usman Raza for contributing an equal part in all the hard days of work to realize the sensor and measurement system from an illustration on a paper into its physical form.

I am thankful to Dr. Nader Hozabri, Mr. Dennis Bueno and Mr. Richard K. Chambers for their technical guidance in semiconductor fabrication at the Shimadzu Institute Nanotechnology Research Center. I am grateful to Mr. Soeren Eyhusen and Mr. Chuong Huynh for allowing access to the focused ion beam at the Zeiss ORION NanoFab facility in Peabody, MA.

I would like acknowledge our collaborators at Dr. Weidanz's lab, Mr. Manoj Kumar Sabnani and Mr. Soroush Ghaffari for providing me with the necessary biological samples in a timely manner, sharing their invaluable expertise in immunology and participating in the healthy scientific brainstorming sessions to improved the quality of my research work.

With profound sense of gratitude, I am grateful to Dr. George Siemens and Lisa Berry for providing me with financial support towards my tuition and stipend through various grants at LINK research lab. I worked here as a graduate research assistant on innovative ideas in digital education and published in academic conferences.

In addition, I would like to thank Dr. Samir M. Iqbal and Dr. Vinay Abhyankar, who played a pivotal role in nurturing my interest in research by providing me with opportunities for publishing my research work at peer-reviewed avenues in the earlier years of my doctoral degree.

Finally, I would like to thank my supervising committee for their valuable inputs in completion of this dissertation work.

## DEDICATION

I dedicate this work to my mother and father. I am always indebted and grateful to my parents for their unconditional love and affection. They were my pillars of strength and support and constantly encouraged me to achieve my goals. My dad's moral and financial support along with my mom's love and prayers helped me complete this dissertation. Kind advice and encouragement from many friends and family members was essential in the successful completion of my doctoral degree. I will always be grateful to every member of LINK research lab for being my support system and my family away from home.

# ABSTRACT

SELF-INDUCED BACK ACTION ACTUATED NANOPORE ELECTROPHORESIS (SANE)  
SENSOR FOR MOLECULAR DETECTION AND ANALYSIS

by

Sai Santosh Sasank Peri, PhD

University of Texas at Arlington, 2019

Supervising Professor: George Alexandrakis

We fabricated a novel single molecule nanosensor by integrating a Solid-State Nanopore (SSNP) and a Double Nanohole (DNH) nanoaperture. The nanosensor employs Self-Induced Back-Action (SIBA) for optical trapping and enables SIBA-Actuated Nanopore Electrophoresis (SANE) for concurrent acquisition of bimodal optical and electrical signatures of molecular interactions. We demonstrated the potential utility of the SANE sensor by trapping and translocating 20 nm silica and gold nanoparticles. The electrical translocation time of the nanoparticles was extended by four orders of magnitude due to opposing electrical and optical forces acting on the nanoparticle, causing high frequency oscillations or bobbing in the electrical signal. Using frequency analysis, we were able to show that bobbing can be used as a signature to distinguish between single and multiple trapping. These promising results enabled us to pursue biomolecular detection with SANE sensor. We used high affinity T-cell receptor-like antibodies (TCRmAbs), and tested their binding to specific peptide-presenting Major Histocompatibility Complex (pMHC) ligands. We used irrelevant TCRmAbs, targeting the same pMHCs as control experiments. We were able to distinguish between individual molecules and their specific and non-

specific mixtures. The optical-electrical metrics enabled measurement of increased bound fraction of the antibody-ligand complexes at lower concentrations than bulk solution equilibrium binding constant ( $K_D$ ). In addition, we detected low affinity ligand-receptor interactions between soluble heterodimer receptors and pMHC ligands. We used irrelevant pMHCs to target the same receptor as a control experiment. We discriminated the optical-electrical signatures for specific and non-specific binding of receptor-ligand interactions, and were able to quantify the dissociation rate constant ( $k_{off}$ ) of the receptor-ligand binding comparable to the commercial technologies. The measurement  $k_{off}$  value can be correlated to the receptor-ligand binding time required for activation of immune response *in vivo*. Therefore, we demonstrated the utility of SANE sensor as a potential screening tool in cancer immunotherapy.

# TABLE OF CONTENTS

ACKNOWLEDGEMENTS.....	i
DEDICATION.....	ii
ABSTRACT.....	iii
TABLE OF CONTENTS.....	v
CHAPTER 1: INTRODUCTION.....	1
CHAPTER 2 :SELF-INDUCED BACK ACTION ACTUATED NANOPORE ELECTROPHORESIS (SANE).....	13
CHAPTER 3 : DETECTION OF SPECIFIC ANTIBODY-LIGAND INTERACTIONS WITH A SELF-INDUCED BACK-ACTION ACTUATED NANOPORE ELECTROPHORESIS (SANE) SENSOR.....	39
CHAPTER 4 : QUANTIFICATION OF LOW AFFINITY KINETICS BETWEEN Qa-1b Qdm LIGANDS AND NK INHIBITORY RECEPTORS CD94/NKG2A WITH A SELF-INDUCED BACK-ACTION ACTUATED NANOPORE ELECTROPHORESIS (SANE) SENSOR .....	70
CHAPTER 5: CONCLUSION .....	95
APPENDIX 1: PERMISSION FROM PUBLISHERS AND AUTHORS .....	97

# CHAPTER 1

## INTRODUCTION

### **Background**

The growing need for knowledge about human health and diagnostics has paved the way for development of molecular diagnostic techniques necessary for the detection of diseases [1-3]. With the advancement of science and technology the diagnostics and cure of many diseases is easily possible [4-6]. The need for more reliable, faster, and robust detection systems has led to the development of biosensors. Biosensors can detect and quantify biomolecular interactions to be used as a marker for disease diagnosis [7-9]. With ever increasing need for sensitivity and specificity in detection of markers and molecules to aid in early detection of life-threatening diseases such as cancer, biosensor research is focused more on detection at the single molecule level.

### **Cancer and Immunotherapy**

Cancer is a condition of abnormal growth of cells and can occur in two forms-benign and malignant. It develops due to mutations in healthy cells leading to altered cell signaling pathways that cause disruption of cell cycle checkpoints and hurdle programmed cell death [10]. Early warning indicators and symptoms of cancer may go unnoticed for a really long period of time. In some cases, the symptoms might not directly indicate the presence of cancer, until a biopsy or x-ray is done and may be misleading for the presence of other disease [11, 12]. Therefore, early and correct diagnosis of cancer is the need of the hour and in order to do so, we need to develop new and advanced diagnostic techniques with high sensitivity and specificity. Detection of cancer at



the benign stage can cause a significant difference in the course of treatment and in some cases may even help in saving the life of a patient, as in the malignant stage the cells have spread through the blood vessels to different sites in the body [13-16]. The rising concern for early detection of cancer is because it is the second most common disease and early detection can help in higher five-year survival rates. Chances of saving a person's life if stage 4 cancer is detected are less as compared to stage 1 cancer [13]. The advancement in the field of proteomics and genomics has led to the early detection of cancer progression. These techniques detect minute changes in DNA base pairs or presence of increased level of cancer biomarkers for the detection of the disease [17, 18]. These cancer specific biomarkers are often called as bio-signatures and represent the molecular changes caused by the tumor cells inside the body. Biomarkers can be identified either at the primary tumor site or secondary tumor site by biopsy of the tumor tissue or by inspecting blood, urine, sweat or saliva in the form of proteins, DNA and RNA [9].

Biomarkers such as proteins are presented on the surface of cancer cells by peptide presenting major histocompatibility complex (pMHC) that enable targeting and lysing by cytotoxic T cells through immune response. Using immunotherapy, the response rate for identification and killing of cancer cells by T cells has been advanced in recent years with the use of recombinant T-Cell-Receptor like monoclonal Antibodies (TCRmAbs) [19-24]. The current challenge in implementing this therapeutic approach is that cancer cells express a wide variety of such receptors, making it difficult for the selection of appropriate TCRmAb to target cancer. When a specific TCRmAb is used, it can target the pMHC and induce an immune response against cancer cells. TCRmAbs are engineered to have precise and tailored binding affinities for the specific pMHC [25]. Advancement in cancer immunotherapy can be possible when the TCRmAb's specificity, sensitivity and binding kinetics can be quantified with precision nanotechnology based

biosensors. Using patient specific biomarkers found through pre-treatment diagnosis, antibodies targeting those pMHCs can be synthesized as a personalized vaccine thereby improving cancer remission and survival.

Advances in the field of nanotechnology have enabled the development of biosensors that can meet this need. Various transduction principles such as electrical, optical, piezoelectric, acoustic, etc. are employed by these sensors to detect and quantify the interaction of proteins and ligands. These interactions are better detected at single molecular level through two popular nanosensing technologies, one is optical trapping through metallic nanoapertures and the other electrical sensing through solid-state nanopores. The aim is to develop efficient, robust and cost-effective nanoscale molecular biosensors for early detection of cancer.

### **Nanoaperture Optical Trapping**

Ashkin's demonstration of manipulating the dynamics of a micrometer sized particle using the forces of light pressure, referred to as optical trapping has been applied extensively in trapping dielectric objects, nanoparticles and biological particles [26]. Particles (<100 nm in size, including biological particles) with a refractive index slightly higher than its immediate surroundings, the gradient force acting on the particle decreases at a rate of third power of size, increases the viscous drag and thermal motion. These conditions make the particle unstable inside the trap and with the only option to increase the intensity of the laser beam, thereby damaging the temperature sensitive biological particles [27, 28].

Nanoapertures, fabricated in metallic films facilitate optical trapping of such dielectric particles (<100 nm diameter), by utilizing the increase in optical transmission due to changes in local electric field at low beam intensities. This approach of nanoaperture based optical trapping

is called as self-induced back action (SIBA) optical trapping [28]. In SIBA optical trapping, when a dielectric particle of slightly higher refractive index than its surroundings enters the laser beam pathway above nanoaperture the diffusion forces are opposed by a photon-mediated feedback force, causing the particle to be trapped and increasing the light transmission through the nanoaperture. This is a label free detection method, enabling characterization of proteins [29-31] and their interactions with other small biomolecules [27, 32-35]. Plasmonic optical trapping has limitations in throughput due to diffusion based delivery of particles to the sensing zone, prolonged trapping of particles with decreasing concentration and sensitivity to the shape of the nanoapertures [27, 36-38]

## **Nanopore Electrophoresis**

The idea behind the working of nanopore biosensors was inspired from nanometer sized biological nanopores like  $\alpha$ -hemolysin (~1.4 nm) present in the lipid membranes of *Staphylococcus Aureus* bacteria. These nanopores mimic the process of uptake of ions, nutrients and exchange of other biomolecules with the extracellular environment *in vivo*. These  $\alpha$ -hemolysin pores have been extracted to perform DNA sequencing by translocating single strand DNA across the pore under optimal electrical bias allowing for the identification of base pair sequence based on the characteristics electrical signature registered for each current blockade event by the nucleotide [39-45]. Though these pores worked as alternative sequencing technology, they had many limitations such as inflexible pore sizes, mechanical stress, inability to capture single base pairs, and instability in higher molar electrolyte solutions [46].

Synthetic nanopores or solid state nanopores (SSNPs) are the robust, reliable and stable counterparts of biological nanopores with a pore size flexibility to accommodate for analyte's

dimensions making them suitable for single detection and analysis [46]. SSNPs are nanometer holes drilled right in dielectric membranes that are suspended in Si chips using focused ion beam (FIB) [47] or transmission electron microscopy (TEM) [48]. Dielectric membranes used in SSNPs are made in silicon nitride, graphene, silicon oxide [49-51]. These membranes are fabricated using standard semiconductor fabrication techniques. The fabricated chip is placed between two containers filled with ionic solution with the analyte in the *cis*-chamber. Analytes are translocated under an electrical bias from *cis* to *trans* chamber, causing a significant reduction in nanopore current that is characteristic of the analyte's size, volume and charge [49, 52-55]. Nanopore electrophoresis has been widely used in the past two decades for detection of DNA, proteins, antigens, antibodies, bacteria and viruses [56-65].

Nanopore sensing has been enhanced with the combination of optical sensing for studying the bimolecular interactions of particles by slowing down the translocation velocity of particles which otherwise go undetected in a normal SSNP. One of the earliest studies was tweezing of a DNA-tethered micrometer bead [66] under a tightly focused laser, which cannot be extended beyond the sub-diffraction limit. Optical excitation of fluorescently labeled analytes to slow down their speed by manipulating the surface charge and using the electroosmotic flow [67]. This technique was limited to small size nanopore only. Bow tie shaped nanoantennas [68-74] in gold were created to enable plasmonic enhancement of optical field over the nanopore which resulted in localized heating due to increased ionic conductance but did not slow down the analyte translocation velocity.

## **SIBA Actuated Nanopore Electrophoresis (SANE)**

In this work, we designed and fabricated a novel bimodal optical-electrical nanosensor by combining both of the above single molecule detection methods, the self-induced back action (SIBA) optical trapping and the Nanopore Electrophoresis (NE), SANE [75]. We placed a classical nanopore in silicon nitride at the center of a gold double nanohole (DNH) nanoperture with tapered walls. The first article describes the fabrication of this sensor and explains the mechanism of how a particle is trapped above mouth of a SSNP using excited wedge plasmons and translocated through SSNP when the electrophoretic force overpowers the optical forces. A proof of concept study is shown with nanoparticles recording concurrent bimodal optical and electrical signatures proportional to the size, volume and charge of the particles. In the second article, the SANE sensor's ability to sense biomolecules has been investigated by detecting the high affinity interactions of Anti-RAH, a TCRmAb and a pMHC, RAH as a means to differentiate bound from unbound antibodies and specific from non-specific binding of TCRmAbs. This work characterized a potential anti-cancer immunotherapeutic antibody capable of triggering a cytotoxic response when deployed in vivo. The final article is another immunotherapy application with the protein receptors (soluble CD94/NKG2A) having low affinity towards their ligands (Qdm/Qa-1<sup>b</sup>) are characterized using SANE sensor for their binding duration and distinguished from non-specific binding to irrelevant ligands. This work has the potential to block the specific ligands displayed on the surface cancer cells evading the immune system and induce a natural killer cells response to lyse them, thereby using natural interactions to kill cancer. Both the biological applications are intended towards the advancement of personalized precision medicine with the aid of nanotechnology-based biosensors.

## REFERENCES

- [1] Sonneborn T M 1965 **Molecular Biology of the Gene**. J. D. Watson. Benjamin, New York, 1965. xxii + 494 pp. Illus. Paper, \$5.95; cloth, \$10 *Science* **150** 1282-
- [2] Savageau M A 1976 *ADDISON WESLEY PUBL.*,
- [3] Josephy P D and Mannervik B 2006 *Molecular toxicology*: Oxford University Press on Demand)
- [4] Sato J, Kawamoto T, Le A, Mendelsohn J, Polikoff J and Sato G 1983 Biological effects in vitro of monoclonal antibodies to human epidermal growth factor receptors *Molecular biology & medicine* **1** 511-29
- [5] Xenarios I, Salwinski L, Duan X J, Higney P, Kim S-M and Eisenberg D 2002 DIP, the Database of Interacting Proteins: a research tool for studying cellular networks of protein interactions *Nucleic acids research* **30** 303-5
- [6] Zhang J-T and Liu Y 2007 Use of comparative proteomics to identify potential resistance mechanisms in cancer treatment *Cancer treatment reviews* **33** 741-56
- [7] Horner S R, Mace C R, Rothberg L J and Miller B L 2006 A proteomic biosensor for enteropathogenic E. coli *Biosensors and Bioelectronics* **21** 1659-63
- [8] Jain K 2003 Current status of molecular biosensors *Medical device technology* **14** 10-5
- [9] Rasooly A and Jacobson J 2006 Development of biosensors for cancer clinical testing *Biosensors and Bioelectronics* **21** 1851-8
- [10] Klein G 2004 Cancer, apoptosis, and nonimmune surveillance *Cell death and differentiation* **11** 13-7
- [11] Utz D C, Hanash K A and Farrow G M 1970 The plight of the patient with carcinoma in situ of the bladder *The Journal of urology* **103** 160-4
- [12] DeAngelis L M 1990 Primary central nervous system lymphoma imitates multiple sclerosis *Journal of neuro-oncology* **9** 177-81
- [13] Goetz T 2008 Why early detection is the best way to beat cancer *WIRED Magazine, December* **22**
- [14] Parikh-Patel A, Bates J H and Campleman S 2006 Colorectal cancer stage at diagnosis by socioeconomic and urban/rural status in California, 1988–2000 *Cancer* **107** 1189-95

- [15] Investigators I E L C A P 2006 Survival of patients with stage I lung cancer detected on CT screening *New England Journal of Medicine* **355** 1763-71
- [16] Lantz P M, Mujahid M, Schwartz K, Janz N K, Fagerlin A, Salem B, Liu L, Deapen D and Katz S J 2006 The influence of race, ethnicity, and individual socioeconomic factors on breast cancer stage at diagnosis *American journal of public health* **96** 2173-8
- [17] Minn A J, Gupta G P, Siegel P M, Bos P D, Shu W, Giri D D, Viale A, Olshen A B, Gerald W L and Massagué J 2005 Genes that mediate breast cancer metastasis to lung *Nature* **436** 518
- [18] Ramaswamy S, Ross K N, Lander E S and Golub T R 2002 A molecular signature of metastasis in primary solid tumors *Nature genetics* **33** 49
- [19] Herrera C E, Lowe D B, Bivens C K, Mobley A S, McCormick A, Wichner T, Sabnani M K, Wood L M and Weidanz J A 2017 TCR-like antibody duocarmycin conjugates promote cytotoxicity of tumor cells expressing low peptide/HLA targets. *Am Assoc Immunol*
- [20] Kim S, Pinto A K, Myers N B, Hawkins O, Doll K, Kaabinejadian S, Netland J, Bevan M J, Weidanz J A and Hildebrand W H 2014 A novel T-cell receptor mimic defines dendritic cells that present an immunodominant West Nile virus epitope in mice *European journal of immunology* **44** 1936-46
- [21] Lowe D B, Bivens C K, Mobley A S, Herrera C E, McCormick A L, Wichner T, Sabnani M K, Wood L M and Weidanz J A 2017 TCR-like antibody drug conjugates mediate killing of tumor cells with low peptide/HLA targets(vol 9): Taylor & Francis) p 603-14
- [22] Verma B, Jain R, Caseltine S, Rennels A, Bhattacharya R, Markiewski M M, Rawat A, Neethling F, Bickel U and Weidanz J A 2011 TCR mimic monoclonal antibodies induce apoptosis of tumor cells via immune effector-independent mechanisms *The Journal of Immunology* **186** 3265-76
- [23] Verma B, Neethling F A, Caseltine S, Fabrizio G, Largo S, Duty J A, Tabaczewski P and Weidanz J A 2010 TCR mimic monoclonal antibody targets a specific peptide/HLA class I complex and significantly impedes tumor growth in vivo using breast cancer models *The journal of immunology* **184** 2156-65
- [24] Wittman V P, Woodburn D, Nguyen T, Neethling F A, Wright S and Weidanz J A 2006 Antibody targeting to a class I MHC-peptide epitope promotes tumor cell death *The Journal of Immunology* **177** 4187-95
- [25] Stone J D, Chervin A S and Kranz D M 2009 T-cell receptor binding affinities and kinetics: impact on T-cell activity and specificity *Immunology* **126** 165-76

- [26] Ashkin A 2000 History of optical trapping and manipulation of small-neutral particle, atoms, and molecules *IEEE Journal of Selected Topics in Quantum Electronics* **6** 841-56
- [27] Al Balushi A A, Kotnala A, Wheaton S, Gelfand R M, Rajashekara Y and Gordon R 2015 Label-free free-solution nanoaperture optical tweezers for single molecule protein studies *Analyst* **140** 4760-78
- [28] Juan M L, Gordon R, Pang Y, Eftekhari F and Quidant R 2009 Self-induced back-action optical trapping of dielectric nanoparticles *Nature Physics* **5** 915
- [29] Al Balushi A A, Zehtabi-Oskuie A and Gordon R 2013 Observing single protein binding by optical transmission through a double nanohole aperture in a metal film *Biomedical optics express* **4** 1504-11
- [30] Pang Y and Gordon R 2011 Optical trapping of a single protein *Nano letters* **12** 402-6
- [31] Wheaton S and Gordon R 2015 Molecular weight characterization of single globular proteins using optical nanotweezers *Analyst* **140** 4799-803
- [32] Al Balushi A A and Gordon R 2015 Label-Free Free Solution Single Protein-Small Molecule Binding Kinetics: An Optical Tweezer Approach: Optical Society of America) p OtT2E. 3
- [33] Al Balushi A A and Gordon R 2014 A label-free untethered approach to single-molecule protein binding kinetics *Nano letters* **14** 5787-91
- [34] Al Balushi A A and Gordon R 2014 Label-free free-solution single-molecule protein–small molecule interaction observed by double-nanohole plasmonic trapping *ACS Photonics* **1** 389-93
- [35] Balushi A A and Gordon R 2014 Dynamic Variation in Protein-Small Molecule Interaction Observed by Double-Nanohole Optical Trapping *arXiv preprint arXiv:1403.3922*
- [36] Kotnala A, DePaoli D and Gordon R 2013 Sensing nanoparticles using a double nanohole optical trap *Lab on a Chip* **13** 4142-6
- [37] Kumar L, Lesuffleur A, Hughes M and Gordon R 2006 Double nanohole apex-enhanced transmission in metal films *Applied Physics B* **84** 25
- [38] Pang Y and Gordon R 2011 Optical trapping of 12 nm dielectric spheres using double-nanoholes in a gold film *Nano letters* **11** 3763-7
- [39] Deamer D W and Akeson M 2000 Nanopores and nucleic acids: prospects for ultrarapid sequencing *Trends in biotechnology* **18** 147-51



- [40] Kasianowicz J J, Brandin E, Branton D and Deamer D W 1996 Characterization of individual polynucleotide molecules using a membrane channel *Proceedings of the National Academy of Sciences* **93** 13770-3
- [41] Venkatesan B M and Bashir R 2011 Nanopore sensors for nucleic acid analysis *Nature nanotechnology* **6** 615
- [42] Keyser U F 2011 Controlling molecular transport through nanopores *Journal of The Royal Society Interface* **8** 1369-78
- [43] Feng Y, Zhang Y, Ying C, Wang D and Du C 2015 Nanopore-based fourth-generation DNA sequencing technology *Genomics, proteomics & bioinformatics* **13** 4-16
- [44] Kowalczyk S W, Blosser T R and Dekker C 2011 Biomimetic nanopores: learning from and about nature *Trends in biotechnology* **29** 607-14
- [45] Ma L and Cockroft S L 2010 Biological Nanopores for Single-Molecule Biophysics *ChemBioChem* **11** 25-34
- [46] Dekker C 2007 Solid-state nanopores *Nature nanotechnology* **2** 209
- [47] Miles B N, Ivanov A P, Wilson K A, Doğan F, Japrun D and Edel J B 2013 Single molecule sensing with solid-state nanopores: novel materials, methods, and applications *Chemical Society Reviews* **42** 15-28
- [48] Storm A, Chen J, Ling X, Zandbergen H and Dekker C 2003 Fabrication of solid-state nanopores with single-nanometre precision *Nature materials* **2** 537
- [49] Shi W, Friedman A K and Baker L A 2016 Nanopore sensing *Analytical chemistry* **89** 157-88
- [50] Yuan Z, Wang C, Yi X, Ni Z, Chen Y and Li T 2018 Solid-State Nanopore *Nanoscale research letters* **13** 56
- [51] Schneider G F, Kowalczyk S W, Calado V E, Pandraud G, Zandbergen H W, Vandersypen L M and Dekker C 2010 DNA translocation through graphene nanopores *Nano letters* **10** 3163-7
- [52] Plesa C and Dekker C 2015 Data analysis methods for solid-state nanopores *Nanotechnology* **26** 084003
- [53] Larkin J, Henley R Y, Muthukumar M, Rosenstein J K and Wanunu M 2014 High-bandwidth protein analysis using solid-state nanopores *Biophysical journal* **106** 696-704
- [54] Fologea D, Ledden B, McNabb D S and Li J 2007 Electrical characterization of protein molecules by a solid-state nanopore *Applied physics letters* **91** 053901
- [55] Smeets R M, Keyser U F, Krapf D, Wu M-Y, Dekker N H and Dekker C 2006 Salt dependence of ion transport and DNA translocation through solid-state nanopores *Nano letters* **6** 89-95

- [56] Ali W, Raza M U, Mahmood M A I, Allen P B, Hall A R, Wan Y and Iqbal S M Differentiation of Specific Cancer Biomarkers with Solid-state Nanopores.
- [57] Butler T Z, Pavlenok M, Derrington I M, Niederweis M and Gundlach J H 2008 Single-molecule DNA detection with an engineered MspA protein nanopore *Proceedings of the National Academy of Sciences* **105** 20647-52
- [58] Freedman K J, Bastian A R, Chaiken I and Kim M J 2013 Solid-state nanopore detection of protein complexes: applications in healthcare and protein kinetics *Small* **9** 750-9
- [59] Freedman K J, Haq S R, Edel J B, Jemth P and Kim M J 2013 Single molecule unfolding and stretching of protein domains inside a solid-state nanopore by electric field *Scientific reports* **3** 1638
- [60] Gershow M and Golovchenko J A 2007 Recapturing and trapping single molecules with a solid-state nanopore *Nature nanotechnology* **2** 775
- [61] Kowalczyk S W, Hall A R and Dekker C 2009 Detection of local protein structures along DNA using solid-state nanopores *Nano letters* **10** 324-8
- [62] Plesa C, Kowalczyk S W, Zinsmeister R, Grosberg A Y, Rabin Y and Dekker C 2013 Fast translocation of proteins through solid state nanopores *Nano letters* **13** 658-63
- [63] Talaga D S and Li J 2009 Single-molecule protein unfolding in solid state nanopores *Journal of the American Chemical Society* **131** 9287-97
- [64] Uram J D, Ke K, Hunt A J and Mayer M 2006 Submicrometer Pore-Based Characterization and Quantification of Antibody–Virus Interactions *Small* **2** 967-72
- [65] Guo P, Hall E W, Schirhagl R, Mukaibo H, Martin C R and Zare R N 2012 Microfluidic capture and release of bacteria in a conical nanopore array *Lab on a Chip* **12** 558-61
- [66] Keyser U, Van der Does J, Dekker C and Dekker N 2006 Optical tweezers for force measurements on DNA in nanopores *Review of Scientific Instruments* **77** 105105
- [67] Di Fiori N, Squires A, Bar D, Gilboa T, Moustakas T D and Meller A 2013 Optoelectronic control of surface charge and translocation dynamics in solid-state nanopores *Nature nanotechnology* **8** 946
- [68] Jonsson M P and Dekker C 2013 Plasmonic nanopore for electrical profiling of optical intensity landscapes *Nano letters* **13** 1029-33

- [69] Li Y, Nicoli F, Chen C, Lagae L, Groeseneken G, Stakenborg T, Zandbergen H W, Dekker C, Van Dorpe P and Jonsson M P 2014 Photoresistance switching of plasmonic nanopores *Nano letters* **15** 776-82
- [70] Nicoli F, Verschueren D, Klein M, Dekker C and Jonsson M P 2014 DNA translocations through solid-state plasmonic nanopores *Nano letters* **14** 6917-25
- [71] Shi X, Verschueren D, Pud S and Dekker C 2018 Integrating Sub-3 nm Plasmonic Gaps into Solid-State Nanopores *Small* **14** 1703307
- [72] Shi X, Verschueren D V and Dekker C 2018 Active Delivery of Single DNA Molecules into a Plasmonic Nanopore for Label-Free Optical Sensing *Nano letters* **18** 8003-10
- [73] Verschueren D, Shi X and Dekker C 2019 Nano-Optical Tweezing of Single Proteins in Plasmonic Nanopores *Small Methods* 1800465
- [74] Verschueren D V, Pud S, Shi X, De Angelis L, Kuipers L and Dekker C 2018 Label-Free Optical Detection of DNA Translocations through Plasmonic Nanopores *ACS nano*
- [75] Raza M U, Peri S S S, Ma L-C, Iqbal S M and Alexandrakis G 2018 Self-induced back action actuated nanopore electrophoresis (SANE) *Nanotechnology* **29** 435501

## CHAPTER 2

# SELF-INDUCED BACK ACTION ACTUATED NANOPORE ELECTROPHORESIS (SANE)<sup>1</sup>

Muhammad Usman Raza<sup>\*1</sup>, Sai Santosh Sasank Peri<sup>\*1</sup>, Liang-Chieh Ma<sup>2</sup>, Samir M. Iqbal<sup>2,3,#</sup>,  
and George Alexandrakis<sup>2,#</sup>

<sup>\*</sup>Equal Author

<sup>1</sup> Department of Electrical Engineering, University of Texas at Arlington, Arlington, TX, 76019,  
USA

<sup>2</sup> Department of Bioengineering, University of Texas at Arlington, Arlington, TX, 76019, USA

<sup>3</sup> Nano-bio Lab, Department of Electrical Engineering, and School of Medicine, University of  
Texas Rio Grande Valley, Edinburg, TX 78539, USA

<sup>#</sup> Email: SMIQBAL@ieee.org and galex@uta.edu

Raza M U, Peri S S S, Ma L-C, Iqbal S M and Alexandrakis G 2018 Self-induced back action  
actuated nanopore electrophoresis (SANE) Nanotechnology 29 435501

---

<sup>1</sup> Used with permission of the publisher, IOP Nanotechnology, 2019. Original content from this work has been used under the terms of the Creative Commons Attribution 3.0 licence.

## ABSTRACT

We present a novel method to trap nanoparticles in Double Nanohole (DNH) nanoapertures integrated on top of solid-state nanopores (ssNP). The nanoparticles were propelled by an electrophoretic force from the cis towards the trans side of the nanopore but were trapped in the process when they reached the vicinity of the DNH-ssNP interface. The Self-Induced Back Action (SIBA) plasmonic force existing between the tips of the DNH opposed the electrophoretic force and enabled simultaneous optical and electrical sensing of a single nanoparticle for seconds. The novel SIBA Actuated Nanopore Electrophoresis (SANE) sensor was fabricated using two-beam GFIS FIB. Firstly, Ne FIB milling was used to create the DNH features and was combined with end pointing to stop milling at the metal-dielectric interface. Subsequently, He FIB was used to drill a 25 nm nanopore through the center of the DNH. Proof of principle experiments to demonstrate the potential utility of the SANE sensor were performed with 20 nm silica and Au nanoparticles. The addition of optical trapping to electrical sensing extended translocation times by four orders of magnitude. The extended electrical measurement times revealed newly observed high frequency charge transients that were attributed to bobbing of the nanoparticle driven by the competing optical and electrical forces. Frequency analysis of this bobbing behavior hinted at the possibility of distinguishing single from multi-particle trapping events. We also discuss how SANE sensor measurement characteristics differ between silica and Au nanoparticles due to differences in their physical properties and how to estimate the charge around a nanoparticle. These measurements show promise for the SANE sensor as an enabling tool for selective detection of biomolecules and quantification of their interactions.

## INTRODUCTION

Nanopore biosensors utilize resistive pulse sensing of ion currents to detect biological analytes. Translocation of the analyte through a nanometer aperture is driven by the applied bias [1-3]. This technique has been used to detect DNA [4-7], proteins [8-14], miRNA [15-18] and other bio-analytes [19]. It has also been proposed as an affordable DNA sequencing tool [20, 21]. Although nanopores have been made from biological membranes [22, 23], solid state nanopores (ssNPs) have been widely used as a more robust alternative [24]. SsNPs are fabricated in silicon chips with suspended dielectric membranes in which the nanopores are etched or milled [25-28]. Over the past two decades, numerous enhancements in nanopore technology have been reported for biosensing, including surface attachment to nanopore walls [7, 16], nanopore arrays [29], optically enhanced nanopores [30] and embedded tunneling electrode nanopores [31]. These technologies were developed to address challenges relating to low throughput, high sensor noise, lack of self-referencing, and high pore translocation speeds [3, 32].

To enhance nanopore sensing further, attempts have been made to combine it with optical sensing. Optical enhancement of nanopore sensing has garnered much interest since Keyser et al [33, 34] used a tightly focused laser on a DNA-tethered micrometer bead translocating through an ssNP. Optical forces acted as a tweezer for controlling bead translocation thus enabling study of biomolecular interactions inside the nanopore by force spectroscopy. However, tweezing cannot be extended to sub-diffraction limit nanoparticles directly due to the exponential reduction in optical trapping force with size. Surface charge control by optical excitation has also been used as an alternative approach employing electroosmotic flow to slow down the translocation of analytes through the nanopores [35]. Nevertheless, this technique only works in small nanopores due to

Debye length restriction and requires fluorescent labeling for optical detection. Jonsson et al. [36] used gold bowtie plasmonic nanoantennas to create optical field enhancement in the nanogap over the mouth of a TEM-milled silicon nitride nanopore. The plasmonic focusing led to increased ionic conductance due to localized heating but did not slow down translocation through the nanopore. They also reported photoresistive switching in plasmonic nanopores [37], which was attributed to plasmon-induced gaseous air bubble formation at the nanopore mouth. Recently, Meller et al. [38] reported a plasmonic nanopore with a circular gold nanowell on the trans side of the nanopore. This resulted in dual-mode detection of nanopore current and plasmonically excited fluorescence from the labelled DNA, without any control on nanopore translocation speed.

Nanoaperture-focused plasmons in metallic films are a potentially enabling technology for controlling analyte translocation through a nanopore, but this has been explored very little to date. Optical trapping at low laser powers can be attained in the immediate vicinity of metallic nanoapertures through a self-induced back action (SIBA) mechanism [39]. In SIBA, when a dielectric nanoparticle has a slightly different refractive index than its surrounding medium a photon-mediated feedback force is actuated due to conservation of momentum against diffusion forces near the nanoaperture. The resulting coupling of light to the far field via the dielectric nanoparticle results in increased light transmission through the plasmonic nanoaperture and therefore enables label-free detection [40]. Double nanohole (DNH) nanoapertures have been reported as SIBA-mediated optical traps by Gordon et al. for high local field enhancement at the intersection of the nanoholes [41]. The Gordon group has reported a series of studies on the design characteristics of the DNH structure [42-44] and their use in many applications, including the trapping of nanoparticles [45-47] and single protein molecules [48-51].

Here we report nanofabrication and proof of principle studies for a DNH-ssNP sensor enabling simultaneous SIBA-mediated optical trapping by the DNH and electrophoresis through the ssNP. We name this a SIBA Actuated Nanopore Electrophoresis (SANE) sensor. The nanopore is milled between the tips of the DNH where the highest plasmonic energy is focused, resulting in trapping of the nanoparticle due to dielectric loading at the mouth of the nanopore. The nanoparticle translocates through the nanopore after it escapes trapping and yields the characteristic drop in ionic current due to pore blockage. Two types of focused ion beam (FIB) milling enabled nanofabrication of the DNH structure in an Au layer deposited on top of a thin silicon nitride layer without damaging it. Furthermore, the DNH structure is known to dissipate heat very effectively with minimal temperature increases at optical trapping powers [52]. In proof of principle experiments, we show that the DNH-nanopore structure trapped 20 nm nanoparticles made of silica or Au for several seconds, while enabling their concurrent electrical sensing during the same time interval. The SANE sensor controlled the nanoparticle translocation through the nanopore, which extended the duration of electrical sensing by up to four orders of magnitude compared to nanopore sensing alone. The extended electrical measurement times revealed a newly observed high frequency charge transient phenomenon related to occupancy of the optical trap by one or more nanoparticles. Finally, we discuss how upon sensor calibration, these bimodal measurements could be used to estimate the total charge around a nanoparticle and how SANE sensor measurements characteristics differ between silica and Au nanoparticles due to differences in their physical properties.



## MATERIALS AND METHODS

### Dual Nanohole – Nanopore Chip Fabrication

The fabrication was done on double side polished, (100) orientation 4-inch silicon. Wet oxidation was done to grow 500 nm  $\text{SiO}_2$  followed by a 60 nm LPCVD non-stoichiometric low stress silicon nitride ( $\text{Si}_x\text{N}_y$ ). For each wafer, individual 15 mm x 15 mm square chips were created with one side patterned using S1813 photoresist with a darkfield backside mask. The first mask contained square windows of 786  $\mu\text{m}$  size in the center. The 786  $\mu\text{m}$  square etch windows were opened in  $\text{Si}_x\text{N}_y$  using DRIE to etch through its entire 60 nm layer thickness and then a 6:1 Buffered Hydrofluoric acid (BHF) solution was used to etch the  $\text{SiO}_2$  to reveal the bare silicon (Fig. 1). The wafers were placed in 22 % tetramethylammonium hydroxide (TMAH) solution at 90 °C to anisotropically etch the wafer all the way to the front side revealing the 100  $\mu\text{m}$  square  $\text{SiO}_2/\text{Si}_x\text{N}_y$  membranes at the other side, henceforth called the front side. The  $\text{SiO}_2$  was a sacrificial layer to protect the membrane during further processing and was etched away at the last step of the chip fabrication. The wafers were cleaned in Piranha solution and inspected under an optical microscope to confirm the design parameters of the anisotropic etch. E-beam evaporation was used to deposit 5 nm of Cr as the adhesion layer on which 100 nm of Au was subsequently deposited on the front side of the wafer on top of the suspended  $\text{Si}_x\text{N}_y$  membranes. The S1813 positive resist was used to coat the front side of the wafer to pattern four diagonal FIB alignment markers in Au. A backside aligner (EVG 620) was used to align the dark field second mask and to expose the front side while aligned to the backside patterns. Au and Cr were wet etched using commercially available wet etchants (Sigma Aldrich). The etched and cleaned wafers were inspected under an optical microscope for proper placement of FIB alignment markers on the suspended  $\text{Si}_x\text{N}_y$

membrane from the front side and the back side [Fig. 1(d)]. The front side of the wafers was coated in thick S1813 photoresist and hard baked. The individual chips were diced and separated from each other. The sacrificial  $\text{SiO}_2$  layer beneath the  $\text{Si}_x\text{N}_y$  was then wet etched from the back side using 6:1 BHF for 8 min and the photoresist layer on the front side was removed in acetone. The individual chips were dried and inspected under an optical microscope to confirm the integrity of the membrane and of the alignment markers on it. The membrane area now consisted of a 50 nm thick  $\text{Si}_x\text{N}_y$  layer with a 5 nm Cr / 100 nm Au metal stack [Fig. 1(c)]. These 15 mm x 15 mm individual chips were now ready for FIB milling [Fig. 1(d)].

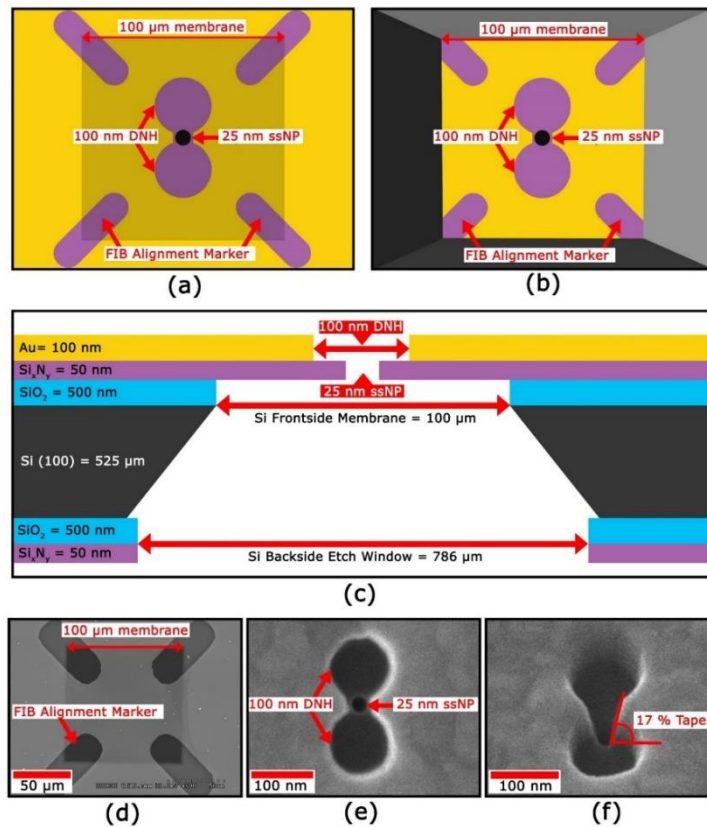


Fig. 1: (a) Front side view of SANE chip. (b) Back side view of SANE chip. (c) Cross-section of the SANE sensor chip. (d) SEM micrograph of front side of the SANE chip before FIB drilling. He ion microscope image of top view (e) and tilted view (f) of milled DNH with 17 % sidewall taper and a 25 nm ssNP drilled at its center.

The FIB milling on these individual chips was done using a mix of Ne and He GFIS focused ion beams (Carl Zeiss, ORION NanoFab, Peabody, MA). The Ga FIB or TEM beam could not be used due to the complex requirements of the dual layer design [Fig. 1(c)]. The dumbbell shape of the DNH was milled into the Au film (Critical Dimension = 25 nm) and the milling had to be stopped at the metal/dielectric interface.

The DNH shape was designed to have 15-20 % tapered edges [Fig. 1(f)], in line with a prior feature optimization study [43], converging towards the metal/dielectric interface. A Ne ion beam was used to mill the DNH shape in the Au/Cr metal stack (500 fA beam current, 25 kV acceleration voltage, 10  $\mu\text{m}$  aperture and 8.5 mm working distance). A beam dose of 0.2 – 0.225  $\text{nC}/\mu\text{m}^2$  was determined to be optimum to reach the Au/Cr –  $\text{Si}_x\text{N}_y$  interface. The secondary electron current was used in the nanopatterning visualization engine to determine when the dielectric interface was reached to terminate the Ne FIB milling. At that point, the beam was switched to He ions and a 25 nm circle was drilled through the suspended  $\text{Si}_x\text{N}_y$  membrane in the middle of the DNH shape (2 pA beam current, 30 kV acceleration voltage with 150  $\text{nC}/\mu\text{m}^2$  dose, 10  $\mu\text{m}$  aperture and 8.5 mm working distance). He FIB nanopore drilling through the  $\text{Si}_x\text{N}_y$  film was stopped when the secondary electron current suddenly decreased to almost zero [Fig. 1(e)].

## **Experimental Setup**

The beam from an 820 nm laser diode (L820P200, Thorlabs) was collimated to a 2 mm diameter and circularly polarized through a QWP (WPQ05M, Thorlab), followed by a Glan-Thompson linear polarizer (GTH10M, Thorlabs) for controlling the polarization of light incident on the chip. The light then passed through a tunable HWP (WPH05M, Thorlabs) to make the

direction of polarization perpendicular to the DNH's long axis to excite maximally wedge plasmons for trapping [46]. A downstream 4x beam expander (Newport) was used in combination with an 8 mm circular aperture (ID.1.0, Newport) to make the intensity profile of the cylindrical beam flatter. The beam then went through a periscope and into the back aperture of a 63x oil immersion objective lens and focused onto the front Au side of the SANE chip. The objective's focal spot was aligned with the DNH center by adjusting the piezoelectric stage controls until polarized light transmission was maximized. Light transmission through the FIB alignment markers was used as a first coarse step to find the DNH on the chip. The light transmitted through the chip's center and any leakage light scattering through alignment markers was collected by a condenser lens and focused onto a photodiode (PDA36A, Thorlabs).

Standard soft lithography techniques were used for fabrication of a flow cell that could house the SANE sensor chip with a cis and a trans chamber for the nanopore and to provide optical access to the DNH. The flow cell was made from polydimethylsiloxane (PDMS) mixed in a 10:1 ratio of polymer to initiator as prescribed by the manufacturer (Dow Corning). This mixture was degassed to remove air bubbles and subsequent fabrication was performed in three steps. In the first step, a flat PDMS slab of 2 mm thickness was created by adding the bubble-free mixture to a cavity created on a polished side of a silicon wafer and curing it on a hotplate at 100°C for 10 min. After peeling this PDMS slab, a pattern was cut into it consisting of a 10 mm square opening at the center and a 2 mm wide rectangular channel connecting it to another 10 mm square opening towards the end of the slab [Fig. 2(a)]. The PDMS slab was bonded onto a 3 in x 2 in glass slide using oxygen plasma (Electro-Technic). In the second step, the SANE sensor was placed over the central square opening using a double-sided tape (3M) sealing the square opening underneath and creating the trans chamber of the nanopore. Another flat PDMS slab of 3 mm thickness was created

using the same procedure and a hollow rectangle was cut and placed over the square opening at the end of the slab using double-sided tape [Fig. 2(b)]. This secondary chamber acted as a reservoir holding enough ionic solution to keep the bottom of the nanopore always wet. The rectangular channel connecting these openings was also covered with the same double-sided tape to completely seal the flow path. In the third step, a 1-inch coverslip of 170  $\mu\text{m}$  thickness (VWR) was plasma-bonded onto a very thin PDMS layer of 200  $\mu\text{m}$  thickness, with a square opening of

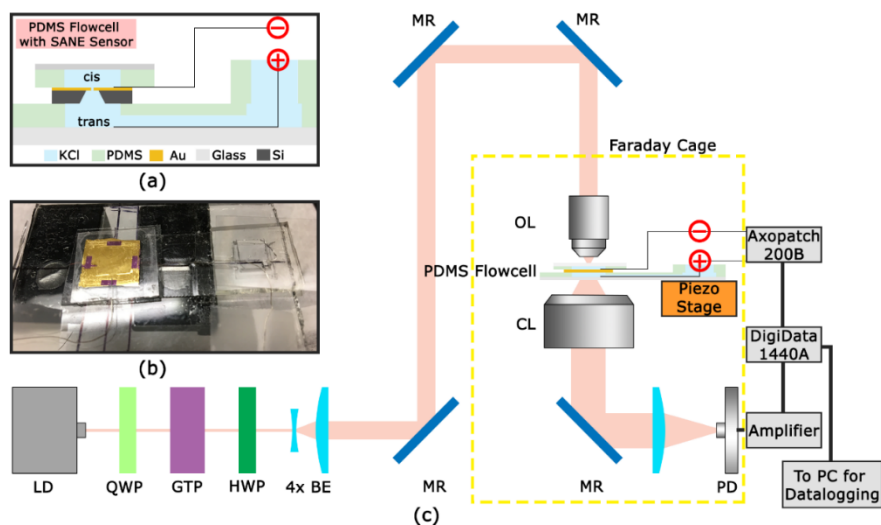


Fig. 2: (a) PDMS flow cell cross-sectional view with SANE sensor. (b) Image of prepared PDMS flow cell with SANE chip ready for placement on piezo-controlled stage. (c) Complete optical setup with PDMS flow cell placement and measurement instruments. LD: Laser Diode, QWP: Quarter Wave Plate, GTP: Glan-Thompson Polarizer, HWP: Half Wave Plate, 4x BE: 4x Beam Expander, MR: Mirror, OL: Carl-Zeiss 1.3 N.A. 63x Objective Lens, CL: Condenser Lens, PD: Photodiode.

10 mm cut through the center of this layer to form a cis chamber over the SANE sensor. An additional 1 mm wide gap was cut at the edge of this PDMS layer to allow introduction of analyte into the cis chamber along with the cis chamber electrode. Subsequently, the trans side was gently

filled with ionic solution using Teflon tubing connected to a syringe up to the brim of the 3 mm PDMS reservoir wall. To complete the electrical path, the trans side electrode was introduced through the reservoir wall and pushed along the rectangular channel until its tip was located right below the sensor.

Finally, the secondary reservoir was topped with a coverslip to confine the ionic solution within the flow cell. This flow cell was attached to a holder and the assembly was screwed onto a piezo-controlled translation stage (MDT6938, Thorlabs) immediately below the objective lens. The prepared PDMS flow cell with the SANE chip is shown in Fig. 2(b).

To implement electrical sensing the cis and trans chamber Ag/AgCl electrodes were attached to the Axon Headstage (CV 203BU) of the Axon Axopatch 200B patch clamp in voltage clamp mode. A custom-made Faraday cage using copper wire mesh (PSY405, Thorlabs) was installed to cover the entire optical assembly and shield the PDMS flow cell from low-frequency electromagnetic noise during highly sensitive patch clamp ionic current recordings. Subsequently, the nanopore was first tested for wetting. If the nanopore was blocked, an alternating  $\pm 5$  volts square wave was applied to the two electrodes for 60 sec to unblock the nanopore through electrophoretic pressure. After wetting, the trans side reservoir of the PDMS flow cell was filled with 7.4 pH 1M KCl solution and the cis reservoir was filled with 200 pM solution of  $20 \pm 4$  nm silica nanoparticles (MEL0010, NanoComposix, zeta potential = -40 mV) suspended in the same solution. Au nanoparticles (C11-20-TM-DIH-50, Nanopartz, zeta potential = -15 mV) of the same size and concentration as silica were also used to fill the cis reservoir in separate experiments. A 2 nm thick methyl polymer coating on the Au nanoparticles helped maintain their stability in KCl solution. The PDMS flow cell was attached to the piezo-controlled stage using screws and the laser beam was aligned to the DNH center as described above. A 250 mV bias was applied through the

patch clamp in voltage clamp mode. The photodiode and Axopatch 200B signals were both sent through an Axon Digidata 1440 ADC to a PC for recording and data analysis in Axon Clampfit 10.6 software. The complete experimental setup schematic is shown in Fig. 2(c). In subsequent data analyses the coefficient of variation was defined as the ratio of standard deviation to the signal mean value and the ionic current translocation time and signal to noise ratio (SNR) during translocation were defined as described previously [53, 54].

## RESULTS

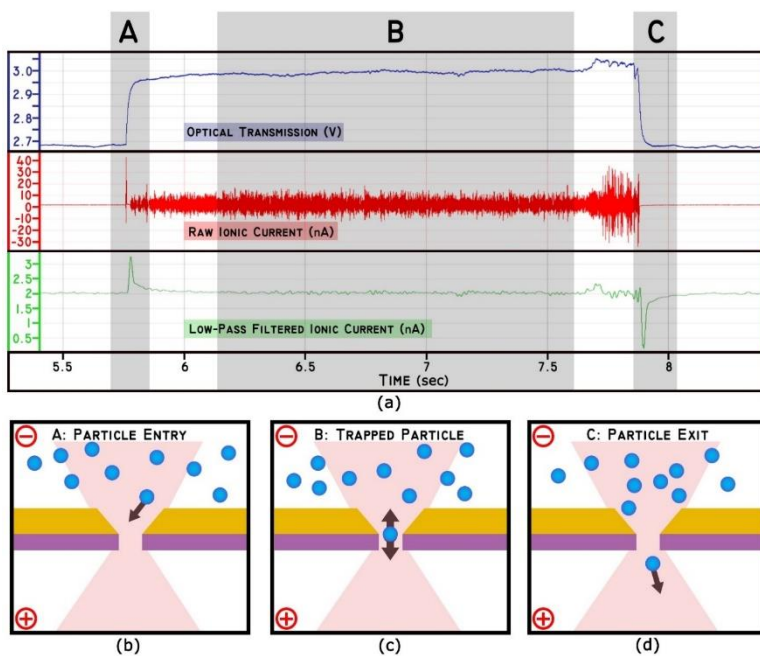


Fig. 3: (a) Plots of simultaneously recorded optical transmission (top, blue; V), raw ionic current (middle, red; nA) and 20 Hz low-pass filtered ionic current [bottom, green; nA) versus time (sec) for the single 20 nm silica nanoparticle trapped in the SANE sensor. Physical interpretation schematics for the signals recorded within gray-shaded regions A, B and C are shown in panels (b), (c) and (d), respectively. (b) Region A: Negatively charged nanoparticle entering

the DNH-ssNP under applied bias. (c) Region B: Nanoparticle trapped and bobbing inside the DNH near the ssNP mouth. (d) Region C: Nanoparticle exiting the optical trap after the electrophoretic force dominates translocation.

Fig. 3 shows the first proof of principle measurements with the SANE sensor that demonstrate multi-second trapping of a single 20 nm silica nanoparticle with concurrent electrophoretic measurements through the nanopore at the center of the DNH. When the 20 nm nanoparticle was trapped by the DNH, a step increase of 11 % in optical transmission was seen due to dielectric loading of the trap [Fig. 3(a)]. Concurrently, high frequency transients were seen in the raw ionic current [Fig. 3(b)], registering a positive charge peak of 38 nA which was 19 times higher than the baseline nanopore current. These ionic current oscillations were likely caused by axial nanoparticle oscillations, which we will henceforth refer to as ‘bobbing’, in the nanopore vicinity due to opposing optical and electrical forces.

It is noteworthy that optical trapping enabled ionic current sensing of the nanoparticle for a few seconds, which is about four orders of magnitude longer than the typical current sensing times for nanoparticle translocation events through a nanopore alone.

The recorded raw ionic current was also filtered with a 20 Hz, low pass 8-pole Bessel filter in Axon Clampfit 10.6 to enable visualization of the nanoparticle movement effects on low frequency ionic current. A distinct positive peak of 26.2 ms was registered during charged nanoparticle entry in the DNH, when the trapping started [Fig. 3(a), Region A, green curve in third row]. The nanoparticle was bobbing inside the DNH trap for about 2.15 sec [Fig. 3(a), Region B] and the low-pass filtered ionic signal did not show any appreciable changes during that time. Towards the end of the trapping period, the amplitude of high frequency transients increased concurrently with a slight increase in optical transmission before the nanoparticle escaped and translocated through the nanopore [Fig. 3(a), Region C]. When the nanoparticle translocated across



the ssNP from the cis to the trans region, a characteristic negative ionic current pulse was seen (third row, green) due to nanopore blockage during translocation ( $1.79 \text{ nA}$ , translocation time  $22.3 \text{ ms}$ ) taking place concurrently with a drop in optical transmission decrease back to the baseline (first row, blue).

In addition to single trapping events, more complex multiple nanoparticle trapping events were recorded and analyzed as well. Fig. 4(a) provides a 1 min trace showing three such trapping events. The gray-shaded Region A in that figure highlights a two-nanoparticle trapping event, as deduced from the nearly doubled optical transmission amplitude compared to the trapping event in Region B ( $8.6 \pm 0.8 \%$  versus  $19.2 \pm 0.5 \%$ ). Frequency spectrum analysis of raw ionic current signals for Regions A and B is shown in Fig. 4(b). Interestingly, the peak of the frequency spectrum for Region A was found in the  $850 \text{ Hz}$  range whereas it was in the  $1\text{kHz}$  range for Region B. The latter had a remarkably similar power spectrum for the single nanoparticle trapping event described in Fig. 3 (frequency spectrum not shown for brevity). Furthermore, the frequency spectrum from a No-Trapping (NT) period is included for comparison in Fig. 4(b), demonstrating a plateau rather than a peak frequency and spectral amplitudes that were up to four orders of magnitude lower than those for trapping events. These spectral differences suggest the possibility of differentiating single versus double nanoparticle trapping events over background signals with the SANE sensor. A representative sequence of multiple nanoparticle trapping events is highlighted in Regions C and D of Fig. 4(a). Fig. 4(c) shows the power spectra of these Regions and compares them to the NT condition. The power spectrum of Region C with an amplitude peak at  $850 \text{ Hz}$  and a  $22.2 \pm 1.2 \%$  increase in optical transmission shows a two-nanoparticle trapping event. Optical transmission in region D was  $8.7 \pm 0.9 \%$  over baseline, indicating single nanoparticle trapping. However, the raw ionic current showed no high

frequency transients in Region D, making its frequency spectrum indistinguishable from the NT condition, even though optical transmission indicated single nanoparticle trapping. We hypothesize, that during this period the nanoparticle attained transient equilibrium in the DNH-ssNP trap and was not bobbing significantly. In Region E, another nanoparticle entered the trapping site, indicated by an increase in optical transmission to  $15.6 \pm 0.4 \%$  and shifted the ionic current fluctuation spectral peak from  $\sim 1\text{kHz}$  to  $850 \text{ Hz}$ . These observations are interpreted as the entry of an additional nanoparticle instigating bobbing for both nanoparticles inside the trap before these translocated through the nanopore.

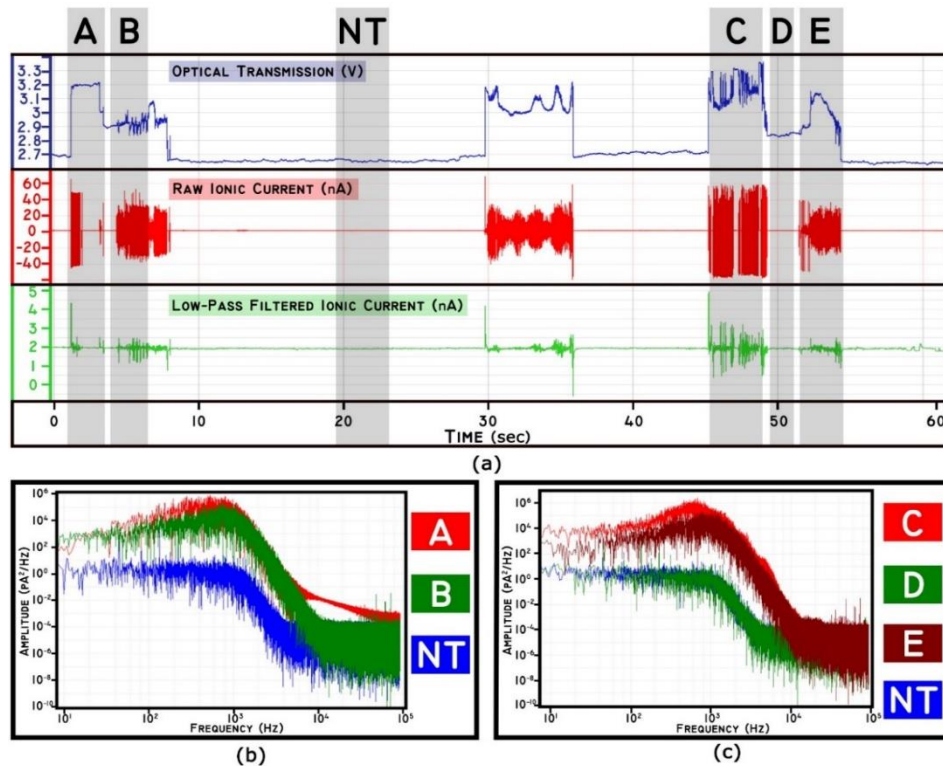


Fig 4: (a) Plots of simultaneously recorded optical transmission (top, blue; V), raw ionic current (middle, red; nA) and 20 Hz low-pass filtered ionic current (bottom, green; nA) versus time (sec) for a 1 min trace with three complex multi-particle trapping events. (b) Power spectrum analysis of the raw ionic current signal for Regions A, B and a No-Trapping (NT) region. (c) Power spectrum analysis of raw ionic current signal for Regions C, D, and E including NT for reference.

To further investigate the influence of charge of individually trapped nanoparticles on SANE sensor measurements, 20 nm methyl functionalized Au nanoparticles were also measured under identical experimental conditions to the silica ones, so as to make comparisons. Fig. 5 shows the trapping event and electrophoretic movement of a single Au nanoparticle. When the nanoparticle was pushed towards the DNH center by the electrophoretic force, its optical trapping caused a rise in optical transmission of 6%. Simultaneously, the raw ionic current through the nanopore registered a positive peak of 8.5 nA for 27.7 ms, as the particle entered the trap [Fig. 5, Region A]. Unlike the silica nanoparticles, the electrical high frequency transients during particle trapping were attenuated to very low levels. At the same time, the coefficient of variation of optical fluctuations during Au nanoparticle trapping reduced to 0.02% compared to the 0.11% seen for the silica nanoparticle fluctuations [Fig. 3, Region B].

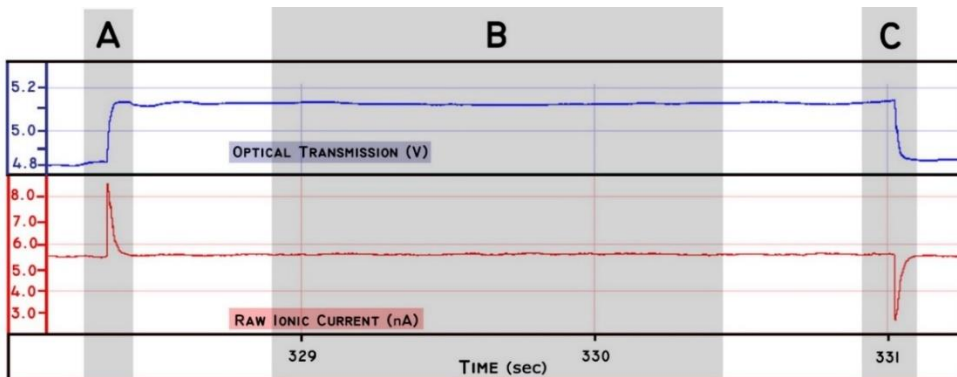


Fig. 5: (a) Plots of simultaneously recorded optical transmission (top, blue; V), raw ionic current (bottom, red; nA) versus time (sec) for the single 20 nm Au nanoparticle trapped in the SANE sensor. Region A: Au nanoparticle entering the DNH-ssNP under applied bias. (c) Region B: Nanoparticle trapped inside the DNH near the ssNP mouth. (d) Region C: Nanoparticle exiting the optical trap after the electrophoretic force dominates translocation.

Typical Au nanoparticle trapping durations were a few seconds, 3.28 sec in [Fig. 5, Region B]. Subsequently they escaped trapping and translocated through the nanopore [Fig. 5, Region C]. A

negative ionic current pulse was measured during translocation, while the Au nanoparticle blocked the nanopore (2.64 nA, translocation time 19.1 ms). At the same time the optical transmission dropped back to the baseline.

Comparisons of SANE sensor measurement characteristics for Au versus silica nanoparticles highlighted a number of differences: (1) Au nanoparticles had a lower optical step increase from baseline compared to silica by a factor of  $2.9 \pm 0.4$  (2) The coefficient of variation for the optical signal during trapping was lower than silica by a factor of  $148.3 \pm 2.4$ . (3) After applying the same 20 Hz low pass 8-pole Bessel filtering to the ionic current during Au nanoparticle optical trapping, the coefficient of variation was lower than silica by a factor of  $5.5 \pm 1.2$ . (4) Translocation times were slower for Au nanoparticles by a factor of  $0.87 \pm 0.05$ . (5) The ionic current during Au nanoparticle translocation was higher than silica nanoparticles by a factor of  $1.7 \pm 0.3$ , resulting in an SNR of  $\sim 72$  compared to  $\sim 43$  for silica. These differences are considered in the Discussion section below.

## DISCUSSION

The dynamics of a nanoparticle in electrophoretic flow through a ssNP have been studied in detail [1]. In our study, the nanoparticle translocation dynamics changed drastically due the SIBA-actuated trapping of the nanoparticle in the DNH nanocavity. The trapping force acting on the nanoparticle remained balanced for several seconds, e.g. 2.15 sec for the particle shown in Fig. 3(a). Furthermore, the characteristic negative peak due to ionic current blockage lasted 22.3 ms for the single 20 nm nanoparticle translocation event shown in Fig. 3(d), which is much longer than the  $200 \pm 30 \mu\text{s}$  translocation times of similar nanoparticles in nanopores [55]. Therefore, optical trapping enabled ionic current recordings in the vicinity of the nanopore that were about

four orders of magnitude longer than typical translocation times for similar nanoparticles and also slowed down their translocation through the nanopore.

The greatly extended ionic current recording times also revealed a newly observed high frequency charge transient phenomenon for silica nanoparticles. We hypothesize that this originates from bobbing of the nanoparticle through the mouth of the nanopore due to the competing electrophoretic and SIBA forces. These high frequency transients were seen both for single [Fig. 3(a)] and multiple [Fig. 4(a)] nanoparticle trapping. At the end of the single trapping event seen in Fig. 3(a) (Region D), the nanoparticle started bobbing, which resulted in larger amplitudes for both ionic current and optical transmission. These observations suggest that the electrophoretic force led the nanoparticle to translocate through the ssNP.

It was observed that the peak amplitude of high frequency transients for raw ionic current decreased as dielectric loading in the trap increased from a one (~1kHz) to two (~850 Hz) silica nanoparticles. Therefore, frequency spectrum analysis of the SANE sensor's raw ionic current shows promise for distinguishing single nanoparticles from more complex trapping events. In addition to periods of high frequency ionic current transients, instances of trapping with relatively quiet ionic current signals were also observed. For example, the single nanoparticle trapping in Fig. 4(a) (Region D), with similar optical transmission amplitude as Region B did not show any high frequency transients. We hypothesize that this behavior was a result of transient equilibrium while the single nanoparticle was blocking the pore and temporarily stopped bobbing. However, when another nanoparticle entered the DNH trap this equilibrium was disturbed and the high frequency charge transients returned with a peak frequency of 850 Hz (Region E) in the raw ionic current trace [Fig. 4(c)]. The latter behavior was consistent with two-nanoparticle trapping. The subsequent gradual decrease in optical transmission and low-amplitude spikes in the low-passed

ionic current in Region E suggest that the two nanoparticles translocated through the nanopore sequentially and not as a single unit. These findings indicate that the SANE sensor can provide information on the dynamics of single and two-nanoparticle dynamics inside the optical trap.

Experiments were performed subsequently with Au nanoparticles of the same size under identical experimental conditions to silica to compare the effect of nanoparticle charge on SANE measurements. The lower change in optical transmission compared to silica when Au nanoparticles entered the optical trap could be attributed to differences in optical interaction cross-sections. Although the scattering cross-section of 20 nm Au nanoparticles in water is ~59% higher than that of the silica ones at 820 nm, the absorption cross-section is about 4 times larger than scattering for the Au nanoparticles [56]. In contrast, silica nanoparticles have negligible absorption. The reduced coefficient of variation in optical signal during Au nanoparticle trapping is therefore expected to be at least in part due to increased absorption. In addition, Au is a conductor and the applied voltage bias across the sensor would exert an electric field force on the Au nanoparticles, which would push towards a preferential direction in nanoparticle displacement. Indirect evidence for the existence of an electric field force was seen in the shorter translocation times of Au nanoparticles even though they had a lower zeta potential relative to the silica nanoparticles. In addition to the reduced translocation time, the observed increase in ionic current amplitude during translocation for Au nanoparticles is consistent with a zeta potential based interpretation [57-59] and resulted in the observed increase in SNR compared to silica. Finally, it was evident that the raw ionic current during Au nanoparticle trapping [Fig. 5, bottom, red, Region B] had significantly reduced high frequency charge transients compared to silica. Although Au nanoparticles had reduced displacement amplitudes within the trap, as discussed above, it is hypothesized that charge fluctuations around the nanoparticle played a major role. Since Au is conducting, it is possible that

charges within the nanoparticle would move around to cancel out charge fluctuations in its immediate vicinity.

Finally, it is worth pointing out the possibility of using calibrated SANE sensor measurements in future work to estimate the number of total surface charges around unknown analytes. The Grahame equation [60] can be used to calculate total surface charge using the experimentally determined zeta potential of the analytes by the SANE sensor. The zeta potential can be deduced from the electrophoretic mobility of the analytes, which entails measurement of their translocation time and knowledge of the applied bias and nanopore size [61]. Concurrent optical measurements of analyte radius can be used to determine which approximation of Smoluchowski's theory is appropriate for deducing the zeta potential [62]. For experimental parameters relevant to this work the appropriate approximation is the Hückel equation, which would yield the zeta potential estimate for the analytes [63]. These considerations indicate the possibility of calibrating the SANE sensor's optical and ionic current signals in future work to estimate the charge around unknown analytes by direct measurement of their radius and electrophoretic mobility.

## **CONCLUSION**

We have demonstrated multi-second optical trapping of electrophoretically translocating nanoparticles through a ssNP. The competing electrophoretic and SIBA forces induced bobbing inside the optical trap that led to high frequency ionic current oscillations sensed through the nanopore. Frequency analysis of these oscillations for silica nanoparticles demonstrated the possibility of distinguishing between one versus two nanoparticles inside the trap. Furthermore, the SANE chip's bimodal sensing ability showcased the possibility of using it as a tool to estimate

the charge around a nanoparticle. Different SANE sensors were used to collect the measurements for this work which demonstrated the repeatability of this approach. In future work, we plan to apply this sensor to study interactions between biological molecules. Our longer term vision is to scale up towards a multiplexed SANE array within a microfluidic channel to facilitate parallel detection of biomolecular interactions to help resolve their heterogeneity in solution.

## ACKNOWLEDGEMENTS

We are grateful to Mr. Soeren Eyhusen and Mr. Chuong Huynh for allowing access and providing technical guidance on focused ion beam milling at the Zeiss ORION NanoFab facility in Peabody, MA. We are also grateful to Mr. Huan (Mick) Nguyen, Mr. Dennis Bueno and Mr. Richard K. Chambers for their invaluable technical guidance on fabrication at the Shimadzu Institute Nanotechnology Research Center, University of Texas at Arlington. Support for this work was provided through a Pilot Research Program for Interdisciplinary Collaboration funded by the Vice-President of Research Office of the University of Texas at Arlington.

## REFERENCES

- [1] Dekker C 2007 Solid-state nanopores *Nature nanotechnology* **2** 209
- [2] Yuan Z, Wang C, Yi X, Ni Z, Chen Y and Li T 2018 Solid-State Nanopore *Nanoscale research letters* **13** 56
- [3] Shi W, Friedman A K and Baker L A 2016 Nanopore sensing *Analytical chemistry* **89** 157-88
- [4] Butler T Z, Pavlenok M, Derrington I M, Niederweis M and Gundlach J H 2008 Single-molecule DNA detection with an engineered MspA protein nanopore *Proceedings of the National Academy of Sciences* **105** 20647-52
- [5] Harrell C C, Choi Y, Horne L P, Baker L A, Siwy Z S and Martin C R 2006 Resistive-pulse DNA detection with a conical nanopore sensor *Langmuir* **22** 10837-43



- [6] Fologea D, Gershow M, Ledden B, McNabb D S, Golovchenko J A and Li J 2005 Detecting single stranded DNA with a solid state nanopore *Nano letters* **5** 1905-9
- [7] Iqbal S M, Akin D and Bashir R 2007 Solid-state nanopore channels with DNA selectivity *Nature nanotechnology* **2** 243
- [8] Hasan M R, Mahmood M A I, Khanzada R R, Mansur N, Adnan A and Iqbale S M 2018 Molecular Dynamics Study of Protein Deformation through Solid-State Nanopore *Functional Nanostructures* **1** 107-13
- [9] Khan M S, Dosoky N S, Mustafa G, Patel D, Berdiev B and Williams J D 2017 Electrophysiology of Epithelial Sodium Channel (ENaC) Embedded in Supported Lipid Bilayer Using a Single Nanopore Chip *Langmuir* **33** 13680-8
- [10] Talaga D S and Li J 2009 Single-molecule protein unfolding in solid state nanopores *Journal of the American Chemical Society* **131** 9287-97
- [11] Nir I, Huttner D and Meller A 2015 Direct sensing and discrimination among Ubiquitin and Ubiquitin chains using solid-state nanopores *Biophysical journal* **108** 2340-9
- [12] Varongchayakul N, Huttner D, Grinstaff M W and Meller A 2018 Sensing Native Protein Solution Structures Using a Solid-state Nanopore: Unraveling the States of VEGF *Scientific reports* **8** 1017
- [13] Freedman K J, Haq S R, Edel J B, Jemth P and Kim M J 2013 Single molecule unfolding and stretching of protein domains inside a solid-state nanopore by electric field *Scientific reports* **3** 1638
- [14] Japrun D, Dogan J, Freedman K J, Nadzeyka A, Bauerdick S, Albrecht T, Kim M J, Jemth P and Edel J B 2013 Single-molecule studies of intrinsically disordered proteins using solid-state nanopores *Analytical chemistry* **85** 2449-56
- [15] Wanunu M, Dadosh T, Ray V, Jin J, McReynolds L and Drndić M 2010 Rapid electronic detection of probe-specific microRNAs using thin nanopore sensors *Nature nanotechnology* **5** 807
- [16] Venkatesan B M and Bashir R 2011 Nanopore sensors for nucleic acid analysis *Nature nanotechnology* **6** 615
- [17] Gu L-Q, Wanunu M, Wang M X, McReynolds L and Wang Y 2012 Detection of miRNAs with a nanopore single-molecule counter *Expert review of molecular diagnostics* **12** 573-84

- [18] Zahid O K, Wang F, Ruzicka J A, Taylor E W and Hall A R 2016 Sequence-specific recognition of microRNAs and other short nucleic acids with solid-state nanopores *Nano letters* **16** 2033-9
- [19] Ali W, Raza M U, Mahmood M A I, Allen P B, Hall A R, Wan Y and Iqbal S M 2016 Differentiation of Specific Cancer Biomarkers with Solid-state Nanopores *Functional Nanostructures* **1** 26-34
- [20] Deamer D, Akeson M and Branton D 2016 Three decades of nanopore sequencing *Nature biotechnology* **34** 518
- [21] Steinbock L and Radenovic A 2015 The emergence of nanopores in next-generation sequencing *Nanotechnology* **26** 074003
- [22] Khan M S, Dosoky N S, Berdiev B K and Williams J D 2016 Electrochemical impedance spectroscopy for black lipid membranes fused with channel protein supported on solid-state nanopore *European Biophysics Journal* **45** 843-52
- [23] Manrao E A, Derrington I M, Laszlo A H, Langford K W, Hopper M K, Gillgren N, Pavlenok M, Niederweis M and Gundlach J H 2012 Reading DNA at single-nucleotide resolution with a mutant MspA nanopore and phi29 DNA polymerase *Nature biotechnology* **30** 349
- [24] Li J, Stein D, McMullan C, Branton D, Aziz M J and Golovchenko J A 2001 Ion-beam sculpting at nanometre length scales *Nature* **412** 166
- [25] Storm A, Chen J, Ling X, Zandbergen H and Dekker C 2003 Fabrication of solid-state nanopores with single-nanometre precision *Nature materials* **2** 537
- [26] Lo C J, Aref T and Bezryadin A 2006 Fabrication of symmetric sub-5 nm nanopores using focused ion and electron beams *Nanotechnology* **17** 3264
- [27] Gierak J, Mailly D, Hawkes P, Jede R, Bruchhaus L, Bardotti L, Prevel B, Mélinon P, Perez A and Hyndman R 2005 Exploration of the ultimate patterning potential achievable with high resolution focused ion beams *Applied Physics A* **80** 187-94
- [28] Emmrich D, Beyer A, Nadzeyka A, Bauerdick S, Meyer J, Kotakoski J and Götzhäuser A 2016 Nanopore fabrication and characterization by helium ion microscopy *Applied Physics Letters* **108** 163103
- [29] Raza M U, Saleem S, Ali W and Iqbal S M 2016 Crosstalk between adjacent nanopores in a solid-state membrane array for multi-analyte high-throughput biomolecule detection *Journal of Applied Physics* **120** 064701

- [30] Gilboa T and Meller A 2015 Optical sensing and analyte manipulation in solid-state nanopores *Analyst* **140** 4733-47
- [31] Ivanov A P, Instuli E, McGilvery C M, Baldwin G, McComb D W, Albrecht T and Edel J B 2010 DNA tunneling detector embedded in a nanopore *Nano letters* **11** 279-85
- [32] Miles B N, Ivanov A P, Wilson K A, Doğan F, Japrun D and Edel J B 2013 Single molecule sensing with solid-state nanopores: novel materials, methods, and applications *Chemical Society Reviews* **42** 15-28
- [33] Keyser U F, Koeleman B N, Van Dorp S, Krapf D, Smeets R M, Lemay S G, Dekker N H and Dekker C 2006 Direct force measurements on DNA in a solid-state nanopore *Nature Physics* **2** 473
- [34] Keyser U, Van der Does J, Dekker C and Dekker N 2006 Optical tweezers for force measurements on DNA in nanopores *Review of Scientific Instruments* **77** 105105
- [35] Di Fiori N, Squires A, Bar D, Gilboa T, Moustakas T D and Meller A 2013 Optoelectronic control of surface charge and translocation dynamics in solid-state nanopores *Nature nanotechnology* **8** 946
- [36] Nicoli F, Verschueren D, Klein M, Dekker C and Jonsson M P 2014 DNA translocations through solid-state plasmonic nanopores *Nano letters* **14** 6917-25
- [37] Li Y, Nicoli F, Chen C, Lagae L, Groeseneken G, Stakenborg T, Zandbergen H W, Dekker C, Van Dorpe P and Jonsson M P 2014 Photoresistance switching of plasmonic nanopores *Nano letters* **15** 776-82
- [38] Assad O N, Gilboa T, Spitzberg J, Juhasz M, Weinhold E and Meller A 2017 Light-Enhancing Plasmonic-Nanopore Biosensor for Superior Single-Molecule Detection *Advanced Materials* **29**
- [39] Juan M L, Gordon R, Pang Y, Eftekhari F and Quidant R 2009 Self-induced back-action optical trapping of dielectric nanoparticles *Nature Physics* **5** 915
- [40] Al Balushi A A, Kotnala A, Wheaton S, Gelfand R M, Rajashekara Y and Gordon R 2015 Label-free free-solution nanoaperture optical tweezers for single molecule protein studies *Analyst* **140** 4760-78
- [41] Kumar L K S and Gordon R 2006 Overlapping double-hole nanostructure in a metal film for localized field enhancement *IEEE Journal of selected topics in quantum electronics* **12** 1228-32
- [42] Kumar L, Lesuffleur A, Hughes M and Gordon R 2006 Double nanohole apex-enhanced transmission in metal films *Applied Physics B* **84** 25

- [43] Ghorbanzadeh M, Jones S, Moravvej-Farshi M K and Gordon R 2017 Improvement of Sensing and Trapping Efficiency of Double Nanohole Apertures via Enhancing the Wedge Plasmon Polariton Modes with Tapered Cusps *ACS Photonics* **4** 1108-13
- [44] Mestres P, Berthelot J, Aćimović S S and Quidant R 2016 Unraveling the optomechanical nature of plasmonic trapping *Light: Science & Applications* **5** e16092
- [45] Pang Y and Gordon R 2011 Optical trapping of 12 nm dielectric spheres using double-nanoholes in a gold film *Nano letters* **11** 3763-7
- [46] Kotnala A, DePaoli D and Gordon R 2013 Sensing nanoparticles using a double nanohole optical trap *Lab on a Chip* **13** 4142-6
- [47] Kotnala A and Gordon R 2014 Quantification of high-efficiency trapping of nanoparticles in a double nanohole optical tweezer *Nano letters* **14** 853-6
- [48] Pang Y and Gordon R 2011 Optical trapping of a single protein *Nano letters* **12** 402-6
- [49] Al Balushi A A, Zehtabi-Oskuie A and Gordon R 2013 Observing single protein binding by optical transmission through a double nanohole aperture in a metal film *Biomedical optics express* **4** 1504-11
- [50] Al Balushi A A and Gordon R 2014 Label-free free-solution single-molecule protein–small molecule interaction observed by double-nanohole plasmonic trapping *ACS Photonics* **1** 389-93
- [51] Al Balushi A A and Gordon R 2014 A label-free untethered approach to single-molecule protein binding kinetics *Nano letters* **14** 5787-91
- [52] Wheaton S and Gordon R 2015 Molecular weight characterization of single globular proteins using optical nanotweezers *Analyst* **140** 4799-803
- [53] Plesa C and Dekker C 2015 Data analysis methods for solid-state nanopores *Nanotechnology* **26** 084003
- [54] Smeets R M, Keyser U F, Dekker N H and Dekker C 2008 Noise in solid-state nanopores *Proceedings of the National Academy of Sciences* **105** 417-21
- [55] Lan W-J, Holden D A, Zhang B and White H S 2011 Nanoparticle transport in conical-shaped nanopores *Analytical chemistry* **83** 3840-7
- [56] Shi Y, Xiong S, Chin L, Zhang J, Ser W, Wu J, Chen T, Yang Z, Hao Y and Liu A 2017 Determination of size and refractive index of single gold nanoparticles using an optofluidic chip *AIP Advances* **7** 095024

- [57] Kejian D, Weimin S, Haiyan Z, Xianglei P and Honggang H 2009 Dependence of zeta potential on polyelectrolyte moving through a solid-state nanopore *Applied Physics Letters* **94** 014101
- [58] Luan B, Stolovitzky G and Martyna G 2012 Slowing and controlling the translocation of DNA in a solid-state nanopore *Nanoscale* **4** 1068-77
- [59] Firnkes M, Pedone D, Knezevic J, Doblinger M and Rant U 2010 Electrically facilitated translocations of proteins through silicon nitride nanopores: conjoint and competitive action of diffusion, electrophoresis, and electroosmosis *Nano letters* **10** 2162-7
- [60] Guan W, Li S X and Reed M A 2014 Voltage gated ion and molecule transport in engineered nanochannels: theory, fabrication and applications *Nanotechnology* **25** 122001
- [61] Arjmandi N, Van Roy W, Lagae L and Borghs G 2012 Measuring the electric charge and zeta potential of nanometer-sized objects using pyramidal-shaped nanopores *Analytical chemistry* **84** 8490-6
- [62] Kim K-M, Kim H M, Lee W-J, Lee C-W, Kim T-i, Lee J-K, Jeong J, Paek S-M and Oh J-M 2014 Surface treatment of silica nanoparticles for stable and charge-controlled colloidal silica *International journal of nanomedicine* **9** 29
- [63] Bhattacharjee S 2016 DLS and zeta potential—What they are and what they are not? *Journal of Controlled Release* **235** 337-51

## CHAPTER 3

# DETECTION OF SPECIFIC ANTIBODY-LIGAND INTERACTIONS WITH A SELF-INDUCED BACK-ACTION ACTUATED NANOPORE ELECTROPHORESIS (SANE) SENSOR.

Sai Santosh Sasank Peri <sup>1</sup>, Manoj Kumar Sabnani <sup>3</sup>, Muhammad Usman Raza <sup>1</sup>, Soroush Ghaffari <sup>3</sup>, Susanne Gimlin <sup>4</sup>, Debra Wawro Weidanz <sup>4</sup>, Jung Soo Lee <sup>5</sup>, Min Jun Kim <sup>5</sup>,  
Jon Weidanz <sup>3</sup>, George Alexandrakis <sup>2,#</sup>

<sup>1</sup> Department of Electrical Engineering, University of Texas at Arlington, Arlington, TX, USA

<sup>2</sup> Department of Bioengineering, University of Texas at Arlington, Arlington, TX, USA

<sup>3</sup> Department of Biology, University of Texas at Arlington, Arlington, TX, USA

<sup>4</sup> Resonant Sensors Incorporated (RSI), Arlington, TX, USA

<sup>5</sup> Department of Mechanical Engineering, Southern Methodist University, Dallas, TX, USA

#Email: galex@uta.edu

In preparation for publication. Used with permission from Manoj Kumar Sabnani, Muhammad Usman Raza, Soroush Ghaffari, Susanne Gimlin, Debra Wawro Weidanz, Jung Soo Lee, Min Jun Kim, Jon Weidanz, and George Alexandrakis.

## ABSTRACT

Recent advances in plasmonic nanopore technologies have enabled the use of concurrently acquired bimodal optical-electrical data for improved quantification of molecular interactions. This work presents the use of a new plasmonic nanosensor employing Self-Induced Back-Action (SIBA) for optical trapping to enable SIBA-Actuated Nanopore Electrophoresis (SANE) for quantifying antibody-ligand interactions. T-cell receptor-like antibodies (TCRmAbs) engineered to target peptide-presenting Major Histocompatibility Complex (pMHC) ligands, representing a model of target ligands presented on the surface of cancer cells, were used to test the SANE sensor's ability to identify specific antibody-ligand binding. Cancer-irrelevant TCRmAbs targeting the same pMHCs were also tested as a control. It was found that the sensor could provide bimodal molecular signatures that could differentiate between antibody, ligand and the complexes that they formed, as well as distinguish between specific and non-specific interactions. Furthermore, the results suggested an interesting phenomenon of increased antibody-ligand complex concentrations near the SANE sensor compared to bulk solution conditions. A possible physical mechanism and potential advantages for the sensor's ability to augment complex formation at concentrations lower than the value of the free solution equilibrium binding constant ( $K_D$ ) are discussed.

## INTRODUCTION

Single molecule detection methods can identify unique biophysical signatures enabling the study of molecular interactions at a level of detail that is often lost by bulk solution interaction analysis methods, such as surface plasmon resonance (SPR) and ELISA [1]. The underlying physical principles of current single molecule detection methods include chemical [2-4], mechanical [5-7], electrical [8-10] and optical [11-16] mechanisms. In recent years, much research effort has been focused on the quantification of electrical molecular signatures by use of solid-state nanopore technology [17, 18] and optical signatures via subwavelength optical trapping [19-22] as a facile means of characterizing molecular interactions.

Solid-state nanopores are drilled by focused ion beam (FIB) [18] or transmission electron microscopy (TEM) [23] through synthetic membranes of nanometer (nm) thickness. These nm-size pores are sandwiched between two compartments filled with electrolyte solution where analytes are driven between compartments through the nanopore by an applied electrical bias [17]. The translocating molecules or molecular complexes obstruct ion flow by displacing charges while translocating through the nanopore. The resulting transient changes in nanopore current depend on analyte size [24], volume [25] and surface charge [26] and are often quantified as current spike amplitude and molecular translocation time [27]. These ionic current metrics are used as molecular signatures for the characterization of single molecules, such as proteins [28, 29] and DNA [30, 31], and their interactions [32-34].

Subwavelength optical sensing methods for single molecule studies rely on confinement of the focused light waves by nanoapertures into intensity hotspots that enable molecular trapping [35]. Although nanoaperture sensing methods are highly sensitive, their throughput is limited



compared to nanopore technologies due to long optical trapping times [22] and diffusion-limited time-to-trap intervals of increasing duration with decreasing analyte concentration [21]. Integration of electrical nanopore with optical nanoaperture technologies could help improve the throughput limitations of optical sensing while allowing detection of bimodal optical-electrical analyte signatures for improved characterization of molecular interactions. Efforts have been made in that direction with the combination of nanopore sensing with gold (Au) bowtie [36] and nanowell [37] structures, where localized plasmonic heating was used to improve convective flow that facilitated nanopore throughput. In other recently published work, bowtie shapes were drilled through consecutive layers of Au and silicon nitride (SiN) to create arrays of inverted bowtie plasmonic nanopores [38-40]. The advantage of inverted structures was that the surrounding Au layer could conduct away efficiently any optically-induced heating, which suppressed the creation of convective flow, but enabled optical trapping and extended measurement times [41].

In our previous work, we reported on a new optical-electrical nanosensor composed of a classical circular nanopore placed at the narrowest point of an Au double nanohole (DNH) structure [42]. This plasmonic nanosensor utilized self-induced back action (SIBA) to effect optical trapping immediately over the nanopore and was coined as the SIBA-induced actuated nanopore electrophoresis (SANE) sensor [42]. Neon (Ne) ion FIB was used to create tapered Au walls at the center of the DNH structure for optimal plasmon excitation [ref], while a nanopore was drilled by Helium (He) ion FIB at the center of this wedge structure through the underlying SiN layer. The SANE sensor was used to demonstrate optical trapping of dielectric (silica) and metal (Au) nanoparticles with concurrent electrical signal acquisition, bobbing of nanoparticles inside the trap due to opposing optical and electrical forces, and extension of translocation times

by up to four orders of magnitude compared to nanopore sensing alone due to slowing down from the optical trap [42].

This work goes beyond nanoparticle trapping to demonstrate the feasibility of using the SANE sensor for the identification of antibodies, their ligands and the complexes they form, while also distinguishing between specific and non-specific binding. Importantly, the proteins used in this proof-of-principle study are of biological relevance, representing a simplified free-solution model of peptide-presenting Major Histocompatibility Complex (pMHC) ligand [43-45] interactions with T-cell receptor-like monoclonal antibodies (TCRmAbs) [46, 47]. When deployed *in vivo*, TCRmAbs could help elicit a systemic immune response against cancer cells presenting specific pMHCs that are not presented by normal cells, thus presenting a possible approach to cancer immunotherapy [43-47]. This work tested the ability of the SANE sensor to distinguish between specific binding for a TCRmAb, engineered to target with high affinity (nM) a cancer-relevant pMHC, and the non-specific binding of a cancer-irrelevant TCRmAb to the same pMHC ligand. It is demonstrated that the SANE sensor enabled identification of formed complexes with different bimodal signatures from individual antibody and ligand signatures, as well as clear separation between specific and non-specific binding for these proteins. Interestingly, the SANE sensor also presented a significantly higher bound fraction for a range of concentrations below the known equilibrium binding constant ( $K_D$ ) for these particular antibody-ligand pairs compared to the bound fraction values measured by a commercial binding assay. The possible reasons for the observed difference are discussed and suggest the presence of a physical mechanism enabling more frequent protein-ligand interactions near the SANE sensor compared to bulk solution conditions. The existence of such an analyte-concentrating mechanism could be beneficial in the future for screening assays where antibodies or target ligands are in limited supply, as is often the case for

TCRmAbs that are time-consuming and expensive to make, or pMHCs that in a clinical scenario would be isolated from tissue biopsy.

## **MATERIALS AND METHODS**

### **SANE Sensor Fabrication**

The detailed fabrication procedure for the SANE sensor has been reported previously [42]. Briefly, sensors were fabricated on clean double side polished 4-inch silicon (Si) wafers (100 orientation) with a 500 nm silicon dioxide ( $\text{SiO}_2$ ) layer grown on top of it by thermal oxidation, followed by a 60 nm stoichiometric ( $\text{Si}_3\text{N}_4$ ), henceforth referred to as SiN, deposition by LPCVD. On one side of the wafer, marked as the backside, a grid pattern was created with a darkfield mask (positive photoresist S1813) to divide the wafer into 21, 15 mm X 15 mm individual chips. The mask also marked a square window of 786  $\mu\text{m}$  per side to etch away the SiN layer using Deep Reactive Ion Etching (DRIE) with tetrafluoromethane ( $\text{CF}_4$ ) gas at an etch rate of 1 nm/min. Then the underlying  $\text{SiO}_2$  layer was also etched away using a 6:1 buffered hydrofluoric (BHF) acid to reach the Si layer. Using a 22% tetramethylammonium hydroxide (TMAH) solution at 90°C, Si was anisotropically etched from the backside to create a 100  $\mu\text{m}$  window on which the overlying SiN/ $\text{SiO}_2$  layers from the front side of the wafer were left suspended. On the front side, 100 nm of gold (Au) were deposited with a 5 nm chromium (Cr) adhesion layer using e-beam evaporation method at a rate of 0.1 nm/sec. On this Au layer, alignment markers for FIB milling were patterned using photolithography and the Au and Cr layers over the marker positions were etched using the respective wet etchants (Sigma Aldrich). A thick layer of photoresist was applied as a protective layer and the wafer was then diced into individual chips. Each chip was then rinsed in acetone to

remove the photoresist layer and the backing SiO<sub>2</sub> layer was removed using 6:1 BHF. Individual chips were then placed inside a GFIS focused ion beam (Carl Zeiss, ORION Nanofab, Peabody, MA) where the DNH nanostructures through the Au layer using a Ne ion beam and the nanopore was milled through the silicon nitride membrane at the center of DNH structure using a He ion beam. Typical dimensions for the DNH structures used in this work were 100 nm diameter circles, with a 15-20% tapered edges converging towards a 25 nm diameter pore in the middle of the DNH.

## **Experimental Setup**

Figure 1 (c) shows a schematic of the experimental setup. A laser diode (820 nm, L820P200, Thorlabs) was collimated by an aspheric lens to form a 2 mm diameter linearly polarized beam that was made circularly polarized using a QWP (WPQ05M, Thorlabs). A Glan-Thompson linear polarizer (GTH10M, Thorlabs) combined with an adjustable HWP (WPH05M, Thorlabs) were then used to select the linear polarization that best aligned with the short axis of the DNH on each chip in order to excite wedge plasmons optimally. A 4x beam expander (Newport) was used to fill the back aperture of a 63x oil immersion objective lens (NA= 1.2, Zeiss C-Apochromat) through a periscope. Precise positioning of the focused laser beam to the center of the DNH was performed with the help of the alignment markers by adjusting the controls of a piezo stage (MDT6938, Thorlabs) holding the chip. The sensor was encased into a transparent PDMS flow cell fabricated as described in our previous work [42] with a coverslip on top, through which light was focused onto the center of the DNH on each chip. The transmitted light was collected using a condenser lens and the beam was subsequently focused onto a photodiode (PDA36A, Thorlabs).

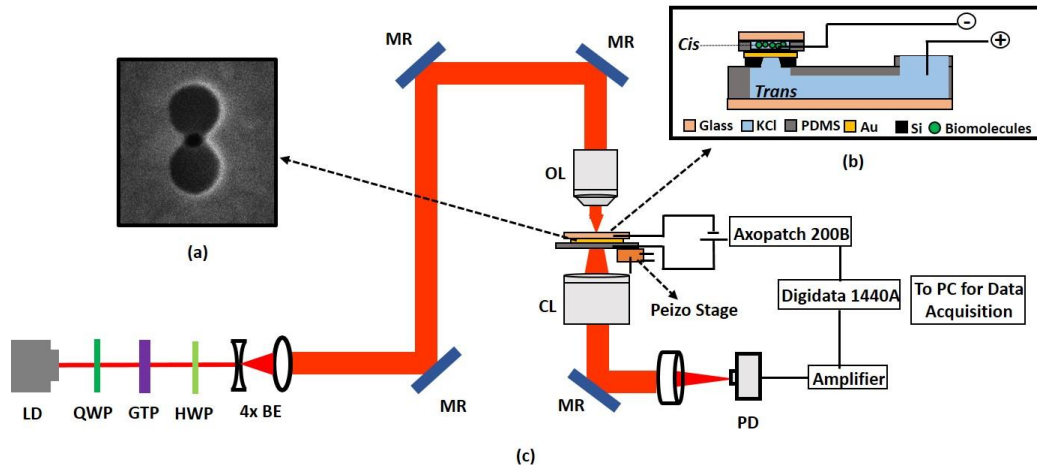


Fig 1: (a) Scanning electron microscope image of FIB milled DNH and nanopores structure on the metal-dielctric membrane. (b) PDMS flow cell cross-sectional view with SANE sensor. (c) Experimental setup with optical and electrical measurement instruments. LD: Laser Diode, QWP: Quarter Wave Plate, GTP: Glan-Thompson Polarizer, HWP: Half Wave Plate, 4x BE: 4x Beam Expander, MR: Mirror, OL: Carl-Zeiss 1.3 N.A. 63x Objective Lens, CL: Condenser Lens, PD: Photodiode.

The PDMS chip holder had a *cis* where protein solutions mixed in potassium chloride (KCl) were dispensed, while the *trans* side contained KCl solution only, of the same molarity. A voltage bias through the nanopore at the center of the DNH structure was enabled using two silver electrodes coated with silver chloride (Ag/AgCl), one placed in the *cis*, and the other in the *trans* chamber. These electrodes were connected to an Axon Headstage (CV 203BU) which was part of an Axon Axopatch 200B patch clamp amplifier and digitizer equipment (Molecular Devices) operating in voltage clamp mode to measure the change in resistance due to ionic current flow through the nanopore. To eliminate low-frequency electromagnetic noise during ionic current recordings a Faraday cage made of aluminum foil (Reynolds) was placed around the piezo-controlled stage. A 100 mV bias was applied across the nanopore through the Ag/AgCl electrodes for electrical measurements of protein translocation events. Any nanopore clogging during experiments was removed by using an AC +/-5V voltage for 60 sec across the nanopore.

Alternatively, a 7.4 pH 1 M KCl ionic solution with no analytes, was used to clear off any proteins clogging the nanopore by forcibly translocating them from *cis* to *trans* at voltages of 500-700 mV.

## Generation and Validation of Antigens and Antibodies

H-2D<sup>b</sup> RAH antigen (RAH) [48], a MHC class I allotype from C57Blk/6 (mouse strain) analogous to HLA (Human) consisted of a purified mouse MHC I heavy chain, H-2D<sup>b</sup> (35 kDa) and a human  $\beta$ 2m (13 kDa) light chain. The peptide RAHYNIVTF<sub>(49-57)</sub> (1 kDa) derived from human papilloma virus-16 (HPV) E7 protein (Genescript, Piscataway, NJ) was loaded onto the RAH antigen by *in vitro* refolding to create a peptide-presenting MHC (pMHC) antigen that was purified by size exclusion chromatography [49]. This HPV-induced RAHYNIVTF peptide is common in ovarian cancers and is known to induce a T-cell response when presented by H-2D<sup>b</sup> in the mouse [48, 50, 51]. To target the RAH antigen, monoclonal antibodies with T-cell Receptor-like specificity Anti-RAH (TCRmAbs) (150 kDa) were generated by classical B cell hybridoma technology [43]. These TCRmAbs specifically recognize RAH/ H-2D<sup>b</sup> pMHCs to form complexes [50]. A different TCRmAb specifically targeting a West Nile virus peptide (Anti-WNV) presented by H-2D<sup>b</sup> pMHC [52] was used as negative control. The RAH antigen and the anti-RAH and Anti-WNV TCRmAbs (150 kDa) were made in-house by Dr. Weidanz's group. The binding kinetics of these molecules were measured using a guided mode resonance based sensor system (ResoSens bioassay system, Resonant Sensors) in separate experiments. This system used an ELISA type plate reader with nanostructures on its surface (Bionetic plate) where the antibodies of interest were surface-immobilized at a fixed concentration while the concentration of the antigen flowing over it was increased up to binding saturation, followed by a wash-out period, in a similar fashion to surface plasmon sensor technologies [53]. The plate was incubated inside the system

while the plate is being constantly scanned for shifts in the wavelength resonance peak due to mass loading. The rate constants of association ( $k_{on}$ ), dissociation ( $k_{off}$ ) and equilibrium dissociation ( $K_D = k_{off}/k_{on}$ ) were estimated for RAH antigen-Anti-RAH TCRmAb interactions by fitting the observed time-dependent traces of wavelength resonance shift to appropriate binding models [53].

## Sample Preparation

The total sample volume that the PDMS flow cell encasing the SANE sensor held on the *cis* side was 70  $\mu$ l. To create stock solutions for studying protein interactions, equal proportions of antigen (RAH, 2 nM) and antibody (Anti RAH or Anti WNV, 2 nM) were incubated together for 30 minutes. The reacted mixtures were then diluted in pH 7.4 KCl electrolyte to attain antibody-antigen concentrations in the 100 nM to 1 nM range while maintaining KCl at 150 mM. The *trans* reservoir of the PDMS flow cell was filled with about 1.5 ml of 7.4 pH, 150 mM KCl solution.

## Experimental Data Acquisition and Analysis

The optical signals detected by the photodiode and the electrical ones detected by Axopatch 200B were both sent through an Axon Digidata 1440 ADC to a computer, where Axon pCLAMP 10.6 software was used to record the signals and perform data analysis. When a molecule entered the optical trap, there was an increase in the optical transmission amplitude, which was proportional to its size. We calculated the percentage change of the transmission amplitude with respect to the baseline (optical step change) and the trapping duration (optical trap time) as the optical modality metrics for characterizing molecular interactions. The concurrently acquired ionic current traces enabled quantification of current amplitude changes relative to baseline current

during nanopore translocation events (translocation current) and transit durations, calculated from the full width half-maximum (FWHM) from the current drop of for each event (translocation time) were the electrical modality metrics used for characterizing molecular interactions [42]. These bimodal optical-electrical molecular signatures were analyzed cumulatively in box plots and any pair-wise statistically significant differences between the signatures detected in the experiments were tested using independent sample t-tests.

## RESULTS

Figures 2a-2c and Figures 2d-2f show examples of optical trapping and concurrent electrical nanopore sensing events for individual antigens (RAH, 150 nM) and specific antibody (Anti-RAH, 300 nM), respectively. For the events shown here, the optical step change and trapping time metrics for antigen (Figures 2(a), 2.25%, 0.63 sec) were lower compared to those for antibody (Figure 2(d), 3.04%, 9.32 sec). The corresponding electrical metrics showed lower translocation current for RAH (Figure 2(c), 686 pA) compared to Anti-RAH (Figures 2(f), 937 pA, 39.86 msec), but translocation times were comparable for RAH and Anti-RAH, at 37.85 msec and 39.86 msec, respectively. These bimodal molecular signatures were used to test the feasibility of discriminating between individual antigen, and antibody versus the complexes that these formed in pure protein mixtures.



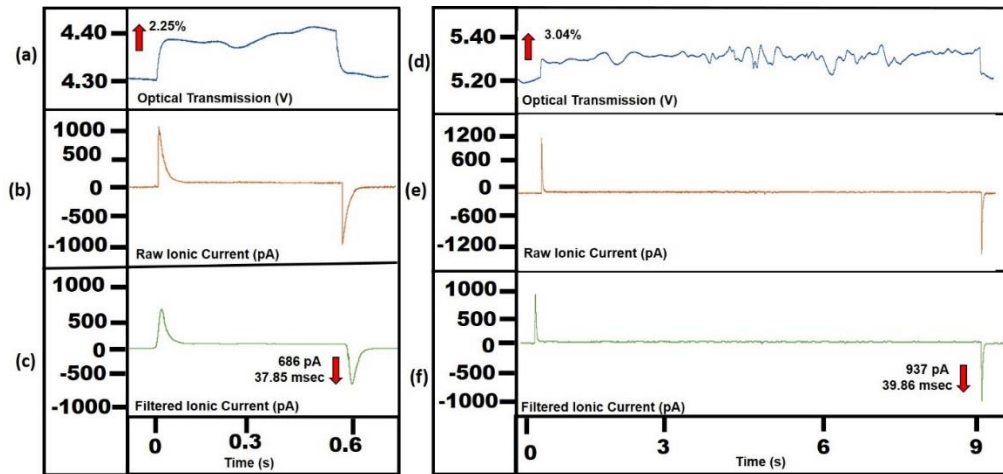


Figure 2: Time traces of individual RAH antigen and Anti RAH antibody molecules. (a & d) Optical transmission, (b & e) Raw ionic Current, (c & f) Filtered Ionic current for antigen (left) and antibody (right).

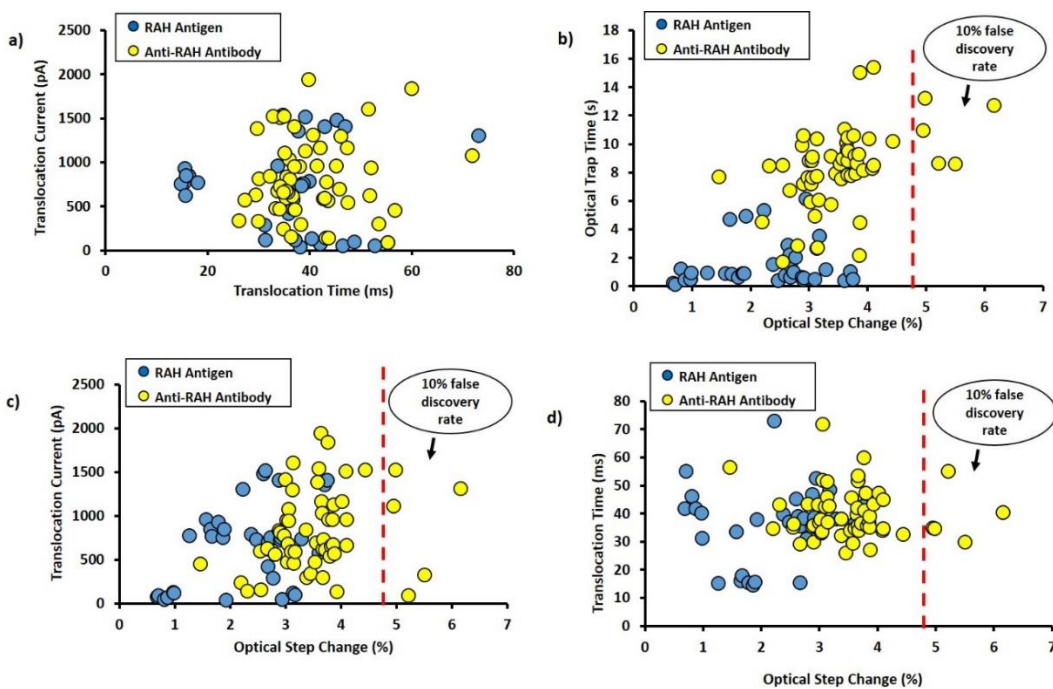


Figure 3: Comparison scatter plots of RAH-Antigen (150 mM) and Anti-RAH Antibody (300 mM) for all data types. (a) Electrical alone. (b) Optical alone. Differences in translocation current (c) and translocation time (d) based on optical step change percentage.

Figure 3 shows a comparison of all data types for antigen and antibody measured in separate experiments at a concentration of 150 mM and 300 mM respectively in a KCl ionic solution. Figure 3 (a) shows that the electrical metrics cannot distinguish between the two groups. Figure 3(b) shows that step changes in optical transmission and optical trapping times showed very little overlap. We empirically chose a highest possible step change that results in a 10 % false discovery rate as threshold criterion, a conservative choice that reflects the compromise between all unbound antibody compared to bound antibody. An optical step threshold of 4.90 % was estimated for the complexes. Using this threshold, we were able to distinguish antigen and antibody molecules by comparing their optical step change to electrical translocation current (Figure 3(c)) and translocation time (Figure 3(d)).

Figure 4(a) shows that using above threshold, the number of antibodies falsely identified as complexes in Figure 4(a) would be 10 %. In contrast when applying the same threshold to 1 nM, 10 nM and 100 nM (Figures 4(b)-4(d), green dots) mixtures of antigen-antibody (in equal proportions) the fraction of detected events exceeding the 4.90% threshold, and therefore presumed as likely antigen-antibody complexes, were 29.51 %, 42.85 %, and 68.42 % respectively. It was also observed that certain event signatures with optical step changes larger than the complex threshold also had very high optical trapping times compared to those for antibodies alone (> 25 sec), while the proportion of those longer trapping times increased with increasing concentration of the antigen-antibody mixture (Figures 2(b)-2(d)). As the Anti-RAH antibodies had two binding sites [54-56], it is presumed that at higher concentrations a larger proportion of bound complexes had both binding sites occupied. Addition of a second antigen to an existing antigen-antibody complex would not increase the optical step change significantly and is estimated at 0.48 %. Therefore, the additional antigen would not shift those events significantly towards the right of the

x-axis in Figures 4(b)-4(d). However, addition of the second antigen could also reduce the overall charge of the complex due to shielding of the antibody binding sites [32]. Charge reduction could lead to prolonged trapping times due to a weaker electrophoretic force pushing the complexes out of the trap for a given voltage bias.

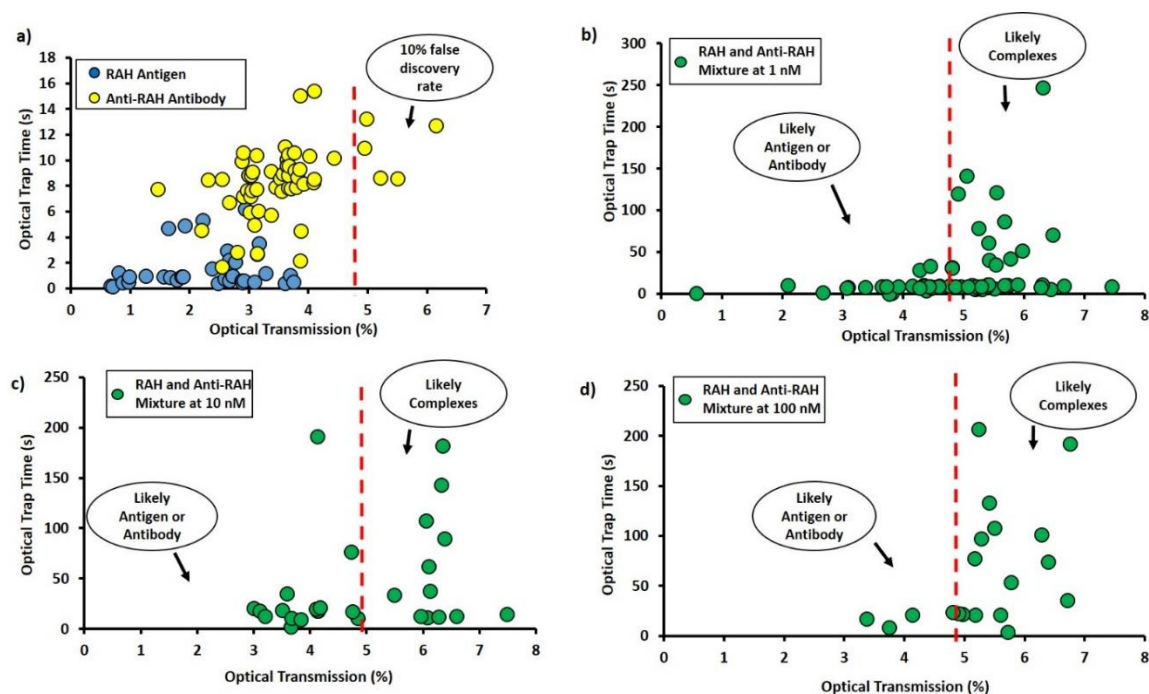


Fig 4: Event density plots for optical metrics. (a) RAH antigen (blue), Anti RAH antibody (yellow). RAH and Anti RAH equal concentration mixtures at (b) 1 nM, (c) 10 nM and (d) 100 nM. The red dotted line indicates the threshold of 4.9 % optical step change.

The optical (step change, trapping time) and electrical (translocation current, nanopore translocation time) data types acquired for RAH antigen, Anti-RAH antibody and for the complexes they formed were compiled and analyzed for statistically significant differences. Figures 5(a)-5(b) show the optical signature comparisons as box plots. The 4.90% optical step threshold discussed above was used to define bound complexes and events with higher trapping times (>25 sec) attributed to likely bivalent binding were plotted separately from lower values,

likely attributed to monovalent binding. In all, optical measurements distinguished RAH antigen clearly from antibody and complexes. Figures 5(c)-5(d) show the corresponding results for the nanopore metrics. The electrical translocation current and translocation times for RAH antigens and Anti-RAH antibodies were not significantly different between them ( $p = 0.07$  and  $p = 0.13$ , respectively; Figure 5(c)-5(d), blue and yellow boxes). Similarly, most pairwise comparisons between Anti-RAH antibody and antigen-antibody complexes were not significant ( $p > 0.05$ ). The only exception was the comparison for nanopore translocation time between the likely bivalent bound complex and antigen ( $p = 0.01$ ).

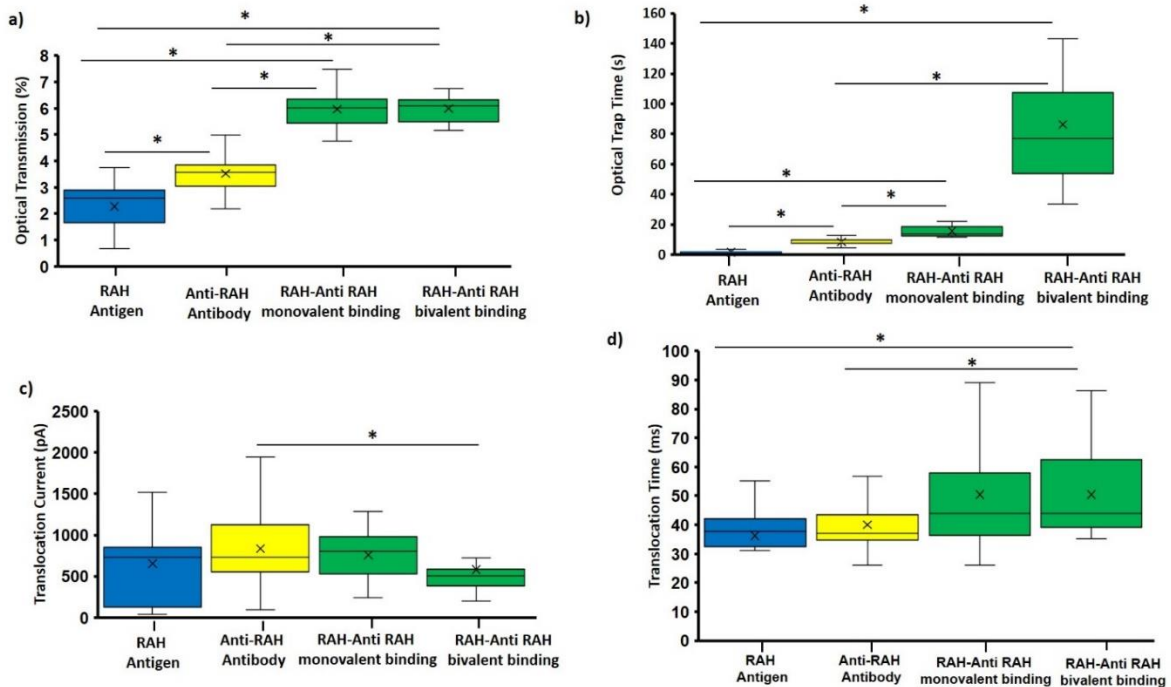


Figure 5: Box plot, demonstrating significant differences between the mean values for RAH antigen, Anti-RAH antibody, and their mixtures. All data types were compiled from equal proportion mixtures at 1 nM, 10 nM and 100 nM. Bound complex events ( $> 4.90\%$  optical step) were sorted as likely monovalent (optical trapping time  $\leq 25$  sec) and bivalent antigen binding ( $> 25$  sec). \*  $p < 0.05$ .

The ability of the SANE sensor to discriminate specific binding of Anti RAH to the RAH antigen, compared to any non-specific binding from an irrelevant antibody Anti-WNV was also evaluated in separate experiments. Typical time traces for both optical and electrical signals for these experiments are shown in Figure 6. Figure 6(a) shows a trapping event for Anti RAH-RAH antigen complex, where initially Anti-RAH antibody was trapped at the DNH (Region A) and after a few seconds the RAH antigen attached to this antibody (Region B) resulting in a total optical step change of 5.77 %. The binding of the antigen to the antibody was not only observed as a step increase in optical transmission (Figure 6(a), Region B) but also as a second positive peak in the ionic current Figure 6(b), Region B). The bound complex translocated through the nanopore at the end of the trapping event duration. Just prior to entering Region C in Figure 6(a) high frequency electrical transients are that are attributed to bobbing near the bottom of the optical trap [42]. After applying a low-pass 20 Hz filter, two electrical translocation events are seen in rapid succession (Figure 6(c), Region C), concurrently with two optical step changes (Figure 6(a), Region C). These observations suggest that as the complex translocated through the nanopore the electric field gradient, combined with the opposing light field gradient likely effected shear forces on the complex [57] separating antigen and antibody, which resulted in them translocating through the pore individually.

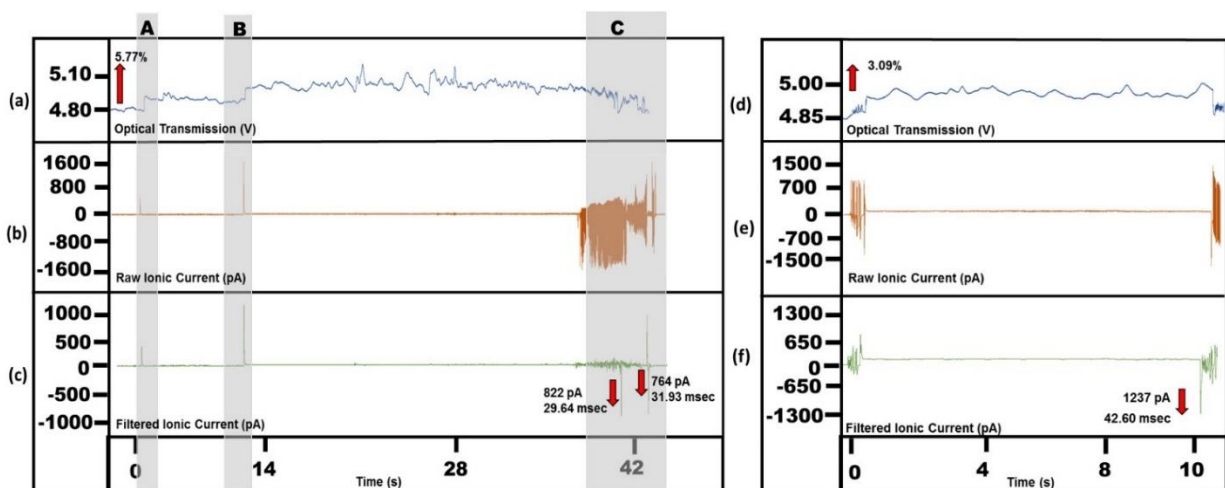


Figure 6: Optical and Electrical time traces of mixture of specific Anti-RAH with RAH antigen (a)-(c), mixture of non-specific Anti-WNV with RAH antigen (d)-(f).

Figures 6(d)-6(f) shows a typical event from the mixture of non-specific Anti-WNV with RAH antigen. The optical signatures (3.09% step change, 10.50 sec trapping time) and electrical signatures (1237 pA translocation current and 42.60 msec translocation time) indicated trapping and translocation of a single molecule consistent with the bimodal signatures of Anti-WNV when measured alone (not shown for brevity). These optical and electrical signatures were therefore consistent with non-binding of Anti-WNV antibody to RAH antigen.

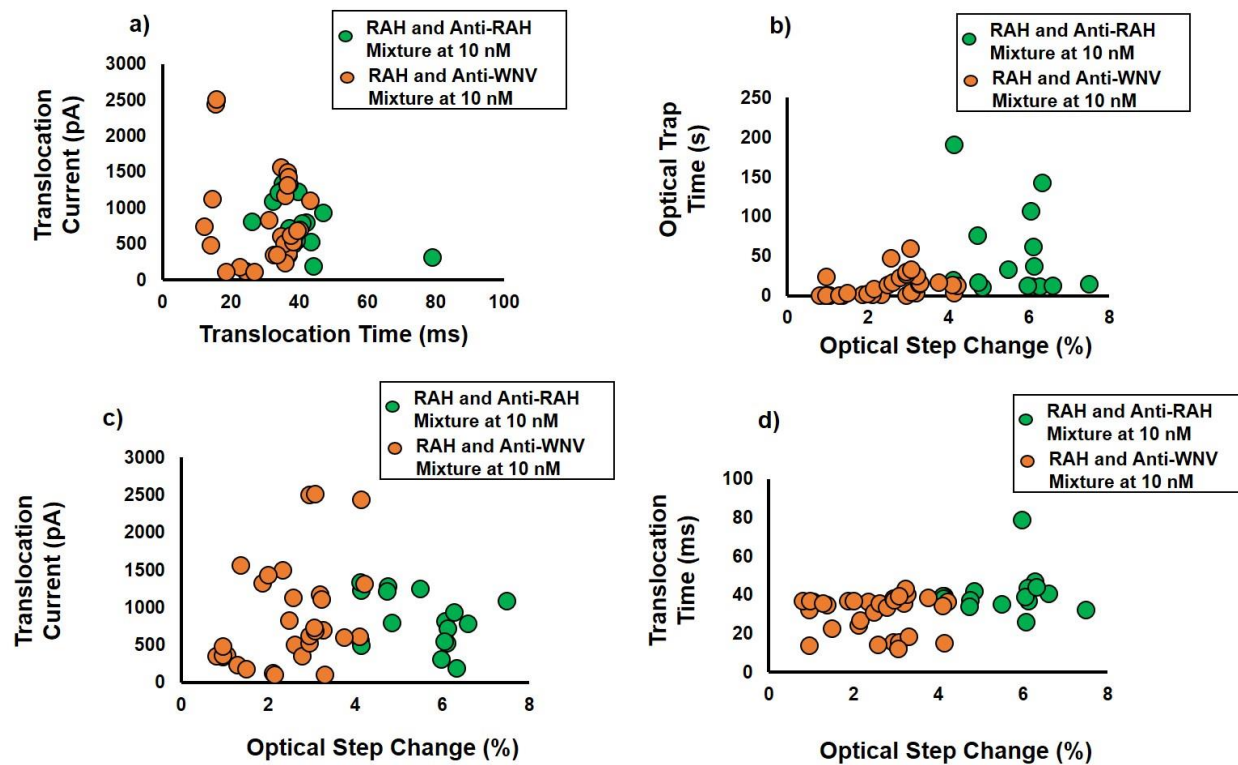


Figure 7: Event density plots of specific vs non-specific mixtures at 10 nM for all data types. (a) Electrical metrics. (b) Optical metrics. Comparison of Translocation Current (c) and Translocation Time (d) with the optical step change of the mixtures.

Figure 7 shows combinations of optical and electrical metrics for mixtures of RAH with Anti RAH (green circles) versus Anti WNV (orange circles), containing equal concentration of antigen and antibody at 10 nM. Events from the mixture with specific targeting were identified as bound complexes (step change greater than 4.9%) as in figure 3. Threshold was applied only to specifically bound events (green circles). Figure 7(a) demonstrates that the electrical signatures alone cannot discriminate between specific and non-specific binding events. Nevertheless, Figures 7(b)-7(d) show that combining optical and electrical signature metrics, or using optical metrics alone can differentiate clearly between specific and non-specific binding for these molecules. All these metric combinations performed similarly in identifying possible complexes and only optical

step change versus optical trapping time are shown here below for brevity. The separation was equally good at higher concentrations of the mixtures.

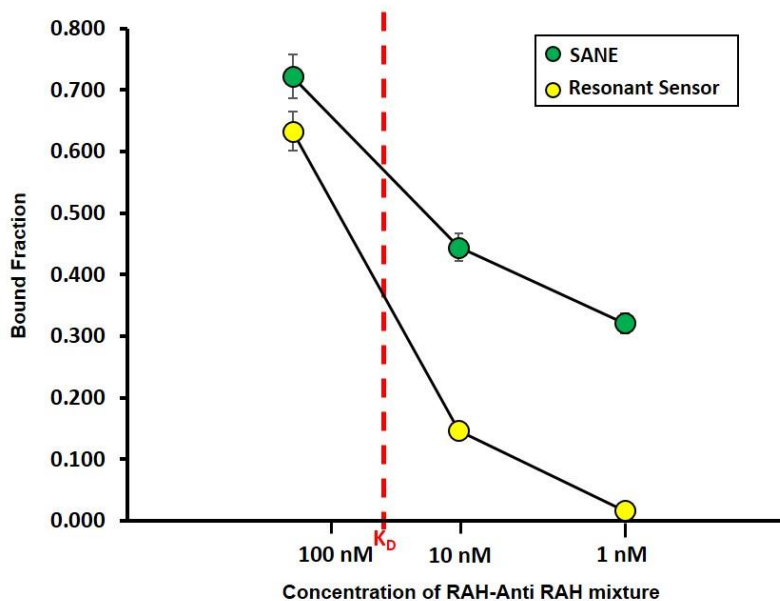


Figure 8: Bound Fraction as a function of the concentration RAH mixture with Anti RAH.

For the case of specific binding, the bound fraction of the antigen-antibody complexes determined by the SANE sensor (using the 4.90 % criterion as in Fig 3) was calculated and compared it with the bound fraction obtained from the commercial Resonant Sensor [53]. The association rate constant  $k_{on}$  was determined as  $7.8 \times 10^2 \pm 2.01 \times 10^2 \text{ M}^{-1}\text{s}^{-1}$  and the dissociation rate constant  $k_{off}$  as  $4.51 \times 10^{-5} \pm 1.22 \times 10^{-6} \text{ s}^{-1}$ , resulting in an equilibrium dissociation constant  $K_D = 58 \pm 17 \text{ nM}$ . Mixtures of RAH antigen and Anti-RAH antibody were then prepared in equal proportions at 100 nM (above  $K_D$ ), and 10 nM and 1 nM (below  $K_D$ ) to quantify the fraction of bound complexes in these mixtures with the SANE sensor. Figure 8 shows that the Resonant Sensor system detected a bound fraction that decreased rapidly at concentrations below the  $K_D$  value. In contrast, the SANE sensor presented a linear reduction in bound fraction with decreasing



concentration, with much increased bound fraction values even at 1 nM, i.e. at concentration ~58 times below the  $K_D$  value. It is hypothesized that the electrical field of the SANE sensor pulls proteins on the *cis* side towards the nanopore where they get slowed down by the optical trap, which results in an increased concentration of reactants immediately over the sensor. Higher local concentrations would result in higher bound fractions. Interestingly, the magnitude of this effect was reduced at 100 nM, which was above the  $K_D$  value, where the available binding sites would be reduced. Also, the resonance shift was almost zero for the RAH – Anti-WNV TCRmAb mixture, confirming the latter as a negative control.

## DISCUSSION

This work presented the use of a novel bimodal optical-electrical SANE sensor technology to identify and differentiate between individual antibodies, their ligands, and the complexes they formed under specific and non-specific binding conditions. The difficulty of identifying bound protein complexes using electrical nanopore translocation current and translocation time metrics has been reported previously and a composite metric of excluded volume was suggested as an improved differentiator metric [58]. Application of this latter method requires knowledge of the charge and volume of the antigen, antibody and mixture, which were not known *a priori* for these proteins that were made in-house. In another study, the overall electrophoretic mobility of the bound complex was shown to increase with respect to its individual components making it difficult to identify based on threshold detection methods [32]. In this work, electrical data (current amplitudes and translocation times) and concurrently acquired optical data (transmitted intensity change and trapping duration), obtained from the nanopore and DNH components of the SANE sensor respectively, were tested for their ability to differentiate between binding conditions.

Similar to the previously reported studies, it was found that using the electrical metrics alone did not allow separating bound from unbound proteins (Figure 3(a)) or specific from non-specific binding (Figure 7 (a)). In contrast, combining optical with electrical metrics or using optical metrics alone enabled differentiating both bound complexes (Figure 4(b)-4(d)) and specific binding (Figure 7(b)-7(d)).

Optical methods identify bound molecules through an increase in optical transmission, but their natural tendency for prolonged trapping times limits the throughput for analyzing sequential trapping events [21]. The results of this work indicate that the bimodal SANE sensor can help address this limitation as the presence of an electric field pushing the trapped molecules through the nanopore, against the opposing optical trapping force, results in bobbing motions followed by a forced translocation (Figure 6(b)), without having to rely on diffusion for un-trapping to occur. The resulting trapping times were in the seconds to tens of seconds in most cases, which was a lot shorter than typical optical trapping times of many minutes observed in the absence of an electric field [59]. Furthermore, the waiting times to detect a trapping event were shortened dramatically in the presence of the electric field bias compared to waiting for an event to trap optically by diffusion alone, especially at lower concentrations (e.g. 40 s versus few min at 1 nM).

Following the previously reported rule of thumb that optical transmission intensity step changes detected by the DNH structure are linearly proportional to the mass of a molecule [60], a threshold of ~4.9 % , representing an empirical chosen 10 % false discovery rate in the highest possible step change , was assumed to be the threshold for detecting bound complex optically. Interestingly, the optical tapping times for events past the defined bound complex threshold showed wide variation, with a higher proportion of longer trapping time events detected with increasing concentration, Figures 4 (b)-4(d). It is hypothesized that the fraction of bound events

with longer trapping times represent complexes with both binding sites of the antibody occupied, while shorter times represent single binding site occupancy. Addition of a second antigen to the antibody-antigen complex would only increase the optical step signal only by 0.48%, which would not permit its easy detection through the optical step metric. Of the electrical metrics, only the nanopore translocation time was found to be different compared to antigen alone (Figure 4(d)), where the overall complex charge was presumed to be lower than that of the antibody. This observation is similar to the result reported in a prior nanopore study where an increase in protein complex charge resulted in increased electrophoretic mobility [32]. This discrepancy could be explained by the bimodal nature of the SANE sensor used in this work, where a surface charging effect of the Au DNH structure edges due to the optical excitation [61] could create an additional repulsive force for the translocating molecules. Some events in Figures 3(b)-3(d) fell below the 4.9 % step threshold, but still had higher optical trapping times than those seen in Figure 3(a) for antibody alone. As these events were very few in number, there was no additional threshold criterion applied for the discrimination of complexes in these data based on optical trapping times, although this will be evaluated further in future work.

The ability of the SANE sensor to differentiate specific from non-specific binding was also tested using an RAH-irrelevant antibody (Anti-WNV), which however had closely matched electrical and optical signatures to the specific antibody (Anti-RAH). Figure 7 shows that the electrical data metrics, derived from the nanopore component of the SANE sensor, could not differentiate specific from non-specific protein mixtures. However, when optical data metrics were included the two mixtures could be separated clearly. The 4.9 % threshold was implicitly applied for the specific binding but no threshold was applied for the non-specific binding. The mixture of

Anti-WNV and RAH antigen did not result in any detected binding events and therefore all the recorded events corresponded to signatures of antibody or antigen only.

One limitation of the SANE sensor, shared by most single molecule analysis technologies, is that it cannot measure the mean life of binding ( $= 1/k_{\text{off}}$ ) for individual high affinity interaction events. The Resonant Sensor measurements for RAH – Anti RAH complex indicated a mean binding life of >6 hours. Given that typical complex trapping times were in the tens of seconds, it would be impossible to measure the mean binding life by direct observation of single molecule on-off binding events. Therefore, attempts to use the SANE sensor for measuring  $K_D$  values would have to be directed at experiments quantifying the changes in bound fraction as a function of ligand concentration. Interestingly, when the bound fraction of specific complex was compared to measurements by the commercial Resonant Sensor system it was found that the SANE sensor detected considerably higher bound fraction values at corresponding antigen concentrations (Figure 8). The SANE and Resonant Sensor experiments are not directly analogous as the latter were performed at excess of antibody immobilized on a surface whereas the former were performed in solutions of equal antigen-antibody proportions. The fact that fewer antigens should be available in the SANE sensor experiments, since they are not available at excess, yet higher bound fractions were still detected than Resonant Sensor, along with an apparently linear reduction in bound fraction with reducing ligand concentration, suggest the existence of an underlying mechanism affecting protein interactions at the SANE sensor. We hypothesized that the applied electric field concentrated the protein solution components immediately over the SANE sensor. This is justified by the fact the top layer of the sensor ship is covered by gold, which is a conductor, except for the nanoscopic area drilled by FIB to make the DNH structure. The proteins pushed by the electric field towards the sensor would likely slow down near the DNH structure due to the

optical trapping of molecules occupying the space over the nanopore, which would offer more opportunities for binding interactions in the vicinity of the optical trap than in bulk solution at a given concentration. Such an interaction augmentation mechanism would need to be characterized further in future work to determine if the SANE sensor could be calibrated with different binding affinity complexes to quantify  $K_D$  from measurements of bound fraction as a function of antibody and ligand concentrations. Nevertheless, the apparent augmentation of bound fraction by the SANE sensor presented in this work demonstrated the existence of a novel phenomenon of potentially great utility. The bound fraction measurements shown in Figure 8 indicate that the SANE sensor could be used to answer yes-no questions on whether a ligand is being targeted or not by a candidate antibody at concentrations that are much lower than the  $K_D$  value, where the bound fraction should be 50% in bulk solution. The resulting savings in protein material could be important in cases where only small protein amounts are available. For example, the Anti-RAH antibodies used in this work are an example of T-cell receptor-like antibodies that bind with high affinity to pMHCs, like the RAH antigen, that are presented on the surface of cancer cells [49]. When used *in vivo*, the binding of such antibodies can be the first step towards helping the immune system mount a response against the cancer [43-47]. The availability of pMHC ligand amounts that can be isolated from tissue biopsy is limited and therefore the SANE sensor-enabled savings of pMHC ligand amounts could enable testing of multiple antibodies to select the best candidate to target a particular tumor.

## CONCLUSION

We have demonstrated the feasibility of using the bimodal SANE sensor to detect specific antibody-ligand interactions. Calibration experiments of individual antigen and antibody solutions were used to calculate typical values for optical and electrical metrics derived from the concurrently acquired bimodal data to identify the specifically bound antigen-antibody complexes found in mixtures. Our results hinted at the possibility of differentiating between monovalent versus bivalent binding, which was possible to occur for the antigen-antibody model used in this work. A mixture of RAH antigen and RAH-irrelevant Anti-WNV was used to show the specificity of antigen binding. In this work, the Anti-WNV antibody showed no detectable binding, which facilitated its differentiation from specific binding. Further experiments to test the separation of non-specific binding with other antibodies that could stick non-specifically to a target antigen will be the object of future work. This work also demonstrated an interesting and novel property of the SANE sensor for enhancing the bound fraction values compared to those expected for the known  $K_D$  of the interaction, which was measured by a commercial Resonant Sensor system that quantifies surface-immobilized binding kinetics. Although this novel SANE sensor behavior requires further characterization to test the feasibility of using it to quantify  $K_D$  values, the present work suggests the potential of using this sensor as a screening tool for antibody-ligand interactions using minimal protein material.

## ACKNOWLEDGEMENTS

We are thankful to Mr. Soeren Eyhusen and Mr. Chuong Huynh for providing us with the access and technical support on focused ion beam milling at the Zeiss ORION NanoFab facility in Peabody, MA. We are also grateful to all the engineers and staff of the nanofabrication facility, Shimadzu Institute Nanotechnology Research Center at the University of Texas at Arlington. The Vice-President of Research Office of the University of Texas at Arlington funded and supported this work through a Pilot Research Program for Interdisciplinary Collaboration.

## REFERENCES

- [1] Spitzberg J D, Zreben A, van Kooten X F and Meller A 2019 Plasmonic-Nanopore Biosensors for Superior Single-Molecule Detection *Advanced Materials* 1900422
- [2] Rissin D M, Kan C W, Campbell T G, Howes S C, Fournier D R, Song L, Piech T, Patel P P, Chang L and Rivnak A J 2010 Single-molecule enzyme-linked immunosorbent assay detects serum proteins at subfemtomolar concentrations *Nature biotechnology* **28** 595
- [3] Todd J, Freese B, Lu A, Held D, Morey J, Livingston R and Goix P 2007 Ultrasensitive flow-based immunoassays using single-molecule counting *Clinical chemistry* **53** 1990-5
- [4] Shim J-u, Ranasinghe R T, Smith C A, Ibrahim S M, Hollfelder F, Huck W T, Klenerman D and Abell C 2013 Ultrarapid generation of femtoliter microfluidic droplets for single-molecule-counting immunoassays *Acs Nano* **7** 5955-64
- [5] Hinterdorfer P and Dufrene Y F 2006 Detection and localization of single molecular recognition events using atomic force microscopy *Nature methods* **3** 347
- [6] Neuman K C and Nagy A 2008 Single-molecule force spectroscopy: optical tweezers, magnetic tweezers and atomic force microscopy *Nature methods* **5** 491
- [7] Hunt H K and Armani A M 2010 Label-free biological and chemical sensors *Nanoscale* **2** 1544-59

- [8] Guo X 2013 Single-Molecule Electrical Biosensors Based on Single-Walled Carbon Nanotubes *Advanced Materials* **25** 3397-408
- [9] Ohshiro T, Matsubara K, Tsutsui M, Furuhashi M, Taniguchi M and Kawai T 2012 Single-molecule electrical random resequencing of DNA and RNA *Scientific reports* **2** 501
- [10] Patolsky F, Zheng G, Hayden O, Lakadamyali M, Zhuang X and Lieber C M 2004 Electrical detection of single viruses *Proceedings of the National Academy of Sciences* **101** 14017-22
- [11] Walt D R 2012 Optical methods for single molecule detection and analysis. ACS Publications)
- [12] Armani A M, Kulkarni R P, Fraser S E, Flagan R C and Vahala K J 2007 Label-free, single-molecule detection with optical microcavities *science* **317** 783-7
- [13] Puchkova A, Vietz C, Pibiri E, Wünsch B, Sanz Paz M a, Acuna G P and Tinnefeld P 2015 DNA origami nanoantennas with over 5000-fold fluorescence enhancement and single-molecule detection at 25  $\mu$ M *Nano letters* **15** 8354-9
- [14] Heylman K D, Thakkar N, Horak E H, Quillin S C, Cherqui C, Knapper K A, Masiello D J and Goldsmith R H 2016 Optical microresonators as single-particle absorption spectrometers *Nature Photonics* **10** 788
- [15] Zhang Z, Kenny S J, Hauser M, Li W and Xu K 2015 Ultrahigh-throughput single-molecule spectroscopy and spectrally resolved super-resolution microscopy *Nature methods* **12** 935
- [16] Yoo S M and Lee S Y 2016 Optical biosensors for the detection of pathogenic microorganisms *Trends in biotechnology* **34** 7-25
- [17] Dekker C 2007 Solid-state nanopores *Nature nanotechnology* **2** 209
- [18] Yuan Z, Wang C, Yi X, Ni Z, Chen Y and Li T 2018 Solid-State Nanopore *Nanoscale research letters* **13** 56
- [19] Al Balushi A A, Kotnala A, Wheaton S, Gelfand R M, Rajashekara Y and Gordon R 2015 Label-free free-solution nanoaperture optical tweezers for single molecule protein studies *Analyst* **140** 4760-78
- [20] Juan M L, Gordon R, Pang Y, Eftekhari F and Quidant R 2009 Self-induced back-action optical trapping of dielectric nanoparticles *Nature Physics* **5** 915
- [21] Kotnala A, DePaoli D and Gordon R 2013 Sensing nanoparticles using a double nanohole optical trap *Lab on a Chip* **13** 4142-6
- [22] Pang Y and Gordon R 2011 Optical trapping of 12 nm dielectric spheres using double-nanoholes in a gold film *Nano letters* **11** 3763-7



- [23] Ali W, Raza M U, Mahmood M A I, Allen P B, Hall A R, Wan Y and Iqbal S M Differentiation of Specific Cancer Biomarkers with Solid-state Nanopores.
- [24] Shi W, Friedman A K and Baker L A 2016 Nanopore sensing *Analytical chemistry* **89** 157-88
- [25] Larkin J, Henley R Y, Muthukumar M, Rosenstein J K and Wanunu M 2014 High-bandwidth protein analysis using solid-state nanopores *Biophysical journal* **106** 696-704
- [26] Fologea D, Ledden B, McNabb D S and Li J 2007 Electrical characterization of protein molecules by a solid-state nanopore *Applied physics letters* **91** 053901
- [27] Plesa C and Dekker C 2015 Data analysis methods for solid-state nanopores *Nanotechnology* **26** 084003
- [28] Freedman K J, Haq S R, Edel J B, Jemth P and Kim M J 2013 Single molecule unfolding and stretching of protein domains inside a solid-state nanopore by electric field *Scientific reports* **3** 1638
- [29] Gershow M and Golovchenko J A 2007 Recapturing and trapping single molecules with a solid-state nanopore *Nature nanotechnology* **2** 775
- [30] Fologea D, Gershow M, Ledden B, McNabb D S, Golovchenko J A and Li J 2005 Detecting single stranded DNA with a solid state nanopore *Nano letters* **5** 1905-9
- [31] Kowalczyk S W, Hall A R and Dekker C 2009 Detection of local protein structures along DNA using solid-state nanopores *Nano letters* **10** 324-8
- [32] Han A, Creus M, Schürmann G, Linder V, Ward T R, De Rooij N F and Staufer U 2008 Label-free detection of single protein molecules and protein– protein interactions using synthetic nanopores *Analytical chemistry* **80** 4651-8
- [33] Plesa C, Kowalczyk S W, Zinsmeister R, Grosberg A Y, Rabin Y and Dekker C 2013 Fast translocation of proteins through solid state nanopores *Nano letters* **13** 658-63
- [34] Talaga D S and Li J 2009 Single-molecule protein unfolding in solid state nanopores *Journal of the American Chemical Society* **131** 9287-97
- [35] Kumar L, Lesuffleur A, Hughes M and Gordon R 2006 Double nanohole apex-enhanced transmission in metal films *Applied Physics B* **84** 25
- [36] Nicoli F, Verschueren D, Klein M, Dekker C and Jonsson M P 2014 DNA translocations through solid-state plasmonic nanopores *Nano letters* **14** 6917-25

- [37] Assad O N, Gilboa T, Spitzberg J, Juhasz M, Weinhold E and Meller A 2017 Light-enhancing plasmonic-nanopore biosensor for superior single-molecule detection *Advanced Materials* **29** 1605442
- [38] Shi X, Verschueren D, Pud S and Dekker C 2018 Integrating Sub-3 nm Plasmonic Gaps into Solid-State Nanopores *Small* **14** 1703307
- [39] Shi X, Verschueren D V and Dekker C 2018 Active Delivery of Single DNA Molecules into a Plasmonic Nanopore for Label-Free Optical Sensing *Nano letters* **18** 8003-10
- [40] Verschueren D V, Pud S, Shi X, De Angelis L, Kuipers L and Dekker C 2018 Label-Free Optical Detection of DNA Translocations through Plasmonic Nanopores *ACS nano*
- [41] Verschueren D, Shi X and Dekker C 2019 Nano-Optical Tweezing of Single Proteins in Plasmonic Nanopores *Small Methods* 1800465
- [42] Raza M U, Peri S S S, Ma L-C, Iqbal S M and Alexandrakis G 2018 Self-induced back action actuated nanopore electrophoresis (SANE) *Nanotechnology* **29** 435501
- [43] Verma B, Jain R, Caseltine S, Rennels A, Bhattacharya R, Markiewski M M, Rawat A, Neethling F, Bickel U and Weidanz J A 2011 TCR mimic monoclonal antibodies induce apoptosis of tumor cells via immune effector-independent mechanisms *The Journal of Immunology* **186** 3265-76
- [44] Verma B, Neethling F A, Caseltine S, Fabrizio G, Largo S, Duty J A, Tabaczewski P and Weidanz J A 2010 TCR mimic monoclonal antibody targets a specific peptide/HLA class I complex and significantly impedes tumor growth in vivo using breast cancer models *The journal of immunology* **184** 2156-65
- [45] Wittman V P, Woodburn D, Nguyen T, Neethling F A, Wright S and Weidanz J A 2006 Antibody targeting to a class I MHC-peptide epitope promotes tumor cell death *The Journal of Immunology* **177** 4187-95
- [46] Herrera C E, Lowe D B, Bivens C K, Mobley A S, McCormick A, Wichner T, Sabnani M K, Wood L M and Weidanz J A 2017 TCR-like antibody duocarmycin conjugates promote cytotoxicity of tumor cells expressing low peptide/HLA targets. *Am Assoc Immunol*)
- [47] Lowe D B, Bivens C K, Mobley A S, Herrera C E, McCormick A L, Wichner T, Sabnani M K, Wood L M and Weidanz J A 2017 TCR-like antibody drug conjugates mediate killing of tumor cells with low peptide/HLA targets(vol 9): Taylor & Francis) p 603-14

- [48] Feltkamp M C, Vreugdenhil G R, Vierboom M P, Ras E, van der Burg S H, Schegget J T, Melief C J and Kast W M 1995 Cytotoxic T lymphocytes raised against a subdominant epitope offered as a synthetic peptide eradicate human papillomavirus type 16-induced tumors *European journal of immunology* **25** 2638-42
- [49] Garboczi D N, Hung D T and Wiley D C 1992 HLA-A2-peptide complexes: refolding and crystallization of molecules expressed in *Escherichia coli* and complexed with single antigenic peptides *Proceedings of the National Academy of Sciences* **89** 3429-33
- [50] van Hall T, van de Rhee N E, Schoenberger S P, Vierboom M P, Verreck F A, Melief C J and Offringa R 1998 Cryptic open reading frames in plasmid vector backbone sequences can provide highly immunogenic cytotoxic T-lymphocyte epitopes *Cancer research* **58** 3087-93
- [51] Hitzeroth I I, Passmore J-A S, Shephard E, Stewart D, Müller M, Williamson A-L, Rybicki E P and Kast W M 2009 Immunogenicity of an HPV-16 L2 DNA vaccine *Vaccine* **27** 6432-4
- [52] Kim S, Pinto A K, Myers N B, Hawkins O, Doll K, Kaabinejadian S, Netland J, Bevan M J, Weidanz J A and Hildebrand W H 2014 A novel T-cell receptor mimic defines dendritic cells that present an immunodominant West Nile virus epitope in mice *European journal of immunology* **44** 1936-46
- [53] Wawro D, Zimmerman S, Magnusson R and Koulen P 2011 Photonic sensor system for screening serum biomarker proteins in ovarian cancer(vol 8090) p 80900S
- [54] Trenevskaja I, Li D and Banham A H 2017 Therapeutic Antibodies against Intracellular Tumor Antigens *Frontiers in Immunology* **8**
- [55] Narayan S, Choyce A, Linedale R, Saunders N A, Dahler A, Chan E, Fernando G J, Frazer I H and Leggatt G R 2009 Epithelial expression of human papillomavirus type 16 E7 protein results in peripheral CD8 T-cell suppression mediated by CD4+ CD25+ T cells *European journal of immunology* **39** 481-90
- [56] Lei J and Zhang G 2012 Potential antitumor applications of a monoclonal antibody specifically targeting human papilloma virus 16 E749-57 peptide *Microbiology and immunology* **56** 456-62
- [57] Pang Y and Gordon R 2011 Optical trapping of a single protein *Nano letters* **12** 402-6
- [58] Freedman K J, Bastian A R, Chaiken I and Kim M J 2013 Solid-state nanopore detection of protein complexes: applications in healthcare and protein kinetics *Small* **9** 750-9
- [59] Al Balushi A A, Zehtabi-Oskuie A and Gordon R 2013 Observing single protein binding by optical transmission through a double nanohole aperture in a metal film *Biomedical optics express* **4** 1504-11

- [60] Wheaton S and Gordon R 2015 Molecular weight characterization of single globular proteins using optical nanotweezers *Analyst* **140** 4799-803
- [61] Di Fiori N, Squires A, Bar D, Gilboa T, Moustakas T D and Meller A 2013 Optoelectronic control of surface charge and translocation dynamics in solid-state nanopores *Nature nanotechnology* **8** 946

## CHAPTER 4

# QUANTIFICATION OF LOW AFFINITY KINETICS BETWEEN Qa- 1<sup>b</sup> Qdm LIGANDS AND NK INHIBITORY RECEPTORS CD94/NKG2A WITH A SELF-INDUCED BACK-ACTION ACTUATED NANOPORE ELECTROPHORESIS (SANE) SENSOR

Sai Santosh Sasank Peri <sup>1</sup>, Manoj Kumar Sabnani <sup>3</sup>, Muhammad Usman Raza <sup>1</sup>, Soroush Ghaffari <sup>3</sup>, Jung Soo Lee <sup>4</sup>, Min Jun Kim <sup>4</sup>, Jon Weidanz <sup>3</sup>, George Alexandrakis <sup>2,#</sup>

<sup>1</sup> Department of Electrical Engineering, University of Texas at Arlington, Arlington, TX, USA

<sup>2</sup> Department of Bioengineering, University of Texas at Arlington, Arlington, TX, USA

<sup>3</sup> Department of Biology, University of Texas at Arlington, Arlington, TX, USA

<sup>4</sup> Department of Mechanical Engineering, Southern Methodist University, Dallas, TX, USA

#Email: galex@uta.edu

In preparation for publication. Used with permission from Manoj Kumar Sabnani, Muhammad Usman Raza, Soroush Ghaffari, Jung Soo Lee, Min Jun Kim, Jon Weidanz, and George Alexandrakis.

## ABSTRACT

A plasmonic nanopore sensor enabling detection of bimodal optical and electrical molecular signatures was fabricated and tested for its ability to characterize low affinity ligand-receptor interactions. This plasmonic nanosensor uses a Self-Induced Back-Action (SIBA) for optical trapping to enable SIBA-Actuated Nanopore Electrophoresis (SANE) through a nanopore located immediately below the optical trap volume. A Natural Killer (NK) cell inhibitory receptor heterodimer molecule CD94/NKG2A was synthesized to target a specific peptide-presenting Qa-1<sup>b</sup> Qdm ligand as a simplified model of low-affinity interactions between immune cells and peptide-presenting cancer cells that occurs during cancer immunotherapy. A cancer-irrelevant GroEL ligand was also targeted by the same receptor as a control experiment to test for non-specific binding. Although the analysis of different pairs of bimodal SANE sensor signatures enabled some level of discrimination between specific and non-specific interactions the separation was not complete, which suggested the need for multi-dimensional data analyses in future work. However, the SANE sensor showed ability to quantify the fast dissociation rate ( $k_{\text{off}}$ ) in this low-affinity model system that was previously shown to be challenging to quantify with commercial technologies. The  $k_{\text{off}}$  value of targeted peptide-presenting ligands is known to correlate with the subsequent activation of immune cells in vivo, suggesting the potential utility of the SANE sensor as a screening tool in cancer immunotherapy.

## INTRODUCTION

Single molecule detection methods have been able to quantify protein-ligand interactions and provide valuable information that is usually unavailable from ensemble methods such as ELISA, Surface Plasmon Resonance (SPR) and other assays [1]. These modalities have utilized either optical or electrical sensing technologies to differentiate between bound and unbound reactants. Current single molecule interaction analysis methods utilizing optical technologies include optical tweezers, atomic force microscopy, single molecule FRET and ultra-high resolution microscopy [2]. Electrical sensors for single molecule analysis predominantly consist of solid-state nanopores (SSNPs) [3] and electrical break junctions [4], of which the former are more popular due to their sensitivity and specificity.

SSNPs are nanometer sized pores milled in suspended dielectric membranes using focused ion beam (FIB) [5] or transmission electron microscopy (TEM) [6] and work as a robust alternative to biological pores [7]. In nanopore sensing two compartments filled with electrolyte solution are joined together with the SSNP at its center and analyte molecules are added to one compartment and translocated through the SSNP into the other using applied bias. The translocation of the molecule causes changes in the ionic current signatures that defines the data metrics (translocation current and translocation time) that SSNP depend on molecular size [8], volume [9] and charge [10] as well as solution pH and salt concentrations [11]. SSNPs have been used to study and characterize protein-ligand interactions [12-16].

On the optical sensing side, an area of focus in recent years has been the development of metallic nanoaperture structures that utilize strong plasmonic confinement to enable using self-induced back action (SIBA) as a mechanism for the optical trapping of protein-size molecules at

low laser powers (12 mW) [17]. Metallic nanoapertures circumvent the difficulty of using high laser powers to trap entities smaller than 100 nm with optical tweezers [18]. SIBA based optical trapping has been reported to quantify protein-small molecule interactions by trapping the molecules in a double nanohole (DNH) structure milled in a gold (Au) film on a glass substrate [19]. However, optical sensor throughput can be limited by long optical trapping times and diffusion-limited molecular transport to the sensing region, as many experiments often use low analyte concentrations. Plasmonic nanopore structures have been previously suggested as a means of using optical illumination to create local heating on plasmonic nanoantennas to augment event detection rate through an SSNP located immediately below [20-22].

Recently, we [23] and others [1, 24-27] have reported on plasmonic nanopores combining the optical trapping of metallic nanoapertures with the electrical sensing of SSNPs, to augment optical event detection rate with the help of an external electrical bias, while also slowing down SSNP event detection by use of the spatially overlapping optical trapping field. In our prior work [23], a DNH nanoaperture had a SSNP placed at its center, which enabled to combine optical trapping by SIBA with electrical nanopore sensing. The resulting bimodal sensor technology was named as a SIBA-Actuated Nanopore Electrophoresis (SANE). The DNH was milled by Neon (Ne) ion FIB and had tapered walls that excited the wedge plasmons such that the molecule was trapped above the mouth of the SSNP. The latter was drilled by Helium (He) ion FIB through a silicon nitride (SiN) layer existing immediately below the Au layer. In initial experiments with nanoparticles the opposing optical and electrical forces generated high frequency oscillations (bobbing) inside the optical trap, while the presence of the optical trap near the SSNP extended the translocation time of nanoparticles up to four orders of magnitude compared to a classical nanopore [3].



This work goes beyond the initial experiments with nanoparticles to test the feasibility of using the bimodal optical-electrical data obtained from the SANE sensor to study low-affinity ligand-receptor interactions in solution and differentiate specific from non-specific binding. The proteins used in this work represent a simplified model of ligand-receptor interactions that are relevant to cancer immunotherapy. CD94 and NKG2A heterodimer receptors are expressed on the cell surface of Natural Killer (NK) lymphocyte cells [28]. These receptors can be cloned and expressed in the mammalian expression system as soluble recombinant protein, CD94/NKG2A heterodimer (henceforth referred to as NK receptor). Heterodimer can recognize a specific peptide-presenting Major Histocompatibility Complex (pMHC) ligand known as Qdm/Qa-1<sup>b</sup> (henceforth referred to as Qdm) [29]. Usually, expression of Qdm ligand is associated with an inhibitory response from the receptors on the NK cells. Tumor cells are also known to express Qdm ligand to evade immune system response. These soluble heterodimers specifically target and block Qdm ligands expressed on the tumor cells. In the absence of inhibitory ligands, activating receptors of the NK cells can kill the tumor cells [30]. Cancer-irrelevant ligands (GroEL) were also used in control experiments. GroEL is an immunodominant epitope expressed by *Salmonella typhimurium* and presented by a Qa-1<sup>b</sup> MHC molecule. It is specifically recognized by CD8<sup>+</sup> cytotoxic T lymphocytes after natural infection in mouse [31, 32].

The SANE sensor bimodal signatures were tested for their ability to discriminate between specific (Qdm-NK receptor) and non-specific (GroEL-NK receptor) interactions in equimolar mixtures over a wide range of concentrations. Furthermore, as the low affinity of NK receptor receptors to Qdm resulted in short binding times that were challenging to quantify in prior SPR experiments [33, 34], the SANE sensor was also tested for its ability to quantify these short binding times. The mean value of detected binding time events yielded an estimate for the dissociation constant ( $k_{off}$ )

that was compared to the corresponding value for NK receptor targeting the human equivalent of Qdm (mouse), estimated in a prior study [34]. The results presented in this work suggest the potential future utility of the SANE sensor as a screening tool in cancer immunotherapy.

## **MATERIALS AND METHODS**

### **SANE Sensor Fabrication**

The SANE sensor was fabricated according to a previously reported procedure [23]. This sensor consists of a metal-dielectric membrane with nanostructures milled using Focused Ion Beam (FIB) on a double side polished 4-inch silicon (Si) wafer (100 orientation). A 500 nm silicon dioxide (SiO<sub>2</sub>) was grown by thermal oxidation, followed by deposition of a 60 nm stoichiometric silicon nitride (SiN) by LPCVD on both sides of the Si wafer. On one side of the wafer (referred to as backside), square windows of side 786 μm were patterned using photolithography process. The SiN layer exposed in these windows were etched away using Deep Reactive Ion Etching (DRIE) with tetrafluoromethane (CF<sub>4</sub>) gas at an etch rate of 1 nm/min. Followed by etching of the SiO<sub>2</sub> layer using 6:1 buffered hydrofluoric (BHF). The underlying Si layer was etched anisotropically using a 22% tetramethylammonium hydroxide (TMAH) solution at 90°C to create a 100 μm window on the front side leaving SiN/SiO<sub>2</sub> layers suspended. On the front side, a 5nm chromium (Cr) layer, followed by 100 nm Au were deposited through e-beam evaporation method at 0.1 nm/s deposition rate, where Cr was used as an adhesion layer for Au. Using a photolithography process, alignment markers were patterned on this Au side to assist in FIB milling. The Au and Cr layers in these marker regions were etched away using respective wet etchants (Sigma Aldrich). The Si wafer was diced into individual chips and the backing SiO<sub>2</sub> layer was etched using 6:1 BHF for each chip. These Si chips with a metal-dielectric membrane were

placed inside a GFIS focused ion beam (Carl Zeiss, ORION Nanofab, Peabody, MA) ultra-high vacuum chamber to mill the nanostructures. A DNH nanoaperture (100 nm diameter circles) was milled through the Au layer with tapered edges having a 15-18% slope for optimal plasmon excitation [35]. In the SiN layer, a 25 nm diameter nanopores was milled using a Ne ion beam such that it was exactly at the middle of the DNH.

## Experimental Setup

Figure 1(a) shows a scanning electron microscope (SEM) image of the milled DNH and nanopore structures comprising the SANE sensor. Figure 1(b) shows the schematic of the experimental setup, that was similar to our previously reported work [23]. Briefly, a near infrared region laser diode (820 nm, L820P200, Thorlabs) was collimated and circularly polarized using a QWP (WPQ05M, Thorlabs) to create a 2 mm diameter beam. This beam was linearly polarized using a Glan-Thompson linear polarizer (GTH10M, Thorlabs). An adjustable HWP (WPH05M, Thorlabs) was used to select the polarization that was parallel to the horizontal axis of the DNH for optimal excitation of wedge plasmons. The beam was expanded using a 4x beam expander (Newport) and passed through a periscope to the back aperture of a 63x oil immersion objective lens (NA= 1.2, Zeiss C-Apochromat). The light beam was focused through a cover slip onto the SANE chip. The chip was enclosed in a transparent PDMS flow cell (Figure 1(b)), fabricated as per previously reported procedure [23]. This PDMS flow cell was attached to a piezo stage (MDT6938, Thorlabs) to perform coarse and fine adjustments and align the short axis of the DNH with the polarization of the laser beam. A condenser lens was used to collect the transmitted light from the DNH and then focused onto a photodiode (PDA36A, Thorlabs). The PDMS flow cell consisted of two chambers, one above the SANE sensor chip (*cis*) and the other below the chip (*trans*). Analytes mixed in 150 mM potassium chloride (KCl) solution were added to the *cis*

chamber. Similar molarity KCl only solution was added to the *trans* chamber. Two silver electrodes were immersed in bleach solution to form a coating of silver chloride (Ag/AgCl). One electrode was inserted in the *cis* and one in the *trans* chamber.

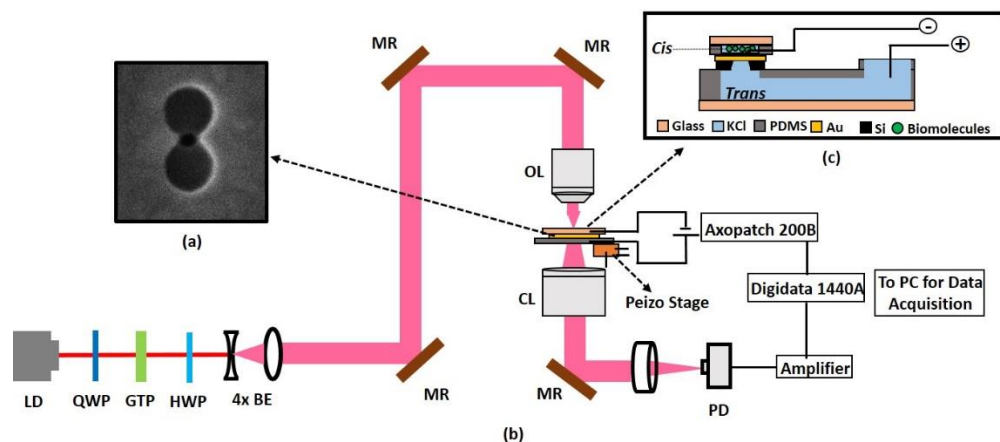


Fig 1: (a) Scanning electron microscope image of FIB milled DNH and nanopores structure on the metal-dielectric membrane. (b) Experimental setup with optical and electrical measurement instruments. LD: Laser Diode, QWP: Quarter Wave Plate, GTP: Glan-Thompson Polarizer, HWP: Half Wave Plate, 4x BE: 4x Beam Expander, MR: Mirror, OL: Carl-Zeiss 1.3 N.A. 63x Objective Lens, CL: Condenser Lens, PD: Photodiode. (c) PDMS flow cell cross-sectional view with SANE sensor.

The electrodes were connected to Axon Axopatch 200B patch clamp amplifier and digitizer equipment (Molecular Devices) through Axon Headstage (CV 203BU) and operated in voltage clamp mode. The change in resistance across the chambers was measured as a drop in ionic current flow when a protein passed through the nanopore while translocating from *cis* to *trans*. A faraday cage was built with aluminum foil (Reynolds) around the piezo-stage with PDMS flow cell to eliminate low-frequency electromagnetic noise while recording the ionic current traces. Protein translocation events were performed at 100 mV voltage bias across the nanopore.

## Generation of Ligands and Receptors

Qa-1<sup>b</sup> Qdm ligand (Qdm) [30], a MHC class Ib allotype from C57Blk/6 (mouse strain) analogous to HLA-E (Human) consisted of a purified mouse MHC I heavy chain, Qa1b (35 kDa) and a human  $\beta$ 2m (13 kDa) light chain. The peptide AMAPRTLTL (1 kDa) derived from leader sequence of H2D<sup>b</sup> and synthesized by Genescript, Piscataway, NJ and refolded *in vitro* to create a peptide-presenting MHC (pMHC) antigen that was purified by size exclusion chromatography [36]. This Qdm peptide is known to induce a NK cell inhibitory response when presented by Qa-1b in the mouse [28, 29]. CD94 (~26 kDa) and NKG2A (~43 kDa) were cloned from murine NK cells and expressed as a soluble recombinant protein in mammalian plasmid in HEK293 cells. The CD94/NKG2A heterodimers specifically recognize Qdm/Qa1b pMHCs to form complexes [30]. Another ligand containing a different peptide, GroEL (refolded in Qa-1<sup>b</sup> similar to Qdm) [31, 32] was used as negative control. Plasmid construct was a generous gift of AbeXXa Biologics Inc., while Dr. Weidanz's group made the Qdm ligand (45 kDa) and the receptors (~ 150 kDa) in-house.

## Sample Preparation

NK receptor molecules were mixed with Qdm/Qa-1<sup>b</sup> and GroEL/Qa-1<sup>b</sup> ligands to create specific and non-specific binding mixtures respectively. Stock solutions of proteins were created with equal proportions of antibody (NK receptor, 1200 nM) and antigens (Qdm or GroEL, 1200 nM) were incubated over ice for 30 minutes. These mixtures were diluted in a KCl electrolyte (pH 7.4, 150 mM) to achieve dilutions of 600 nM to 10 nM range. 70  $\mu$ l of sample solution was dispensed onto the *cis* reservoir of the sensor. The *trans* reservoir was filled with 1.5 ml of 7.4 pH, 150 mM KCl solution.

## Experimental Data Acquisition and Analysis

The detected optical (photodiode) and electrical (Axopatch 200 B) signals were processed as patch-clamp data through an Axon Digidata 1440 ADC connected to a computer, where Axon pCLAMP 10.6 software was used for data acquisition, recording and analysis. Optical signals were recorded as changes in transmission amplitude proportional to the size of the particle in the optical trap. The optical modality metrics calculated from the optical signals were percentage change in the optical amplitude (optical step change) from the baseline and the total trapping duration (optical trap time) of that particle. Electrical signals were recorded as changes in the ionic current proportional to the charge and volume of the particles. The electrical modality metrics calculated from the concurrent ionic current traces were drop in current amplitude from the baseline (translocation current) and the transit duration from the full width half-maximum (FWHM) of the current drop for every event (translocation time). These concurrent bimodal metrics were used to characterize the protein interactions.

Qdm antigen and NK receptor antibody mixtures were evaluated for any statistical differences in the optical and electrical metrics derived from the bimodal traces as a function of concentration. Equimolar concentrations of 600 nM, 300 nM, 100 nM and 10 nM were used for both ligands and receptors. Statistical significance was evaluated for all of the six possible pairwise comparisons between the above-mentioned solution concentrations using a two-tailed unequal variance t-test for the optical (step change, trap time) and electrical (translocation current, translocation time) metrics (where  $p = 0.05$ ). The differences between specific (Qdm and NK receptor) and non-specific binding events for all bimodal data types at each concentration were evaluated through two-tailed unequal variance t-tests for all concentrations.

The Qdm-NK receptor mean lifetime of binding interactions was estimated from the average duration of time traces that had optical step change values above the threshold for ligand or receptor alone. The dissociation rate constant ( $k_{\text{off}}$ ) for ligand-receptor interactions was then determined as  $k_{\text{off}} = 1/(\text{mean lifetime})$ . Optical trap durations were compared for statistical differences between specific and non-specific binding using two tailed unequal variance t-tests ( $p < 0.05$ ).

## RESULTS

Figures 2(a)-2(c) show typical concurrent bimodal molecular signatures for a binding event of NK receptor to Qdm ligand in an equimolar 600 nM mixture. Figure 2(a) shows optical time-series data for a NK receptor that was initially trapped at the DNH (Region A) causing an optical step change of 3.71% and after about 8 s a Qdm ligand is attached to the receptor (Region B) resulting in a total step change of 5.54%. In the total optical trap time of the ligand-receptor complex (12.47 s), the ligand was bound only for a short duration (~2 s) before leaving the trap and translocating through the nanopore (Region C). The step change in optical transmission coincided with a positive peak in ionic current (Region A, Figure 2(b)) as the receptor was trapped by the DNH, near the nanopore. The subsequent high-frequency charge transients just before Region B in Figure 2(b) are attributed to the initial approach of the ligand into the optical trap, while the higher amplitude transients within Region B are attributed to the bound ligand-receptor complex. The occurrence of these transients has also been reported in our previous work characterizing the SANE sensor with dielectric nanoparticles [23], where it was interpreted to be a result of the opposing electric bias and optical trap forces that caused bobbing at similar frequencies before the particle stabilized over the nanopore. When the electrical signal was filtered

using a low-pass 20 Hz filter a small positive spike was discernible in Region B of Figure 2(c), indicating the charge added by the ligand when it bound to the receptor, as seen in the concurrent increase in the optical step. High frequency charge transients began once again at the start of Region C in Figure 2(b), near the end of the bound complex duration, indicating the imminent escape of the complex components from the optical trap and the overtaking of the electric field bias that forced their translocation through the nanopore.

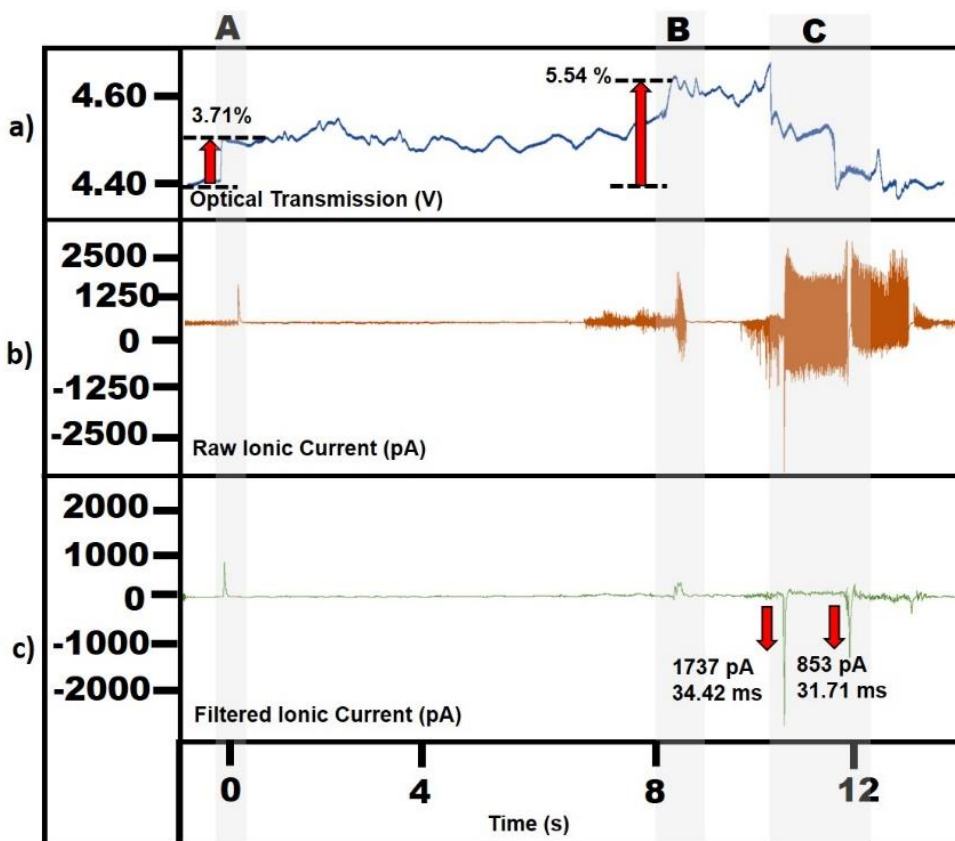


Figure 2: Time traces of an event from NK receptor and Qdm ligand mixture. (a) Optical transmission, (b) Raw ionic Current, (c) Filtered Ionic current for a single receptor and ligand binding.



Interestingly, two separate translocation events were observed in Region C, one likely due to the ligand (1737 pA) first, followed by one due to the receptor (853 pA). It would appear that once unbinding occurred, the higher charge ligand experienced higher electrophoretic mobility and translocated first, followed by the lower charge receptor. Optical step change reductions in Region C or Figure 2(a) are concurrent with the electrical translocation spikes in current for these events. High-frequency charge transients persisted even after the receptor translocation, past Region C, indicating that the optical trap still kept that receptor in the vicinity of the nanopore even after translocation and eventually these oscillations end after a few seconds as seen at the end of the trace in Figure 2(b).

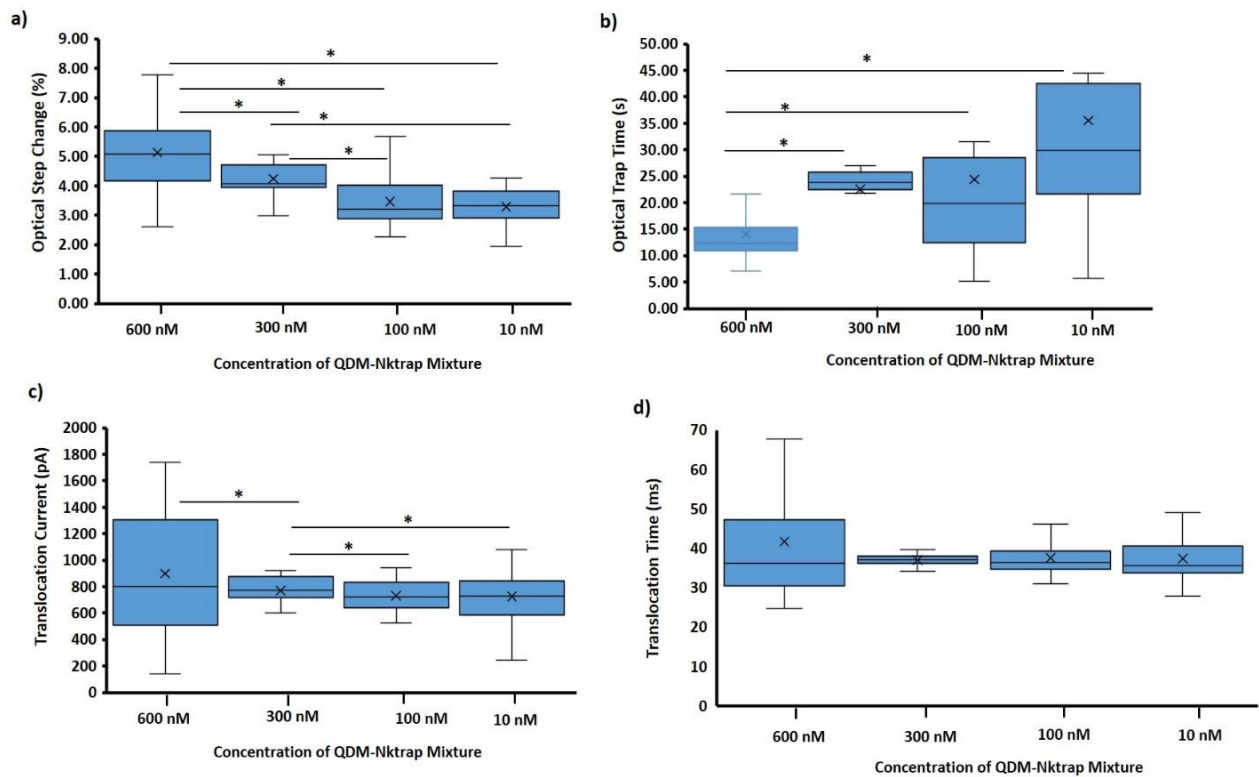


Figure 3: Box plot, demonstrating significant differences between the mean values for NK receptor and Qdm ligand mixtures for different data types. An equal proportion of receptor and ligand mixture at 1200 nM was diluted to 600 nM, 300 nM, 100 nM and 10 nM. \*p<0.05.

To investigate if there is any effect of concentration of mixtures on the molecular interactions, the optical (step change, trapping time) and electrical metrics (translocation current, nanopore translocation time) were acquired for different dilutions of the ligand and receptor mixtures and compared for their significant statistical differences using a two-tailed unequal variance t-test. Figures 3(a)-3(b) show comparison of optical metrics as box plots. Optical step change measurements clearly distinguished ( $p < 0.05$ ) all groups except between 100 nM & 10 nM ( $p = 0.50$ ). Optical step change was significantly different only for pairs formed with 600 nM concentration. The mean value trends reported for optical step change (decreasing) and optical trapping time (increasing) were opposite as a function of decreasing concentration. Figures 3(c)-3(d) report the electrical characteristics of these molecules at different concentrations. Translocation current was significantly different between 600 nM & 300 nM, and all pairs of 300 nM. Translocation time was not statistically distinguishable among the mixture concentrations.

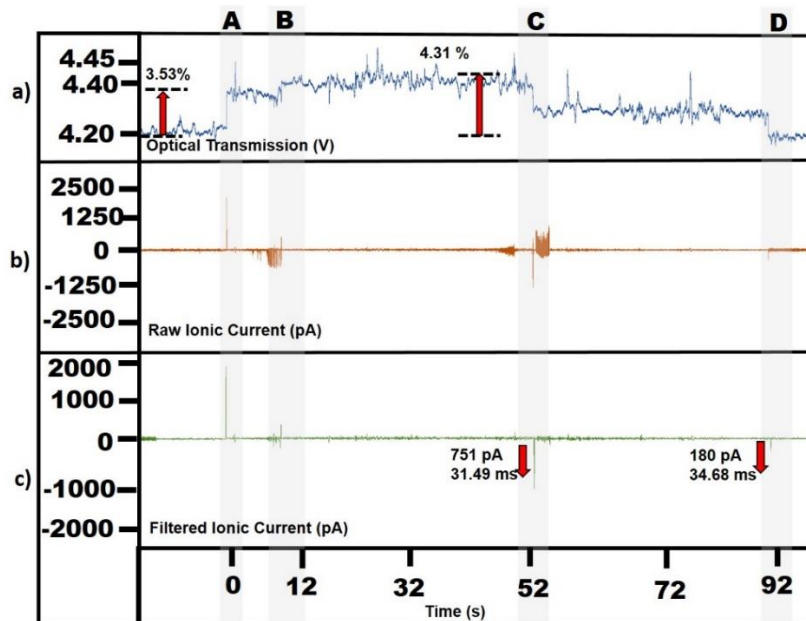


Figure 4: Time traces of an event from NK receptor and Qdm ligand mixture. (a) Optical transmission, (b) Raw ionic Current, (c) Filtered Ionic current for a single receptor and ligand binding.

In separate experiments, mixtures of irrelevant ligand (GroEL) were mixed with receptor (NK receptor) to evaluate whether the SANE sensor could differentiate non-specific interactions from the specific binding events of NK receptor with Qdm ligand observed in the prior experiments. Equimolar mixtures of GroEL and NK receptor were prepared at 600 nM, 300 nM, 100 nM and 10 nM. Figure 4 shows a typical time trace of such an event at 600 nM. Figure 4(a) shows the optical metrics (3.53% first step and total 4.31 %, 91.75 s) and Figure 4 (b) shows the raw ionic current. The translocation metrics (751 pA , 31.49 ms and 180 pA, 34.68 ms) was revealed after applying a low-pass 20 kHz filter in Figure 4(c).

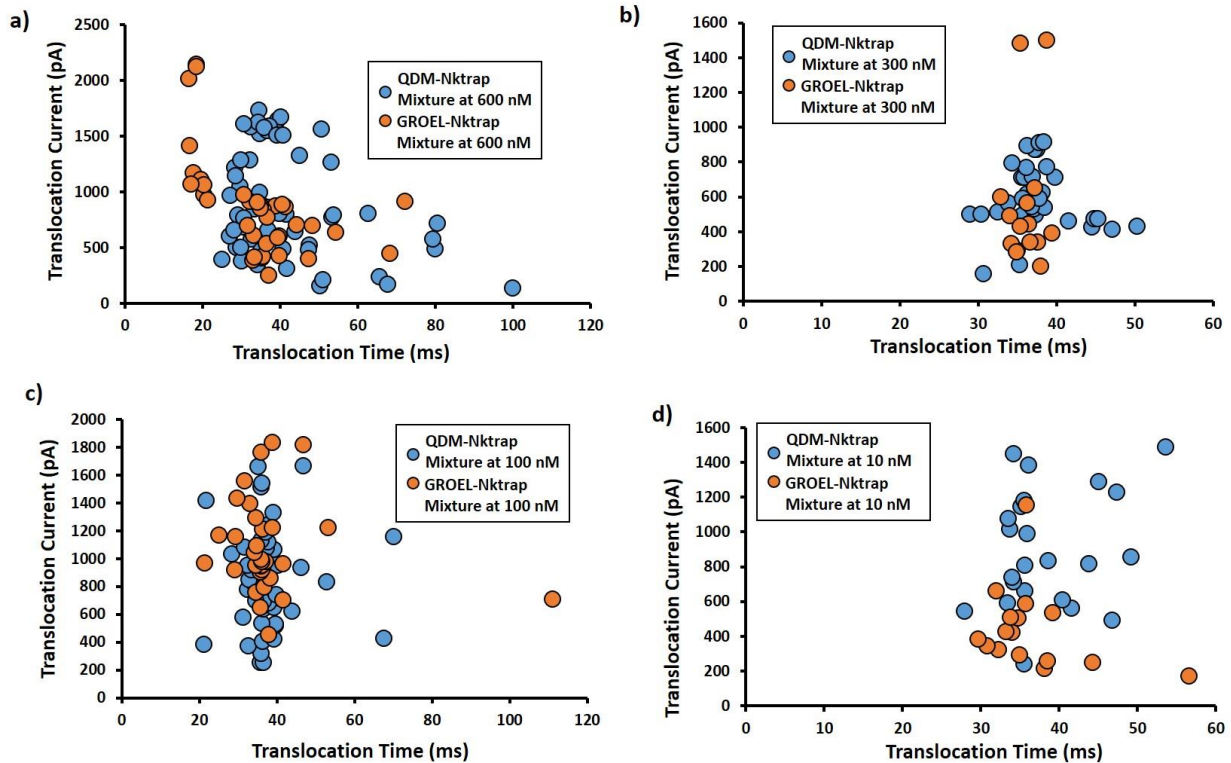


Figure 5: Event density plots comparing of the specific mixture (Qdm-NK receptor) with non-specific mixture (GroEL-NK receptor) based on electrical metrics alone.

Figures 5(a)-5(d) compare the electrical metrics of Qdm-NK receptor (blue circles) and GroEL -NK receptor (orange circles) mixtures at 600 nM, 300 nM, 100 nM and 10 nM. The translocation current was statistically distinguishable at the lower concentrations of 100 nM and 10 nM with no difference at 600 nM ( $p = 0.80$ , Figure 5(a)) and 300 nM ( $p = 0.69$ , Figure 5(b)). The translocation time was statistically different for the specific and non-specific groups only at 600 nM (Figure 5(a)) concentration and no difference at other concentrations ( $p = 0.10, 0.90, 0.32$  at 300 nM, 100 nM and 10 nM respectively). Majority of specific binding events are seen above  $\sim 400$  pA at 10 nM (Figure 5(d)). As the mixture concentration decreases in Figures 5(a)-5(d) a switch is seen in the data trends for translocation time where the specific complexes have higher values at higher concentrations compared to the non-specific mixture events (Figure 5(b)), but lower values at lower concentrations (Figure 5(d)).

As the electrical metric plots in Figures 5(a)-5(d) did not yield statistically significant separation between specific binding and non-specific interaction events, the metric of optical trapping time was also plotted against translocation current to test whether it could improve specific event discrimination. We did not add optical step change into these comparisons because optical step change was significantly different only at 600 nM, with other concentrations having no significant difference ( $p = 0.67, 0.17, 0.32$  at 300 nM, 100 nM and 10 nM respectively). Figures 6(a)-6(d) show data for these bimodal metrics for the same mixture concentrations. Optical trapping time was significantly different across all concentrations. A similar trend was observed as in Figure 5, where at the lowest mixture concentration of 10 nM a reversal in relative optical trapping times was observed, with the non-specific mixture reducing in values, consistent with our hypothesis of reduced level of non-specific mixture agglomeration. These results indicate the

multi-dimensional data metric analyses may be needed to improve the discrimination of specific binding events.

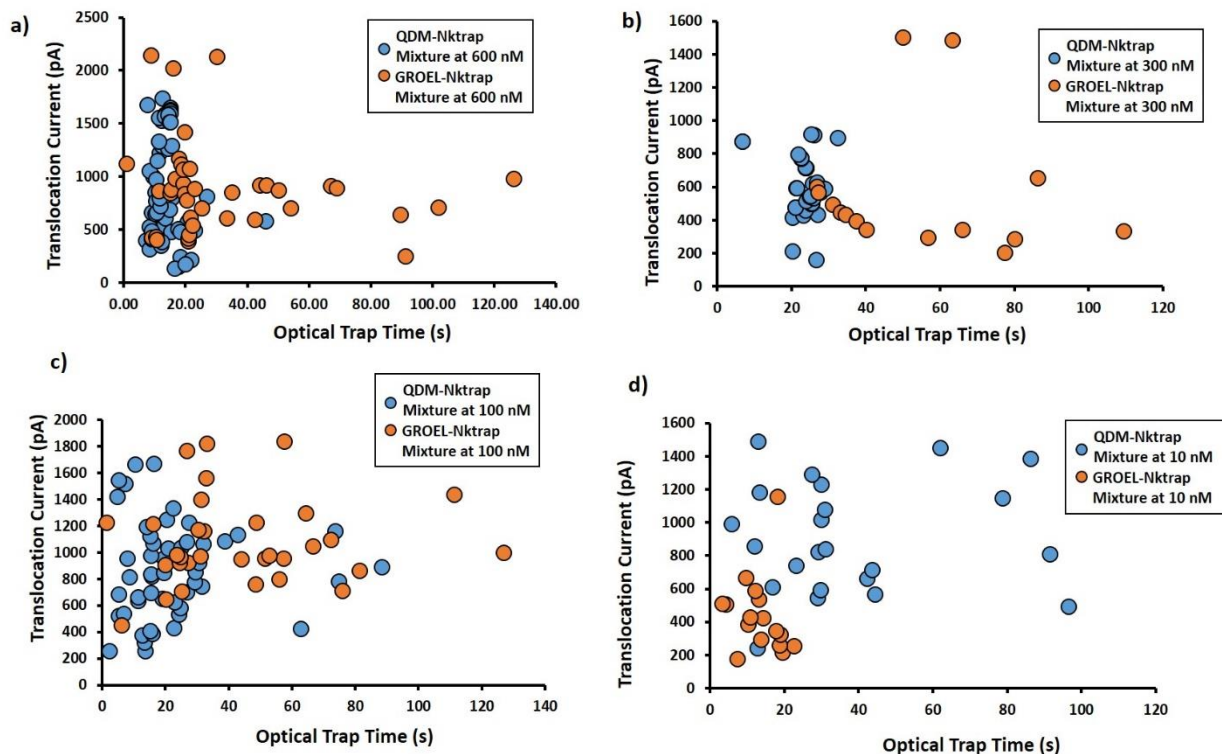


Figure 6: Event density plots comparing the specific mixture (Qdm-NK receptor) with non-specific mixture (GroEL-NK receptor) based on combined electrical and optical metrics.

The ability to measure the duration Qdm-NK receptor binding events with the SANE sensor, also enabled the estimation of a mean binding time averaged over all detected events, which in turn enabled estimation of a Koff value for this interaction. The binding duration corresponds to the mean lifetime of the ligand-receptor interaction. Figure 7(a) shows a typical optical signature of a specific binding event, where the entry of ligand can be seen as rise in optical amplitude (Region B) above the existing optical step change (Region A). Qualitatively similar step changes were observed in the non-specific mixtures (Figure 7 (b)), but we attribute those to mass loading

of agglomerates entering and leaving the optical trap. Figure 7(c) shows average binding duration as a box plot for specific binding of Qdm to NK trap receptor and non-specific binding of GroEL receptor. The results show a statistically significant difference ( $p < 0.01$ ) between specific and non-specific events, where binding durations extracted from the optical data were pooled from experiments across all concentrations. The mean value of binding duration for specific binding was  $4.54 \pm 2.62$  s and  $k_{\text{off}}$  approximately between  $0.14 - 0.52$   $\text{s}^{-1}$ , which is closer to the reported  $k_{\text{off}}$  value of  $0.42$   $\text{s}^{-1}$  for an analogous human pMHC (HLA-E, ref).

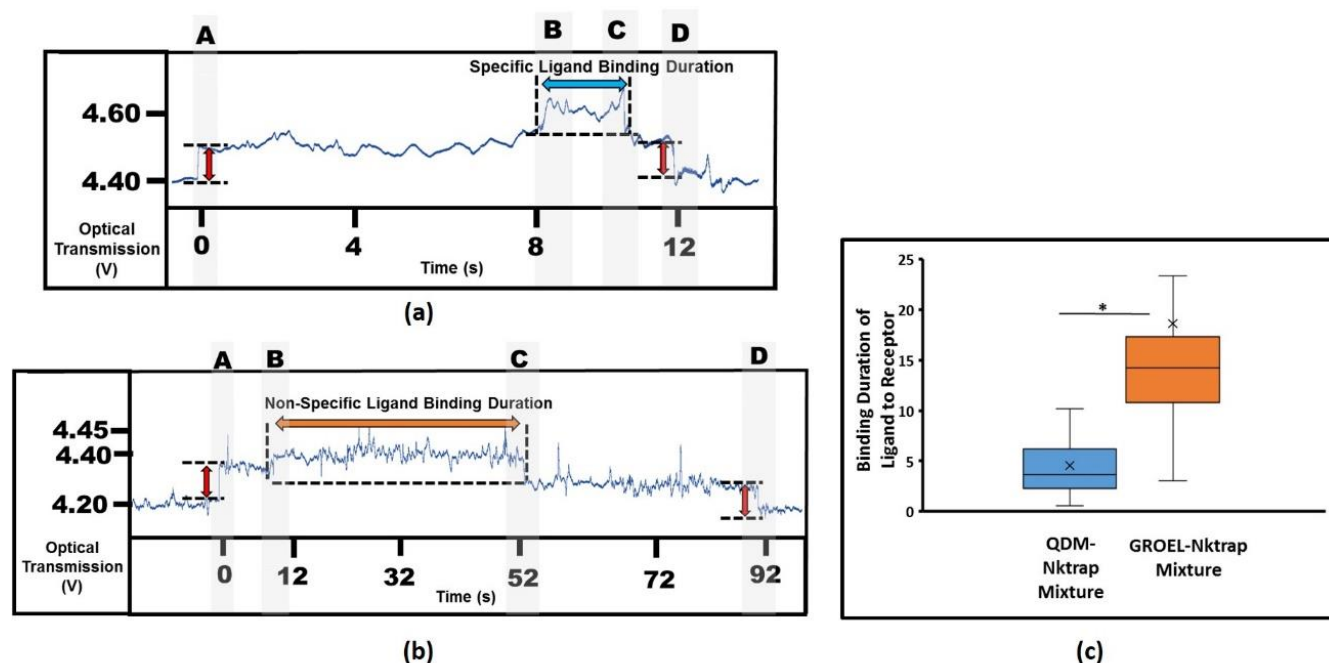


Figure 7 (a): Detection of binding duration for NK receptor- Qdm ligand complex. (b) Detection of binding duration for NK receptor- GroEL ligand complex (b): Box plot, ligand-receptor interaction duration,  $k_{\text{off}} = 1/(\text{mean residence time})$ ,  $*p < 0.01$ .

## DISCUSSION

This work presents the use of a bimodal optical-electrical SANE sensing technique to differentiate complexes as specific or non-specific based on whether a relevant or an irrelevant ligand was interacting with the receptors. Optical data (optical amplitude change and trapping duration) and electrical data (current drop amplitude and translocation time) was recorded to differentiate between these types of interactions. Figure 2 and Figure 4 show the time traces with for both binding conditions. Non-specific binding (Figure 4(a)) had lower optical step change than specific binding (Figure 2(a)). This difference was statistically significant only at 600 nM mixture probably due to the greater availability of specific ligands at higher concentrations that allow for multiple bound complexes. Other mixtures did not show any statistically significant difference for optical step change. The optical trapping time is longer for non-specific binding at 600 nM concentration due to likely agglomerate formation (Figure 6(a)). This behavior was completely opposite at 10 nM according to our hypothesis of reduction in agglomeration (Figure 6(d)). The mean value of translocation current for specific binding events did not change significantly between mixture concentrations at 600 nM ( $p = 0.80$ , Figure 5(a)) and 300 nM ( $p=0.69$ , Figure 5(a)). At 100nM (Figure 5(c)) the mean translocation current of specific binding was lower than non-specific binding. At 10 nM (Figure 5(d)) it was the opposite trend (Figure 5(d)). It is hypothesized that the observed trend reversal occurred due to reduced agglomerate formation in the non-specific mixture with decreasing concentration (Figure 6 (d)). The translocation time was significantly higher for specific binding at 600 nM only. Other mixtures did not show any significant difference for translocation time. The lack of a clear trend across the concentrations or data types could possibly be due the availability of the binding molecules, influence of the total

charge of the molecules and the laser induced surface charge effects. Multi-dimensional data metric analyses can be used to improve the discrimination of events in these binding conditions. This work presents with a method to measure kinetics of interaction between low affinity ligands and NK cell inhibitory receptors. Weak affinities lead to fast association and dissociation kinetics which is difficult to detect in an optical plasmon resonance system [33]. It is previously reported, fast translocation times for antigen-antibody complexes make it difficult to be detected through nanopores [37]. Optically, the molecules can be trapped for prolonged times, limiting the detection of these interactions [17, 38]. Using the SANE sensor to study the Qdm-NK receptor interactions, the mean binding duration of ligand and receptor binding (Figure 2 (a), Region B) was estimated from the optical transmission signals, which led to the estimation of  $k_{off}$ . It is likely that the bound complex gets pulled by the optical field gradient [39] (Figure 2(a), Region C) while it is forced to translocate. It is possible that this pulling effect could increase the apparent  $k_{off}$  value compared to bulk solution conditions. However, the comparison with  $k_{off}$  measured by plasmon resonance in another study indicates that this effect may not be significant [40, 41]. Figure 7(a) shows shorter binding duration of the Qdm ligand to the NK receptor compared to the GroEL ligand (Figure 7 (b)). The inverse value of this mean binding time is equivalent to the  $k_{off}$  and our estimation is comparable to the reported value from another study [34].



## **CONCLUSION**

We have demonstrated the feasibility of using the bimodal SANE sensor to quantify low affinity kinetics between specific ligand-receptor interactions and discriminate from irrelevant ligand binding. Optical and electrical metrics from the concurrent bimodal signals were used to differentiate specific from non specific binding. Qdm ligand and NK receptor mixture was used to show specific ligand and receptor binding. GroEL ligand and NK receptor mixture was used to show non-specific binding. Different dilutions of the mixtures were made to compare the effect of concentration of binding molecules on the optical and electrical metrics and estimate the event detection limit of the SANE sensor. Multi-dimensional analysis of the data types and ionic current power spectrum analysis would improve the separation of specific from non-specific binding. We were able to show possible agglomeration of non-specific molecules through prolonged optical trapping times at higher concentrations and a reverse in the trend at lower concentrations due to reduction of this agglomeration. Our results indicated a possibility of estimating dissociation rate kinetics ( $k_{\text{off}}$ ) for low affinity and fast kinetic rates molecules comparable to reported values. With further characterization the SANE sensor can be used as a potential screening tool for immunotherapeutic receptor-ligand interactions.

## **ACKNOWLEDGEMENTS**

We thank Mr. Soeren Eyhusen and Mr. Chuong Huynh for permitting us with the access and providing technical guidance on focused ion beam milling at the Zeiss ORION NanoFab facility in Peabody, MA. We are also thankful to all the engineers and staff at the Shimadzu Institute Nanotechnology Research Center at the University of Texas at Arlington for their support

and guidance. This work was supported through a Pilot Research Program for Interdisciplinary Collaboration funded by the Vice-President of Research Office of the University of Texas at Arlington.

## REFERENCES

- [1] Spitzberg J D, Zreben A, van Kooten X F and Meller A 2019 Plasmonic-Nanopore Biosensors for Superior Single-Molecule Detection *Advanced Materials* 1900422
- [2] Neuman K C and Nagy A 2008 Single-molecule force spectroscopy: optical tweezers, magnetic tweezers and atomic force microscopy *Nature methods* **5** 491
- [3] Dekker C 2007 Solid-state nanopores *Nature nanotechnology* **2** 209
- [4] Ilyas A, Asghar W, Allen P B, Duhon H, Ellington A D and Iqbal S M 2012 Electrical detection of cancer biomarker using aptamers with nanogap break-junctions *Nanotechnology* **23** 275502
- [5] Yuan Z, Wang C, Yi X, Ni Z, Chen Y and Li T 2018 Solid-State Nanopore *Nanoscale research letters* **13** 56
- [6] Trenevskaya I, Li D and Banham A H 2017 Therapeutic Antibodies against Intracellular Tumor Antigens *Frontiers in Immunology* **8**
- [7] Butler T Z, Pavlenok M, Derrington I M, Niederweis M and Gundlach J H 2008 Single-molecule DNA detection with an engineered MspA protein nanopore *Proceedings of the National Academy of Sciences* **105** 20647-52
- [8] Shi W, Friedman A K and Baker L A 2016 Nanopore sensing *Analytical chemistry* **89** 157-88
- [9] Larkin J, Henley R Y, Muthukumar M, Rosenstein J K and Wanunu M 2014 High-bandwidth protein analysis using solid-state nanopores *Biophysical journal* **106** 696-704
- [10] Fologea D, Ledden B, McNabb D S and Li J 2007 Electrical characterization of protein molecules by a solid-state nanopore *Applied physics letters* **91** 053901
- [11] Smeets R M, Keyser U F, Krapf D, Wu M-Y, Dekker N H and Dekker C 2006 Salt dependence of ion transport and DNA translocation through solid-state nanopores *Nano letters* **6** 89-95
- [12] Freedman K J, Haq S R, Edel J B, Jemth P and Kim M J 2013 Single molecule unfolding and stretching of protein domains inside a solid-state nanopore by electric field *Scientific reports* **3** 1638

- [13] Gershow M and Golovchenko J A 2007 Recapturing and trapping single molecules with a solid-state nanopore *Nature nanotechnology* **2** 775
- [14] Kowalczyk S W, Hall A R and Dekker C 2009 Detection of local protein structures along DNA using solid-state nanopores *Nano letters* **10** 324-8
- [15] Plesa C, Kowalczyk S W, Zinsmeister R, Grosberg A Y, Rabin Y and Dekker C 2013 Fast translocation of proteins through solid state nanopores *Nano letters* **13** 658-63
- [16] Talaga D S and Li J 2009 Single-molecule protein unfolding in solid state nanopores *Journal of the American Chemical Society* **131** 9287-97
- [17] Pang Y and Gordon R 2011 Optical trapping of a single protein *Nano letters* **12** 402-6
- [18] Pang Y and Gordon R 2011 Optical trapping of 12 nm dielectric spheres using double-nanoholes in a gold film *Nano letters* **11** 3763-7
- [19] Kumar L, Lesuffleur A, Hughes M and Gordon R 2006 Double nanohole apex-enhanced transmission in metal films *Applied Physics B* **84** 25
- [20] Jonsson M P and Dekker C 2013 Plasmonic nanopore for electrical profiling of optical intensity landscapes *Nano letters* **13** 1029-33
- [21] Li Y, Nicoli F, Chen C, Lagae L, Groeseneken G, Stakenborg T, Zandbergen H W, Dekker C, Van Dorpe P and Jonsson M P 2014 Photoresistance switching of plasmonic nanopores *Nano letters* **15** 776-82
- [22] Nicoli F, Verschueren D, Klein M, Dekker C and Jonsson M P 2014 DNA translocations through solid-state plasmonic nanopores *Nano letters* **14** 6917-25
- [23] Raza M U, Peri S S S, Ma L-C, Iqbal S M and Alexandrakis G 2018 Self-induced back action actuated nanopore electrophoresis (SANE) *Nanotechnology* **29** 435501
- [24] Shi X, Verschueren D, Pud S and Dekker C 2018 Integrating Sub-3 nm Plasmonic Gaps into Solid-State Nanopores *Small* **14** 1703307
- [25] Shi X, Verschueren D V and Dekker C 2018 Active Delivery of Single DNA Molecules into a Plasmonic Nanopore for Label-Free Optical Sensing *Nano letters* **18** 8003-10
- [26] Verschueren D, Shi X and Dekker C 2019 Nano-Optical Tweezing of Single Proteins in Plasmonic Nanopores *Small Methods* 1800465

- [27] Verschuereen D V, Pud S, Shi X, De Angelis L, Kuipers L and Dekker C 2018 Label-Free Optical Detection of DNA Translocations through Plasmonic Nanopores *ACS nano*
- [28] Brooks A G, Posch P E, Scorzelli C J, Borrego F and Coligan J E 1997 NKG2A complexed with CD94 defines a novel inhibitory natural killer cell receptor *Journal of Experimental Medicine* **185** 795-800
- [29] Vance R E, Kraft J R, Altman J D, Jensen P E and Raulet D H 1998 Mouse CD94/NKG2A is a natural killer cell receptor for the nonclassical major histocompatibility complex (MHC) class I molecule Qa-1b *Journal of Experimental Medicine* **188** 1841-8
- [30] Kraft J R, Vance R E, Pohl J, Martin A M, Raulet D H and Jensen P E 2000 Analysis of Qa-1b Peptide Binding Specificity and the Capacity of Cd94/Nkg2a to Discriminate between Qa-1–Peptide Complexes *Journal of Experimental Medicine* **192** 613-24
- [31] Lo W-F, Ong H, Metcalf E S and Soloski M J 1999 T cell responses to Gram-negative intracellular bacterial pathogens: a role for CD8+ T cells in immunity to Salmonella infection and the involvement of MHC class Ib molecules *The Journal of Immunology* **162** 5398-406
- [32] Lo W-F, Woods A S, DeCloux A, Cotter R J, Metcalf E S and Soloski M J 2000 Molecular mimicry mediated by MHC class Ib molecules after infection with gram-negative pathogens *Nature medicine* **6** 215
- [33] Kaiser B K, Barahmand-pour F, Paulsene W, Medley S, Geraghty D E and Strong R K 2005 Interactions between NKG2x immunoreceptors and HLA-E ligands display overlapping affinities and thermodynamics *The Journal of Immunology* **174** 2878-84
- [34] Valés-Gómez M, Reyburn H T, Erskine R A, López-Botet M and Strominger J L 1999 Kinetics and peptide dependency of the binding of the inhibitory NK receptor CD94/NKG2-A and the activating receptor CD94/NKG2-C to HLA-E *The EMBO journal* **18** 4250-60
- [35] Ghorbanzadeh M, Jones S, Moravvej-Farshi M K and Gordon R 2017 Improvement of sensing and trapping efficiency of double nanohole apertures via enhancing the wedge plasmon polariton modes with tapered cusps *ACS Photonics* **4** 1108-13
- [36] Garboczi D N, Hung D T and Wiley D C 1992 HLA-A2-peptide complexes: refolding and crystallization of molecules expressed in Escherichia coli and complexed with single antigenic peptides *Proceedings of the National Academy of Sciences* **89** 3429-33

- [37] Han A, Creus M, Schürmann G, Linder V, Ward T R, De Rooij N F and Stauffer U 2008 Label-free detection of single protein molecules and protein– protein interactions using synthetic nanopores *Analytical chemistry* **80** 4651-8
- [38] Kotnala A, DePaoli D and Gordon R 2013 Sensing nanoparticles using a double nanohole optical trap *Lab on a Chip* **13** 4142-6
- [39] Juan M L, Gordon R, Pang Y, Eftekhari F and Quidant R 2009 Self-induced back-action optical trapping of dielectric nanoparticles *Nature Physics* **5** 915
- [40] Lin J J, Low-Nam S T, Alfieri K N, McAfee D B, Fay N C and Groves J T 2019 Mapping the stochastic sequence of individual ligand-receptor binding events to cellular activation: T cells act on the rare events *Sci. Signal.* **12** eaat8715
- [41] Yousefi O S, Guenther M, Hoerner M, Chalupsky J, Wess M, Brandl S M, Smith R W, Fleck C, Kunkel T and Zurbriggen M D 2019 Optogenetic control shows that kinetic proofreading regulates the activity of the T cell receptor *eLife* **8** e42475

## CHAPTER 5

### CONCLUSION

In this work, we demonstrated methods for design and fabrication of a bimodal optical-electrical sensor for single molecule detection and analysis. The Self-Induced Back-Action (SIBA) Actuated Nanopore Electrophoresis (SANE) Sensor is a combination of Solid-State Nanopore (SSNP) and a double nanohole (DNH) metallic nanoaperture for electrical and optical characterization of nanoparticles and biomolecules. Chapter 2 in this dissertation describes the design and fabrication of the SANE sensor on a metal-dielectric membrane in a silicon substrate with the SSNP and DNH nanostructures milled using a focused ion beam (FIB) tool. The sensor successfully trapped dielectric and metallic nanoparticles for multiple seconds at the DNH and translocated them through the SSNP while recording concurrent optical and electrical metrics for each event. We differentiated single and multiple particle trapping using frequency analysis of ionic current oscillations. This work also showed a possible method to estimate charges on individual nanoparticles.

In chapter 3, the SANE sensor's ability to study biomolecular interactions was demonstrated by detection of interactions between cancer specific TCR-like monoclonal antibodies and peptide presenting surface ligands. Baseline experiments helped quantify the optical and electrical metrics of individual RAH antigen and Anti-RAH antibody molecules as well as identify specifically bound antigen-antibody complexes in a mixture. A possible antibody bivalent binding was detected from the acquired data. An irrelevant antibody Anti-WNV was used as negative control to demonstrate the capability of the SANE sensor to distinguish specific and non-specific binding. An interesting result in this work was the possibility of calculation of bound

fraction of the antigen-antibody interaction. The bound fraction was significantly enhanced in the SANE sensor compared to a value estimated from the surface-immobilized binding kinetics of a commercial Resonant Sensor system. These results demonstrated SANE sensor as a potential screening tool to investigate antibody-ligand interactions using minimal protein material.

In chapter 4, we quantified the low affinity binding kinetics between a cancer specific ligand and a soluble recombinant NK receptor as well as distinguish them from non-specific binding using the optical and electrical metrics derived from concurrent bimodal signatures of the SANE sensor. Qdm ligand was shown to specifically bind to CD94/NKG2A NK receptor and GroEL ligand was used as a negative control. We tested for the event detection limit of the sensor by reducing the concentration of ligand and receptor mixtures and measured their statistical differences. An interesting outcome in this work is the possibility for estimation of fast (sub-second to seconds) dissociation rate kinetics ( $k_{off}$ ) for low affinity interactions and achieving results comparable to reported values attained with commercial assays.

All the experiments were performed with different SANE sensors on different days demonstrating the repeatability of this single molecule characterization work. Multi-dimensional analysis of the optical and electrical metrics as well as power spectrum analysis of ionic current will enhance the power of data analysis for better discrimination of biomolecules. This sensor has the potential to screen immunotherapeutic antibody-ligand interactions label-free at the single molecule level. A future vision would be to have an array of SANE sensors on a chip integrated with microfluidics so as to achieve higher throughput screening of molecular interactions. This novel technology could possibly find application in the identification of which pMHCs expressed by cancer cells are targeted by T-cell receptors or high-affinity biologics and thus help guide personalized immunotherapy.

# APPENDIX 1

## PERMISSION FROM PUBLISHERS AND AUTHORS

### Chapter 2- Permission from Publisher

5/12/2019

Mail - Peri, Sai Santosh Sasank - Outlook

**Re: Request for written approval of using published article (NANO-117791.R1) for PhD dissertation**

Permissions <permissions@iopublishing.org>

Tue 3/19/2019 11:13 AM

To: Peri, Sai Santosh Sasank <saisantoshsasank.peri@mavs.uta.edu>

Cc: Nano <nano@iopublishing.org>

Dear Sai Santosh Sasank Peri,

Thank you for your request to reproduce content from <https://iopscience.iop.org/article/10.1088/1361-6528/aad7d1>

The content you have requested was published under a [CC BY](#) licence which permits reuse for any purposes, even commercial, provided the licence terms are adhered to.

Therefore you may reuse the content without permission, so long as you reference it adequately and adhere to the terms of the CC BY licence.

Please note this does not apply to any content/figure which is credited to another source in our publication or has been obtained from a third party, which is not available under a suitable open access licence. Express permission for such content/figures must be obtained from the copyright owner.

Kind regards,  
Christina

#### Copyright & Permissions Team

Gemma Alaway – Senior Rights & Permissions Adviser

Christina Colwell - Rights & Permissions Assistant

#### Contact Details

E-mail: [permissions@iop.org](mailto:permissions@iop.org)

For further information about copyright and how to request permission:

<https://publishingsupport.iopscience.iop.org/copyright-journals/>

See also: <https://publishingsupport.iopscience.iop.org/>

Please see our Author Rights Policy <https://publishingsupport.iopscience.iop.org/author-rights-policies/>

**Please note:** We do not provide signed permission forms as a separate attachment. Please print this email and provide it to your publisher as proof of permission.

**Please note:** Any statements made by IOP Publishing to the effect that authors do not need to get permission to use any content where IOP Publishing is not the publisher is not intended to constitute any sort of legal advice. Authors must make their own decisions as to the suitability of the content they are using and whether they require permission for it to be published within their article.

---

<https://outlook.office.com/mail/search/id/AAQkADAyOGU1OWQwLTgzMzgtNDI4Ni05Y2QzLWUyMDIyOGZhY2M3OAAQAJKwLsJ6htf9Qqe5HM0xOM...> 1/2



## Chapter 2- Permission from Publisher

5/12/2019

Mail - Peri, Sai Santosh Sasank - Outlook

**From:** Peri, Sai Santosh Sasank <saisantosh.sasan.peri@mavs.uta.edu>  
**Sent:** 18 March 2019 16:51  
**To:** Nano  
**Cc:** Nanotechnology  
**Subject:** Request for written approval of using published article (NANO-117791.R1) for PhD dissertation

Dear IOP Nanotechnology Team,

I am a PhD Candidate in Electrical Engineering department at University of Texas at Arlington (UTA), Arlington, Texas. I am graduating this spring semester and currently working on my dissertation.

We published an article "Self-induced back action actuated nanopore electrophoresis (SANE)" in your journal on 21 August, 2018, Volume 29, Number 43.

I would like to request your written permission to use the article in my dissertation as I am an equal author on this article.

We have a style called "article-based" dissertation, in our university, UT Arlington, which allows us to use the published article as it is for our dissertation without need to re-write it. For this, I require your permission letter that I need to attach it along with my dissertation.

Kindly accept my request and provide me an approval in my name:  
First name: Sai Santosh Sasank  
Last name : Peri

Let me know if you need any further information.

Thank you,  
Sai Santosh Sasank Peri

---

As part of some systems improvements we're making in February and March 2019, IOP Publishing email addresses will change from @iop.org to @iopublishing.org, except those of our legal and finance teams, which will switch to @ioplegal.org and @iopfinance.org respectively.

This email (and attachments) are confidential and intended for the addressee(s) only. If you are not the intended recipient please immediately notify the sender, permanently and securely delete any copies and do not take action with it or in reliance on it. Any views expressed are the author's and do not represent those of IOPP, except where specifically stated. IOPP takes reasonable precautions to protect against viruses but accepts no responsibility for loss or damage arising from virus infection. For the protection of IOPP's systems and staff, emails are scanned automatically.

**IOPP Publishing Limited**

Registered in England under Registration No 00467514.

Registered Office: Temple Circus, Bristol BS1 6HG England

Your privacy is important to us. For information about how IOPP uses your personal data, please see our [Privacy Policy](#).

<https://outlook.office.com/mail/search/id/AAQkADAyOGU1OWQwLTgzMzgtNDI4Ni05Y2QzLWUyMDIyOGZhY2M3OAAQAJKwLsJ6hf9Oqe5HM0xOM...> 2/2

# Chapter 3 and Chapter 4- Permissions from co-authors



## Multiple Author Release for Master's Thesis or Doctoral Dissertation

Thesis / Dissertation Writer Name: Sai Santosh Sasank Peri

Co-Author Name: Manoj K Sabnani

Title(s) of Co-Authored Work(s):

Director of Specific Instructional Support with a Self-Managed Work Arrangement/Temporary Employment (DANS) Service

---

Assistant Professor/Associate Professor/Assistant Professor/Associate Professor/Assistant Professor (AP) Service

---

---

---

---

### Co-Author Statement of Consent:

As the co-author of the above named work(s), I acknowledge the above-named thesis / dissertation writer as the primary author of the work(s) listed above. I authorize the thesis / dissertation writer named above to use the listed work(s) in their thesis / dissertation. I further agree that the thesis / dissertation writer may use this work to comply with requirements for graduation.

Co-Author Signature: 

Date: 05/10/2019

**Please maintain a copy of this completed form for your records.**

You may be entitled to know what information The University of Texas at Arlington (UT Arlington) collects concerning you. You may review and have UT Arlington correct this information according to procedures set forth in UTS 139. The law is found in sections 552.021, 552.023 and 559.004 of the Texas Government Code.

## Multiple Author Release for Master's Thesis or Doctoral Dissertation

Thesis / Dissertation Writer Name: Sai Santosh Sasank Peri

Co-Author Name: Muhammad Usman Raza

Title(s) of Co-Authored Work(s):

Detection of Specific Antibody-Ligand Interactions with a Self-Induced Back-Action Induced Nanopore Electrode (2018) Under Review

Quantum Coherence in a Single Electron Transistor with a Self-Induced Back-Action Induced Nanopore Electrode (2018) Under Review

\_\_\_\_\_

\_\_\_\_\_

\_\_\_\_\_

\_\_\_\_\_

**Co-Author Statement of Consent:**

As the co-author of the above named work(s), I acknowledge the above-named thesis / dissertation writer as the primary author of the work(s) listed above. I authorize the thesis / dissertation writer named above to use the listed work(s) in their thesis / dissertation. I further agree that the thesis / dissertation writer may use this work to comply with requirements for graduation.

Co-Author Signature: 

Date: May 13, 2019

**Please maintain a copy of this completed form for your records.**

You may be entitled to know what information The University of Texas at Arlington (UT Arlington) collects concerning you. You may review and have UT Arlington correct this information according to procedures set forth in UTS 139. The law is found in sections 552.021, 552.023 and 559.004 of the Texas Government Code.

## **Multiple Author Release for Master's Thesis or Doctoral Dissertation**

Thesis / Dissertation Writer Name: Sai Santosh Sasank Peri

Co-Author Name: Soroush Ghaffari

Title(s) of Co-Authored Work(s):

Detection of Specific Antigen-Antibody Interactions with a Self-Induced Electro-Active Polymer Electrodeposited (SIP-EA) Sensor

Antibody-Modified Electrodeposited Polymers for the Detection of Heavy Metals (Preliminary Report)

\_\_\_\_\_

\_\_\_\_\_

\_\_\_\_\_

\_\_\_\_\_

**Co-Author Statement of Consent:**

As the co-author of the above named work(s), I acknowledge the above-named thesis / dissertation writer as the primary author of the work(s) listed above. I authorize the thesis / dissertation writer named above to use the listed work(s) in their thesis / dissertation. I further agree that the thesis / dissertation writer may use this work to comply with requirements for graduation.

Co-Author Signature: Ghaffari, Soroush Digitally signed by Ghaffari,  
Soroush  
Date: 2019.05.10 15:26:14 -0500

Date: 5.10.19

**Please maintain a copy of this completed form for your records.**

You may be entitled to know what information The University of Texas at Arlington (UT Arlington) collects concerning you. You may review and have UT Arlington correct this information according to procedures set forth in UTS 139. The law is found in sections 552.021, 552.023 and 559.004 of the Texas Government Code.



UNIVERSITY OF  
**TEXAS**  
ARLINGTON

OFFICE OF  
GRADUATE STUDIES

## Multiple Author Release for Master's Thesis or Doctoral Dissertation

Thesis / Dissertation Writer Name: Sai Santosh Sasank Peri

Co-Author Name: Susanne Gimlin

Title(s) of Co-Authored Work(s):

Detection of Specific Antibody-Ligand Interactions with a Self-Induced Back-Action Activated Nanopore Electrode (SAB) Sensor

\_\_\_\_\_  
\_\_\_\_\_  
\_\_\_\_\_  
\_\_\_\_\_  
\_\_\_\_\_

### Co-Author Statement of Consent:

As the co-author of the above named work(s), I acknowledge the above-named thesis / dissertation writer as the primary author of the work(s) listed above. I authorize the thesis / dissertation writer named above to use the listed work(s) in their thesis / dissertation. I further agree that the thesis / dissertation writer may use this work to comply with requirements for graduation.

Co-Author Signature: Susanne Gimlin

Date: 05/10/2019

**Please maintain a copy of this completed form for your records.**

You may be entitled to know what information The University of Texas at Arlington (UT Arlington) collects concerning you. You may review and have UT Arlington correct this information according to procedures set forth in UTS 139. The law is found in sections 552.021, 552.023 and 559.004 of the Texas Government Code.

## Multiple Author Release for Master's Thesis or Doctoral Dissertation

Thesis / Dissertation Writer Name: Sai Santosh Sasank Peri

Co-Author Name: Debra Wawro Weidanz

Title(s) of Co-Authored Work(s):

Detection of Specific Antigen/Antibody Interactions with a Self-Healing Electrochromic (SE) Sensor

---

---

---

---

---

**Co-Author Statement of Consent:**

As the co-author of the above named work(s), I acknowledge the above-named thesis / dissertation writer as the primary author of the work(s) listed above. I authorize the thesis / dissertation writer named above to use the listed work(s) in their thesis / dissertation. I further agree that the thesis / dissertation writer may use this work to comply with requirements for graduation.

Co-Author Signature: 

Date: May 13, 2019

**Please maintain a copy of this completed form for your records.**

You may be entitled to know what information The University of Texas at Arlington (UT Arlington) collects concerning you. You may review and have UT Arlington correct this information according to procedures set forth in UTS 139. The law is found in sections 552.021, 552.023 and 559.004 of the Texas Government Code.

## Multiple Author Release for Master's Thesis or Doctoral Dissertation

Thesis / Dissertation Writer Name: Sai Santosh Sasank Peri

Co-Author Name: Jung Soo Lee

Title(s) of Co-Authored Work(s):

Detection of Specific Antibody/Agglutination with a Self-Induced Electrokinetic Activated Nanopore Electrode (2019) Doctor

Development of a Self-Induced Electrokinetic Activated Nanopore Electrode for the Detection of Specific Antibody/Agglutination (2019) Doctor

\_\_\_\_\_

\_\_\_\_\_

\_\_\_\_\_

\_\_\_\_\_

\_\_\_\_\_

**Co-Author Statement of Consent:**

As the co-author of the above named work(s), I acknowledge the above-named thesis / dissertation writer as the primary author of the work(s) listed above. I authorize the thesis / dissertation writer named above to use the listed work(s) in their thesis / dissertation. I further agree that the thesis / dissertation writer may use this work to comply with requirements for graduation.

Co-Author Signature: 

Date: 05-10-2019

**Please maintain a copy of this completed form for your records.**

You may be entitled to know what information The University of Texas at Arlington (UT Arlington) collects concerning you. You may review and have UT Arlington correct this information according to procedures set forth in UTS 139. The law is found in sections 552.021, 552.023 and 559.004 of the Texas Government Code.

## Multiple Author Release for Master's Thesis or Doctoral Dissertation

Thesis / Dissertation Writer Name: Sai Santosh Sasank Peri

Co-Author Name: MinJun Kim

Title(s) of Co-Authored Work(s):

Detection of Specific Antigen-Antibody Interactions with a Self-Induced Electro-Acceptor (2019) Doctor

\_\_\_\_\_

\_\_\_\_\_

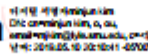
\_\_\_\_\_

\_\_\_\_\_

\_\_\_\_\_

**Co-Author Statement of Consent:**

As the co-author of the above named work(s), I acknowledge the above-named thesis / dissertation writer as the primary author of the work(s) listed above. I authorize the thesis / dissertation writer named above to use the listed work(s) in their thesis / dissertation. I further agree that the thesis / dissertation writer may use this work to comply with requirements for graduation.

Co-Author Signature: minjun kim 

Date: 05/10/2019

**Please maintain a copy of this completed form for your records.**

You may be entitled to know what information The University of Texas at Arlington (UT Arlington) collects concerning you. You may review and have UT Arlington correct this information according to procedures set forth in UTS 139. The law is found in sections 552.021, 552.023 and 559.004 of the Texas Government Code.



## Multiple Author Release for Master's Thesis or Doctoral Dissertation

Thesis / Dissertation Writer Name: Sai Santosh Sasank Peri

Co-Author Name: Jon Weidanz

Title(s) of Co-Authored Work(s):

Detection of Specific Antigen/ligand Interactions with a Self-Induced Electro-Acceptor (SEAC) Sensor

Author(s): Sai Santosh Sasank Peri, Jon Weidanz, Sai Santosh Sasank Peri, Jon Weidanz, Sai Santosh Sasank Peri, Jon Weidanz

### Co-Author Statement of Consent:

As the co-author of the above named work(s), I acknowledge the above-named thesis / dissertation writer as the primary author of the work(s) listed above. I authorize the thesis / dissertation writer named above to use the listed work(s) in their thesis / dissertation. I further agree that the thesis / dissertation writer may use this work to comply with requirements for graduation.

Co-Author Signature: 

Date: 5/10/2019

**Please maintain a copy of this completed form for your records.**

You may be entitled to know what information The University of Texas at Arlington (UT Arlington) collects concerning you. You may review and have UT Arlington correct this information according to procedures set forth in UTS 139. The law is found in sections 552.021, 552.023 and 559.004 of the Texas Government Code.

## Multiple Author Release for Master's Thesis or Doctoral Dissertation

Thesis / Dissertation Writer Name: Sai Santosh Sasank Peri

Co-Author Name: George Alexandrakis

Title(s) of Co-Authored Work(s):

Detection of Specific Antibody/ligand Interactions with a Self-Induced Electro-Acetic Transport Electrodeless (SDE) Sensor

Author(s): Alexandrakis, George; Peri, Sai Santosh Sasank; Alexandrakis, George; Alexandrakis, George; Alexandrakis, George

\_\_\_\_\_

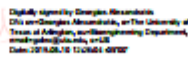
\_\_\_\_\_

\_\_\_\_\_

\_\_\_\_\_

**Co-Author Statement of Consent:**

As the co-author of the above named work(s), I acknowledge the above-named thesis / dissertation writer as the primary author of the work(s) listed above. I authorize the thesis / dissertation writer named above to use the listed work(s) in their thesis / dissertation. I further agree that the thesis / dissertation writer may use this work to comply with requirements for graduation.

Co-Author Signature: Georgios Alexandrakis 

Date: 05/10/19

**Please maintain a copy of this completed form for your records.**

You may be entitled to know what information The University of Texas at Arlington (UT Arlington) collects concerning you. You may review and have UT Arlington correct this information according to procedures set forth in UTS 139. The law is found in sections 552.021, 552.023 and 559.004 of the Texas Government Code.